

ผลของไอน้ำต่อทรายรีฟอรั่มิงของมีเทนโดยใช้ตัวเร่งปฏิกิริยานิกเกิลรองรับบน
ซีเรียมเซอร์โคเนียออกไซด์

นางฐิตินาถ สุขคนเขตร์

วิทยานิพนธ์นี้เป็นส่วนหนึ่งของการศึกษาตามหลักสูตรปริญญาวิทยาศาสตรดุษฎีบัณฑิต

สาขาวิชาปิโตรเคมี

คณะวิทยาศาสตร์ จุฬาลงกรณ์มหาวิทยาลัย

ปีการศึกษา 2552

ลิขสิทธิ์ของจุฬาลงกรณ์มหาวิทยาลัย

EFFECTS OF STEAM ON DRY REFORMING OF METHANE USING Ni
CATALYST SUPPORTED ON CERIUM ZIRCONYL OXIDE

Mrs. Thitinat Sukonket

A Dissertation Submitted in Partial Fulfillment of the Requirements
for the Degree of Doctor of Philosophy Program in Petrochemistry

Faculty of Science

Chulalongkorn University

Academic Year 2009

Copyright of Chulalongkorn University

Thesis Title EFFECTS OF STEAM ON DRY REFORMING OF
 METHANE USING Ni CATALYST SUPPORTED ON
 CERIUM ZIRCONYL OXIDE
By Mrs. Thitinat Sukonket
Field of Study Petrochemistry
Thesis Advisor Associate Professor Supawan Tantayanon, Ph.D.
Thesis Co-Advisor Professor Rahhael Idem, Ph.D.

Accepted by the Faculty of Science, Chulalongkorn University in Partial
Fulfillment of the Requirements for the Doctoral Degree

.....Dean of the Faculty of Science
(Professor Supot Hannongbua, Dr.rer.nat.)

THESIS COMMITTEE

.....Chairman
(Professor Pattarapan Prasassarakich, Ph.D.)

.....Thesis Advisor
(Associate Professor Supawan Tantayanon, Ph.D.)

.....Thesis Co-Advisor
(Professor Raphael Idem, Ph.D.)

.....Examiner
(Associate Professor Wimonrat Trakarnpruk, Ph.D.)

.....Examiner
(Assistant Professor Korbratna Kriausakul, Ph.D.)

.....External Examiner
(Associate Professor Navadol Laosiripojana, Ph.D.)

ฐิตินาถ สุขคนเขตร์: ผลของไอน้ำต่อดรายรีฟอร์มมิงของมีเทนโดยใช้ตัวเร่งปฏิกิริยานิกเกิลรองรับบนซีเรียมเซอร์โคเนียออกไซด์ (EFFECTS OF STEAM ON DRY REFORMING OF METHANE USING Ni CATALYST SUPPORTED ON CERIUM ZIRCONYL OXIDE) อ.ที่ปรึกษาวิทยานิพนธ์หลัก: รศ.ดร.ศุภวรรณ ตันตยานนท์, อ.ที่ปรึกษาวิทยานิพนธ์ร่วม: Professor Raphael Idem, Ph.D., 124 หน้า

ได้เตรียมตัวเร่งปฏิกิริยานิกเกิลบนตัวรองรับซีเรียมเซอร์โคเนียออกไซด์ $5\%Ni/Ce_{0.6}Zr_{0.4}O_2$ 4 ชนิด ตัวรองรับถูกสังเคราะห์ด้วยวิธีเซอร์แฟกแทนท์แอสซิสเทดเทมเพลตติง โดยใช้เซทิลโทรเมทิล-แอมโมเนียมโบรไมด์ (ซีทีเอบี) ในปริมาณต่างๆ และได้วางนิกเกิลด้วยวิธีการฝังตัว ตัวเร่งปฏิกิริยานิกเกิลบนตัวรองรับซีเรียมเซอร์โคเนียออกไซด์อีกชนิดหนึ่งถูกสังเคราะห์โดยวิธีการตกตะกอนร่วมเพื่อใช้ในการเปรียบเทียบ ตัวเร่งปฏิกิริยาถูกตรวจสอบด้วยการดูดซับทางกายภาพไนโตรเจน การเลี้ยวเบนรังสีเอกซ์รามานสเปกโทรสโกปี เอกซ์เรย์โฟโตอิเล็กตรอนสเปกโทรสโกปี รีดักชันแบบโปรแกรมอุณหภูมิ การวิเคราะห์ทางความร้อนโดยวัดการเปลี่ยนน้ำหนักของสารร่วมกับการเปลี่ยนพลังงานความร้อน ได้ตรวจวัดความสามารถในการเร่งปฏิกิริยาและการสะสมคาร์บอนบนตัวเร่งปฏิกิริยาในปฏิกิริยาดรายรีฟอร์มมิงของมีเทนที่เติมไอน้ำและไม่เติมไอน้ำ คอนเวอร์ชันของมีเทนและคาร์บอนไดออกไซด์รวมทั้งการเกิดไฮโดรเจนและคาร์บอนมอนอกไซด์ถูกวิเคราะห์ในเวลาเดียวกันด้วยแก๊สโครมาโทกราฟีเป็นเวลา 8 ชั่วโมงของปฏิกิริยา ผลการทดลองได้แสดงให้เห็นว่าตัวเร่งปฏิกิริยาทั้งหมดที่เตรียมด้วยวิธีเซอร์แฟกแทนท์แอสซิสเทดเทมเพลตติง มีประสิทธิภาพและเสถียรภาพดีกว่าตัวเร่งปฏิกิริยาที่เตรียมด้วยวิธีการตกตะกอนร่วม การเติมไอน้ำในปฏิกิริยาไม่เพิ่มคอนเวอร์ชันของมีเทนแต่ช่วยลดการสะสมคาร์บอน นอกจากนี้ได้เตรียมตัวรองรับออกไซด์ผสมแบบเทอร์นารี $CeZrMO_2$ จำนวน 10 ชนิด ซึ่ง M เป็นไอออนของโลหะทรานซิชัน โลหะทรานซิชันแบบอินเนอร์ หรือโลหะที่ไม่ใช่ทรานซิชัน ด้วยวิธีเซอร์แฟกแทนท์แอสซิสเทดเทมเพลตติงแล้วจึงฝังนิกเกิล พบว่าโลหะที่เติมเข้าไปได้ช่วยเพิ่มความจุหน่วยเก็บออกซิเจนและเสถียรภาพต่อความร้อนให้กับตัวรองรับเมื่อเปรียบเทียบกับออกไซด์ผสมแบบไบนารี ซึ่งส่งผลให้ความสามารถในการเร่งปฏิกิริยาดรายรีฟอร์มมิงของมีเทนดีขึ้น การเติมไอน้ำในปฏิกิริยาที่ใช้ตัวเร่งปฏิกิริยาออกไซด์ผสมแบบเทอร์นารีได้เพิ่มค่าคอนเวอร์ชันของมีเทนเล็กน้อย และได้ลดคาร์บอนได้อย่างสำคัญ นอกจากนี้แล้วตัวเร่งปฏิกิริยาได้แสดงเสถียรภาพที่ดีในปฏิกิริยาดรายรีฟอร์มมิงของมีเทน ถึงแม้ว่าจะทำที่อุณหภูมิต่ำถึง 500 องศาเซลเซียส

สาขาวิชา.....ปีโตรเคมี..... ลายมือชื่อนิสิต.....
 ปีการศึกษา.....2552..... ลายมือชื่อ อ. ที่ปรึกษาวิทยานิพนธ์.....
 ลายมือชื่อ อ. ที่ปรึกษาวิทยานิพนธ์ร่วม.....

4873818023 : MAJOR PETROCHEMISTRY

KEYWORDS : DRY REFORMING/ CERIUM-ZIRCONIUM OXIDE/ NICKEL-BASED CATALYST/ TERNARY MIXED OXIDE

THITINAT SUKONKET : EFFECTS OF STEAM ON DRY REFORMING OF METHANE USING Ni CATALYST SUPPORTED ON CERIUM ZIRCONYL OXIDE. THESIS ADVISOR : ASSOC. PROF. SUPAWAN TANTAYANON, Ph.D., THESIS CO-ADVISOR : PROF. RAPHAEL IDEM, Ph.D., 124 pp.

Four nickel catalysts supported on cerium zirconyl oxide, 5%Ni/Ce_{0.6}Zr_{0.4}O₂, were prepared. The supports were synthesized by surfactant-assisted templating route using cetyltrimethyl ammonium bromide (CTAB) at various amounts, and nickel deposition was then introduced by impregnation. Another Ni catalyst supported on cerium zirconyl oxide prepared by co-precipitation method was used for comparison. The catalysts were characterized by N₂ physisorption, XRD, RS, XPS, TPR, and TG-DSC. The catalytic performance and carbon deposition in the catalytic dry reforming of CH₄ (CDRM) with and without steam were investigated. The CH₄ and CO₂ conversion as well as the formation of H₂ and CO were concomitantly analysed by gas chromatography for 8 hours of reaction. The results showed that all catalysts prepared by surfactant-assisted templating route had higher activity and stability than the catalyst prepared by co-precipitation method. The addition of steam to the reaction did not increase the CH₄ conversion but decreased the carbon deposition. In addition, ten ternary mixed oxide supports, CeZrMO₂, where M is a transition, inner-transition or non-transition metal ion were prepared by surfactant-assisted templating route and then impregnated with Ni. It was found that the doping metals enhanced oxygen storage capacity and thermal stability of the supports comparing to the binary mixed oxides, resulting in a better catalytic performance in CDRM. The addition of steam in the reaction using ternary mixed oxide catalysts slightly increase the conversion of CH₄ and significantly decrease in carbon deposition. Moreover, the catalysts showed good stability in CDRM even at temperature as low as 500°C.

Field of Study:Petrochemistry.....	Student's Signature.....
Academic Year:2009.....	Advisor's Signature.....
	Co-Advisor's Signature.....

ACKNOWLEDGEMENTS

First of all I would like to express my sincere gratitude and appreciation to my adviser, Associate Professor Dr. Supawan Tantayanon, for her support, guidance, and encouragement throughout my education at Chulalongkorn University. She has given me the great opportunity for every thing. I would like to thank I would like to thank Professor Dr. Paitoon Tontiwachwuthikul and Professor Dr. Raphael Idem, from university of Regina, who support the instruments, financial and knowledge. Their wealth of information and input has been proved invaluable to this project. Moreover, I would like to thank my committee members, Professor Dr. Pattarapan Prasassarakich, Associate Professor Dr. Wimonrat Trakarnpruk, Assistant Professor Dr. Korbratna Kriausakul and Associate Professor Dr. Navadol Laosiripojana. I would like to thank Office of the Higher Education Commission and Suan dusit Rajabhat University for research fund and National Center of Excellence for Petroleum, Petrochemicals, and Advance Materials, NCE-PPAM for the support. I gratefully acknowledge the material support from Bangkok Industrial Gas Co., Ltd.

I would like to extend my deepest gratitude to Dr. Ataullah Khan and Dr. Sutteerawat Smingprai for their sincere help and standing beside me. Next I would like to thank all my friends especially, Mr. Bappy Saha for giving me a hand in the experimental, Miss Wannarudee Temnin, Miss Saranya Ploypradub, Miss Maslin Shotirat, Miss Chantimas Tochai, Mr. Jareonporn Chokboribal, and Thai people in Canada. Without all direct or indirect supports from them this thesis can not be completely successful.

Last but not the least; I would like to thank my parents and my family for all the love, trust, support, worries and encouragement.

CONTENTS

	Page
ABSTRACT IN THAI	iv
ABSTRACT IN ENGLISH	v
ACKNOWLEDGEMENTS	vi
CONTENTS	vii
LIST OF TABLES	xii
LIST OF FIGURES	xiii
LIST OF ABBREVIATIONS	xvii
CHAPTER I: INTRODUCTION	1
1.1 Introduction.....	1
1.2 Objective	4
CHAPTER II: THEORETICAL STUDIES AND LITERATURE REVIEW	5
2.1 Theoretical studies.....	5
2.1.1 Hydrogen production.....	5
2.1.1.1 Reforming of methane	6
2.1.1.2 Carbon formation on metal surfaces.....	9
2.1.1.3 Sintering of metal.....	9
2.1.2 Catalyst for dry reforming.....	10
2.1.2.1 Support and catalyst preparation.....	10
2.1.2.1.1 Precipitation methods.....	10
2.1.2.1.2 Impregnation methods.....	11

	Page
2.1.2.1.3 Drying.....	12
2.1.2.1.4 Calcination.....	13
2.1.2.1.5 Reduction.....	13
2.1.2.2 Catalyst Characterization.....	14
2.1.2.2.1 Nitrogen adsorption/ desorption technique: BET.....	14
2.1.2.2.2 Oxygen storage capacity (OSC).....	18
2.1.3.2.3 Temperature programmed reduction (TPR).....	19
2.1.3.2.4 X-ray diffraction spectroscopy (XRD).....	20
2.1.3.2.5 Raman spectroscopy (RS).....	23
2.1.3.2.6 X-ray photoelectron spectroscopy (XPS).....	24
2.2 Literature review	26
2.2.1 Ni/CeZrO ₂ catalyst for dry reforming reaction.....	26
2.2.2 Ni/CeZrMO ₂	28
2.2.3 Dry reforming with steam	31
CHAPTER III: EXPERIMENTAL.....	34
3.1 Materials, equipments and instruments.....	34
3.1.1 Materials.....	34
3.1.2 Equipments.....	35
3.1.3 Instruments.....	35
3.2 Experimental procedures.....	36
3.2.1 Binary mixed oxide catalyst preparation.....	36
3.2.1.1. Support preparation.....	36

	Page
3.2.1.1.1 Co-precipitation method.....	36
3.2.1.1.2 Surfactant-assisted templating route	36
3.2.1.2 Supported-nickel catalyst preparation.....	37
3.2.2 Ternary mixed oxide catalyst preparation.....	37
3.2.3 Catalyst characterization.....	38
3.2.3.1. Surface area and pore size distribution analysis.....	38
3.2.3.2 Oxygen storage capacity: OSC.....	38
3.2.3.3 X-ray diffraction: XRD.....	39
3.2.3.4 Raman spectroscopy: RS.....	39
3.2.3.5 Temperature-programmed reduction: TPR	39
3.2.3.6 X-ray photoelectron spectroscopy: XPS.....	40
3.2.4 Catalytic reaction.....	40
3.2.4.1 Equations used for calculating conversion, selectivity and yield.....	42
3.2.5 Carbon deposition evaluation.....	43
3.2.6 Long-term stability test of 5%Ni/CeZrMO ₂	43
CHAPTER IV: RESULTS AND DISCUSSION.....	45
4.1 Binary mixed oxide catalysts.....	45
4.1.1 Characteristics of the supports and catalysts.....	45
4.1.1.1 BET surface area and oxygen storage capacity	45
4.1.1.2 X-ray diffraction.....	48
4.1.1.3 Raman spectroscopy.....	50

	Page
4.1.1.4 Temperature program reduction	52
4.1.1.5 X-ray photoelectron spectroscopy.....	54
4.1.2 Catalytic performance.....	57
4.1.2.1 Effect of preparation method and CTAB/[Ce+Zr] molar ratio on catalyst performance for typical dry reforming of CH ₄	57
4.1.2.2 Effect of steam/methane ratio on the resultant catalytic activity	59
4.1.2.3 Effect of the addition of steam on the performance of NCZ catalysts for dry reforming of CH ₄	60
4.1.2.4 Effect of temperature on catalytic activity for typical dry reforming of CH ₄	61
4.1.3 Carbon deposition results.....	63
4.1.4 The structure-activity relationships (SAR) of the catalysts.....	64
4.2 Ternary mixed oxide catalyst.....	67
4.2.1 Characteristics of the supports and catalysts.....	67
4.2.1.1 BET surface area.....	67
4.2.1.2 Oxygen storage capacity (OSC).....	68
4.2.1.3 X-ray diffraction.....	70
4.2.1.4 Raman spectroscopy.....	72
4.2.1.5 Temperature program reduction.....	73
4.1.1.6 X-ray photoelectron spectroscopy.....	76
4.2.2 Catalytic performance.....	83
4.2.2.1 Effect of doped metals on catalytic performance of 5%Ni/CeZrMO ₂ for typical dry reforming of CH ₄	83
4.2.2.2 Effect of the addition of steam on the performance of 5%Ni/CeZrMO ₂ catalysts for dry reforming of CH ₄	86
4.2.2.3 Effect of temperature on catalytic performance of 5%Ni/CeZrMO ₂ for dry reforming of CH ₄	88

	Page
4.2.3 Long-term stability test.....	91
4.2.3.1 Long-term stability test of 5%Ni/CeZrCaO ₂	91
4.2.3.2 Long-term stability test of 5%Ni/CeZrYO ₂	92
4.2.3.3 Long-term stability test of 5%Ni/CeZrCaO ₂ in the presence of steam.....	93
4.2.4 The structure-activity relationships (SAR) of the catalysts.....	94
CHAPTER V: CONCLUSIONS.....	97
5.1 Binary mixed oxide catalyst.....	97
5.2 Ternary mixed oxide catalyst.....	97
5.3 Further works.....	98
REFERENCES.....	99
APPENDICES.....	110
Appendix A.....	111
Appendix B.....	122
VITAE.....	124

LIST OF TABLES

		Page
Table 2.1	IUPAC classification of pores	14
Table 4.1	Characteristics of supports and catalysts after calcination at 650°C for 3 h.....	45
Table 4.2	XPS characterization.....	54
Table 4.3	The amount of carbon deposition in the reaction.....	63
Table 4.4	Textural characteristics of ternary mixed oxide supports and catalysts calcined at 650°C for 3 h.....	67
Table 4.5	Oxygen Storage Capacity of ternary mixed oxide supports calcined at 650°C for 3 h.....	68
Table B1	The productivity calculation of 5%NiCe _{0.6} Zr _{0.4} , CTAB 1.25, without steam, 800 °C	122
Table B2	The productivity calculation of 5%NiCe _{0.6} Zr _{0.4} , CTAB 1.25, with steam 0.03 cc/min, 800 °C.....	123

LIST OF FIGURES

		Page
Figure 2.1	Patterns of activation and reaction of methane with carbon dioxide on the nickel catalyst.....	8
Figure 2.2	The IUPAC standard adsorption isotherms.....	17
Figure 2.3	A schematic of the N ₂ adsorption instrument.....	18
Figure 2.4	Oxygen storage and release.....	18
Figure 2.5	TPR spectra of the ternary mixed oxide support and catalyst calcinated at 650 °C (a) CaO (b) CeZrCa (c) Ni/CeZrCa	20
Figure 2.6	Schematic of an x-ray powder diffractometer.....	21
Figure 2.7	Reflection of x-rays from two planes of atoms in a solid.....	22
Figure 2.8	Raman spectroscopy	24
Figure 2.9	Concept of XPS technique.....	25
Figure 3.1	Schematic diagram of the experimental setup for the CO ₂ dry reforming of methane, CDRM, using packed bed tubular reactor, PBTR.....	41
Figure 4.1	X-ray diffraction patterns of titled Ce _{0.6} Zr _{0.4} O ₂ supports and 5Ni/Ce _{0.6} Zr _{0.4} O ₂ catalysts.....	48
Figure 4.2	Raman spectra of titled Ce _{0.6} Zr _{0.4} O ₂ supports and 5% Ni/Ce _{0.6} Zr _{0.4} O ₂ catalysts.....	50
Figure 4.3	TPR profiles of the supports and catalysts with various CTAB ratios (1.25 0.8 and 0.5) calcined at 650 °C.....	52
Figure 4.4	XPS spectra of supports and catalysts with various CTAB ratios (1.25 and 0.5): (a) Ce3d, (b) Zr3d, and (c) O1s	55
Figure 4.5	Performance evaluation of titled 5% Ni/Ce _{0.6} Zr _{0.4} O ₂ catalysts for dry reforming reaction: (a) CH ₄ conversion, (b) CO ₂ conversion, (c) H ₂ yield, (d) H ₂ selectivity, (e) H/CO ratio, (f) CO ₂ /CH ₄ ratio, and (g) CO/CO ₂ ratio.....	58

	Page	
Figure 4.6	Influence of steam/methane ratio on the catalytic activity of titled 5Ni/Ce _{0.6} Zr _{0.4} O ₂ CTAB 1.25 catalyst for dry reforming reaction at 800 °C in the presence of steam: H ₂ O:CH ₄ :CO ₂ = 0.625:1:1 H ₂ O:CH ₄ :CO ₂ :N ₂ = 1:1:1 and H ₂ O:CH ₄ :CO ₂ = 1.24:1:1.....	59
Figure 4.7	Screening of titled %5Ni/Ce _{0.6} Zr _{0.4} O ₂ catalysts for dry reforming reaction at 800 °C in the presence of steam (H ₂ O:CH ₄ :CO ₂ = 1:1:1).....	61
Figure 4.8	Influence of temperature on the catalytic activity of titled 5Ni/CeZrO ₂ (CTAB 0.5 and 1.25) catalyst for dry reforming reaction.....	62
Figure 4.9	Structure/activity correlation plots for dry reforming of CH ₄ reaction: (a) Activity vs. average pore diameter; (b) Surface cerium/nickel content vs. activity, (C) Activity vs. reducibility, and (D) Activity vs. OSC.....	64
Figure 4.10	X-ray diffractograms of the ternary mixed oxide supports calcined at 650 °C	70
Figure 4.11	Raman spectra of the ternary mixed oxide supports.....	72
Figure 4.12	TPR profiles of the ternary mixed oxide supports	73
Figure 4.13	TPR profiles of Ni-based catalysts supported on ternary mixed oxide.....	75
Figure 4.14	XPS spectra of CeZrMO ₂ for (a) Ce3d, (b) Zr3d, (c) O1s, and (d) C1s	76
Figure 4.15	XPS spectra of CeZrMO ₂ for (a) Ca2p, (b) Hf4f, (c) La3d, (d) Pr3d, (e) Sm 3d and (f) Tb4d	78
Figure 4.16	XPS spectra of 5%Ni/CeZrMO ₂ for (a) Ce3d, (b) Zr3d, (c) O1s, (d) C1s, and (e) Ni2p.....	81
Figure 4.17	XPS spectra of Ni/CeZrMO ₂ for (a) Ca2p, (b) Hf4f, (c) Pr3d, (d) Tb3d, (e) Sm3d and (f) Sm4d	82
Figure 4.18	Performance evaluation of titled 5%Ni/CeZrMO ₂ catalysts for dry reforming reaction: (a) CH ₄ conversion, (b) CO ₂ conversion, (c) H ₂ yield, (d) H ₂ selectivity, (e) H/CO ratio, (f) CO ₂ /CH ₄ ratio, and (g) CO/CO ₂ ratio.....	84

	Page	
Figure 4.19	Effect of steam content (0.03 cc/min) on dry reforming reaction using 5%Ni/CeZrMO ₂ for (a) CH ₄ conversion, (b) CO ₂ conversion, (c) H ₂ yield, (d) H ₂ selectivity, (e) H/CO ratio, (f) CO ₂ /CH ₄ ratio, and (g) CO/CO ₂ ratio.....	86
Figure 4.20	Effect of temperature on dry reforming reaction using 5%Ni/CeZrMO ₂ at steam 0.03 cc/ min for (a-b) CH ₄ conversion, and H ₂ yield of 5%Ni/CeZrCaO ₂ (c-d) CH ₄ conversion, and H ₂ yield of 5%Ni/CeZrLaO ₂ (e-f) CH ₄ conversion, and H ₂ yield of 5%Ni/CeZrYO ₂	89
Figure 4.21	The long-term stability of Ni/CeZrCaO ₂ on dry reforming reaction at 800 °C, without steam for 100 h for (a) CH ₄ , CO ₂ conversion, and H ₂ yield, (b) ratio.....	91
Figure 4.22	The long-term stability of 5%Ni/CeZrYO ₂ for typical dry reforming reaction at 800 °C for 25 h for (a) CH ₄ , CO ₂ conversion, and H ₂ yield, (b) ratio.....	92
Figure 4.23	The long-term stability of 5%Ni/CeZrYO ₂ on dry reforming reaction at 800 °C, steam 0.03 cc/ min for 25 h for (a) CH ₄ , CO ₂ Conversion, and H ₂ yield, (b) ratio.....	93
Figure 4.24	Structure/activity correlation plots of activity vs. reducibility for dry reforming of CH ₄ reaction in the presence of steam.....	94
Figure 4.25	Structure/activity correlation plots of activity vs. OSC for dry reforming of CH ₄ reaction in the presence of steam.....	95
Figure A1	TPR profiles of the ternary mixed oxide support and catalyst calcinated at 650 °C (a) CaO (b) CeZrCa (c) 5%Ni/CeZrCa	111
Figure A2	TPR profiles of the ternary mixed oxide support and catalyst calcinated at 650 °C (a) Sm ₂ O ₃ (b) CeZrSm (c) 5%Ni/CeZrSm	111
Figure A3	TPR profiles of the ternary mixed oxide support and catalyst calcinated at 650 °C (a) Tb ₂ O ₃ (b) CeZrTb (c) 5%Ni/CeZrTb...	112
Figure A4	TPR profiles of the ternary mixed oxide support and catalyst calcinated at 650 °C (a) Y ₂ O ₃ (b) CeZrY (c) 5%Ni/CeZrY.....	112
Figure A5	TPR profiles of the ternary mixed oxide support and catalyst calcinated at 650 °C (a) La ₂ O ₃ (b) CeZrLa (c) 5%Ni/CeZrLa...	113

	Page
Figure A6	TPR profiles of the ternary mixed oxide support and catalyst calcinated at 650 °C (a) Pr ₂ O ₃ (b) CeZrPr (c) 5%Ni/CeZrPr..... 113
Figure A7	TPR profiles of the ternary mixed oxide support and catalyst calcinated at 650 °C (a) HfO ₂ (b) CeZrHf (c) 5%Ni/CeZrHf.... 114
Figure A8	TPR profiles of the ternary mixed oxide support and catalyst calcinated at 650 °C (a) Al ₂ O ₃ (b) CeZrAl (c) 5%Ni/CeZrAl... 114
Figure A9	TPR profiles of the ternary mixed oxide support and catalyst calcinated at 650 °C (a) Sr ₂ O ₃ (b) CeZrSr (c) 5%Ni/CeZrSr..... 115
Figure A10	RS spectrum of CeZrCa O ₂ 116
Figure A11	RS spectrum of CeZrHfO ₂ 116
Figure A12	RS spectrum of CeZrLa O ₂ 117
Figure A13	RS spectrum of CeZrPr O ₂ 117
Figure A14	RS spectrum of CeZrSm O ₂ 118
Figure A15	RS spectrum of CeZrTb O ₂ 118
Figure A16	XRD pattern of CeZrCa O ₂ 119
Figure A17	XRD pattern of CeZrHf O ₂ 119
Figure A18	XRD pattern of CeZrLa O ₂ 120
Figure A19	XRD pattern of CeZrPr O ₂ 120
Figure A20	XRD pattern of CeZrSm O ₂ 121
Figure A21	XRD pattern of CeZrTb O ₂ 121

LIST OF ABBREVIATION

CDRM	Catalytic dry reforming of methane
CH ₄	Methane
CO ₂	Carbon dioxide
PBTR	Packed bed tubular reactor
CTAB	Cetyltrimethylammonium bromide
OSC	Oxygen storage capacity
BET	Brunauer-Emmett-Teller
TG/DSC	Thermogravimetric analysis/differential scanning calorimetry
TPR	Temperature- programmed reduction
XRD	X-ray diffraction
RS	Raman spectroscopy
XPS	X-ray photoelectron spectroscopy
GHSV	Gas hourly space velocity
Co-ppt	Co-precipitation
SATR	Surfactant-assisted templating route
°C	Degree Celsius
g	gram
eV	Electron volt
h	Hour
mL	Milliliter
mm	Millimeter
cc/min	Cubic centimeter/ minute

CHAPTER I

INTRODUCTION

1.1 Introduction

The catalytic dry reforming of methane (CDRM) to produce synthesis gas has attracted attention from academia and industry in recent years because this reaction involves gases that are intimately related to the greenhouse effect and energy supply. This reaction directly converts two potent greenhouse gases (CH_4 and CO_2) to synthesis gas with low H_2/CO ratio (~ 1), which satisfies the requirement of many important processes, such as Fischer-Tropsch synthesis and carbonyl production [1]. However, CO_2 reforming uses a high C/H feedstock which results in carbon deposition on the catalyst by CO disproportionation ($2\text{CO} \rightarrow \text{CO}_2 + \text{C}$) and/or methane decomposition ($\text{CH}_4 \rightarrow 2\text{H}_2 + \text{C}$). This problem has become the major issue in CO_2 reforming of methane [2]. Thus, current intense research efforts have been focused in developing catalysts which show high activity and are also resistant to carbon formation and sintering. With its relative availability, low cost and activity comparable to noble metal catalyst, Ni-based catalysts have shown good potential as a catalyst for the reforming of methane [3]. Nickel has been supported on various materials such as MgO [4-5], Al_2O_3 [6-7], SiO_2 [8-9], $(\text{MgFe})_2\text{SiO}_4$ [10], and CeO_2 [11], ZrO_2 [12], and $\text{Ce}_{1-x}\text{Zr}_x\text{O}_2$. Currently, the $\text{Ce}_{1-x}\text{Zr}_x\text{O}_2$ system has been considered as a promising support [13-16] or combined support [17-19] materials for Ni-based catalyst. The addition of ZrO_2 to CeO_2 has been found to improve the oxygen storage capacity, redox property, thermal stability and catalytic activity [1, 13-14, 16, 20-21]. Moreover, the Zr content affects the structure and redox properties of the ceria-zirconia mixed oxides. Usually, there are two phases (tetragonal and cubic) in the $\text{Ce}_x\text{Zr}_{1-x}\text{O}_2$ samples with $x \leq 0.5$ [22]. However, only a cubic fluorite phase is formed in the $\text{Ce}_x\text{Zr}_{1-x}\text{O}_2$ samples when x is higher than 0.5 [23]. Generally, $\text{Ce}_x\text{Zr}_{1-x}\text{O}_2$ with x ranging from 0.6 to 0.8 are preferred for the purposes of catalysis especially when they are used for the deposition of noble metals. In this case, Zr^{4+} ions are

incorporated into the CeO_2 matrix, and a solid solution is formed. Several methods have been used to prepare $\text{Ce}_x\text{-Zr}_{1-x}\text{O}_2$ solid solutions for catalytic applications. These included the high-temperature firing or high-energy milling of a mixture of the oxides [24-25], co-precipitation [1, 20-22, 26-28], sol-gel techniques [13-16] and surfactant-assisted templating route [29-33]. Among these methods, the surfactant-assisted templating route, a modified co-precipitation assisted with the surfactant, has attracted considerable interest due to the effective soft template effect, reproducibility and simple maneuverability [29]. This method can be used to prepare the solid solutions with high surface area and thermal stability, which favors the application of the solid solutions at high temperature [32, 33]. The $\text{Ce}_{0.6}\text{Zr}_{0.4}\text{O}_2$ systems have already been identified by our group as a promising support material for nickel based catalysts for the CDRM process. It has also been reported that 5%Ni/ $\text{Ce}_{0.6}\text{Zr}_{0.4}\text{O}_2$ prepared by using the surfactant approach has shown to be a good catalyst as the activity was stable for up to 100 h at 650 and 700 °C, while at 800 °C the catalyst activity remained stable for more than 230 h [32-34]. However, Ni-based catalysts are readily deactivated by carbon deposition at low temperature operating conditions. Much effort has been devoted towards coke suppression in the case of nickel catalysts. Recently, the addition of a small amount of steam to the dry reforming feedstock was attempted in order to eliminate carbon formation [2, 35-45]. Hence, the simultaneous steam and carbon dioxide reforming of methane, known as the 'mixed reforming' reaction allows some limited control of the H_2/CO synthesis gas ratio while avoiding carbon deposition. In our previous study [32, 33], a surfactant/metal molar ratio of 1.25 was used. Although the catalyst activity was excellent, the waste generated during support preparation was large. In the present study, we aim to develop Ni-based catalysts supported on carriers prepared using surfactant assisted route with optimal utilization of surfactant, thereby reducing the chemical wastes and production costs.

Accordingly, $\text{Ce}_{0.6}\text{Zr}_{0.4}\text{O}_2$ supports were prepared by surfactant-assisted templating route with different surfactant/metal molar ratios. The catalytic activity of the resulting catalysts when 5% Ni was impregnated on these supports was examined for dry reforming reaction both in the presence and absence of steam, and compared with those of 5%Ni impregnated on supports prepared by the conventional co-

precipitated method. The results of these comparisons are presented and discussed in Chapter IV section 4.1 of this dissertation.

The 5%Ni/CeZrO₂ binary oxide-based catalysts obtained from surfactant assisted route exhibited reasonably good performance in dry reforming reaction. However, were prone to deactivation when steam was introduced along with the dry reforming feed gas. The inherent hydrophilic nature of the ceria-zirconia support is the main cause for the apparent deactivation in the presence of steam. In order to overcome the deficiencies associated with binary oxide catalysts, a series of new generation ternary mixed oxide-based catalysts with a nominal composition 5%Ni/CeZrMO₂ (M = transition/inner transition/non-transition metal ion) were developed in the current study. The so developed catalysts made use of optimal amount of surfactant during the course of their preparation. The huge incentive in developing catalysts for low temperature steam assisted dry reforming reaction is that it will open up the option for membrane reactor application. It is reported in literature, that doping the CeZrO₂ binary oxide system with rare earth elements having variable oxidation states, results in the enhancement of the redox properties and thermal stability of CeZrO₂ [46-48]. For instance the various dopant ions evaluated for the above purpose in the literature are Al³⁺[49-50], Y³⁺ [51], La³⁺[51], Tb³⁺ [52], Pr³⁺ [53], Ba²⁺[54], and Ca²⁺ [55]. From the point of cost reduction, the use of cheap dopants with acceptable electrochemical properties is more preferable.

Hence a series of CeZrMO₂ (M = transition/inner transition/non-transition metal ion) supports were prepared by surfactant-assisted templating route with optimal surfactant/metal molar ratio = 0.5. The catalytic activity of the resulting catalysts when 5%Ni was impregnated on these supports was examined for dry reforming reaction both in the presence and absence of steam, and compared with those of 5%Ni impregnated on CeZrO₂ binary oxide supports prepared by the surfactant-assisted templating route with surfactant/metal molar ratio = 0.5. Furthermore, the low temperature activity of the ternary mixed-oxide based catalysts was evaluated in a range of temperatures, with the lowest being 500 °C. The results of these comparisons are presented and discussed in Chapter IV section 4.2 of this dissertation.

Objectives

- 1.2.1 To develop the high performance catalysts for dry reforming of CH₄ reaction.
- 1.2.2 To study the effect of steam on dry reforming of CH₄ reaction.
- 1.2.3 To investigate the catalyst performance in dry reforming of CH₄ at low temperature.

CHAPTER II

THEORETICAL STUDIES AND LITERATURE REVIEW

2.1 Theoretical studies

2.1.1 Hydrogen production

Today, hydrogen is primarily used as a feedstock, or as an intermediate chemical and specialty chemical. However, most industries and academics envision a robust hydrogen future, in which hydrogen will be used as an energy carrier for vehicle fuel or, as presented here, stationary power.

Most of the technologies required for hydrogen production, storage, and utilization have already been developed. Few of them are at a level where they can compete with the existing energy technologies. Production of hydrogen requires feedstock (logical sources being hydrocarbon fuels C_xH_y and H_2O) and energy. The amount of energy required to produce hydrogen is always greater than the energy that can be released by hydrogen utilization. Presently, hydrogen is mostly being produced from fossil fuels (natural gas, oil, and coal). Hydrogen is used in refineries to upgrade crude oil (hydrotreating and hydrocracking), in the chemical industry to synthesize various chemical compounds (ammonia, methanol, etc.), and in metallurgical processes as a reduction or protection gas. Technologies for hydrogen production from fossil fuels have been developed and are used to produce industrial hydrogen. These include steam reforming of natural gas, partial oxidation of hydrocarbons and coal gasification. However, these technologies depend on fossil fuels and emit CO_2 . The only method that can generate hydrogen from fossil fuels without generation of CO_2 is direct thermal and catalytic cracking of hydrocarbons. This method has been used to produce carbon, but for cost effective hydrogen generation it is still in the early development phase. Water electrolysis is relatively efficient (>70%), but because it needs electricity, hydrogen produced by water-electrolysis is expensive [56].

2.1.1.1. Reforming of methane

The preparation of synthesis gas from natural gas, which is the most important step in the gas-to-liquid transformation, has attracted increasing attention in the last decade. Steam reforming, partial oxidation, and CO₂ reforming are the three major processes that can be employed to prepare synthesis gas. The history of the development of methane conversion to synthesis gas is summarized as an introduction [1].

In the 1930s, Standard Oil of New Jersey was the first company to employ on a commercial scale the indirect conversion of methane, the main component of natural gas, via steam reforming to give synthesis gas, which is a mixture of H₂ and CO, with the H₂/CO ratio depending on the reactant composition. CO₂ is also formed in synthesis gas production, and sulfur compounds are present as impurities. Synthesis gas can be used as a feedstock for numerous chemicals and fuels and as a source of pure hydrogen or carbon monoxide. The steam reforming process is widely employed today.



The reaction is energy intensive because of its endothermic nature, the requirement for low space velocities, and the high H₂/CO ratio (3/1), which is unsuitable for synthesis of methanol or the long-chain hydrocarbons made in the Fischer–Tropsch process. The other two main processes for conversion of methane into synthesis gas are partial oxidation and CO₂ reforming. In the 1940s, Prettre et al. first reported the formation of synthesis gas by the catalytic partial oxidation of CH₄.



They used a Ni-containing catalyst. In contrast to steam reforming of methane, methane partial oxidation is exothermic. However, the partial oxidation requires pure oxygen, which is produced in expensive air separation units that are responsible for up to 40% of the cost of a synthesis gas plant (in contrast, the steam reforming process does not require pure oxygen). Therefore, the catalytic partial oxidation of methane

did not attract much interest for nearly half a century, and steam reforming of methane remained the main commercial process for synthesis gas manufacture.

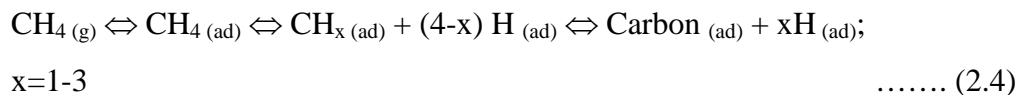
CO₂ reforming was investigated as early as 1888. Although this process, like steam reforming, is also endothermic, it produces synthesis gas with a lower H₂/CO ratio than steam reforming, and is, therefore, suitable for the Fischer–Tropsch synthesis of longchain hydrocarbons.



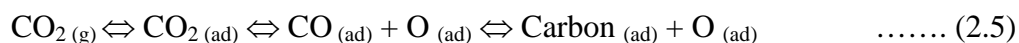
Furthermore, it can be carried out with natural gas from fields containing large amounts of CO₂, without the pre-separation of CO₂ from the feed. Because CO₂ is a greenhouse gas that causes warming of the earth and climate change, there are incentives for reducing its concentration in the atmosphere. CO₂ reforming of methane may provide a practical method for consumption of the two greenhouse gases—CH₄ and CO₂. Unfortunately, no industrial technology for CO₂ reforming of methane has yet been developed, because no effective, economic catalysts have been discovered; furthermore, high energy costs may be another drawback preventing commercialization. The partial oxidation of methane is reviewed with emphasis on hot spots in reactors, major developments in the reduction of O₂ separation costs, and reaction mechanisms. The various catalysts employed in CO₂ reforming are examined, with emphasis on inhibition of carbon deposition and sintering [57].

The possible reaction processes of carbon dioxide reforming with methane was inferred as follows: methane is firstly decomposed into hydrogen and different surface carbon species, then the adsorbed CO₂ reacts with surface carbons to form CO. The proposed mechanism is as follows [58].

- 1) Dissociative adsorption of methane is the rate-determining step.



- 2) Dissociative adsorption of carbon dioxide



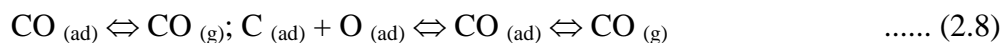
- 3) Formation of water



- 4) Formation of hydrogen



- 5) Formation of carbon monoxide and decarbonation



This mechanism is actually the synergic decomposition process of methane and carbon dioxide as shown in Figure 2.1

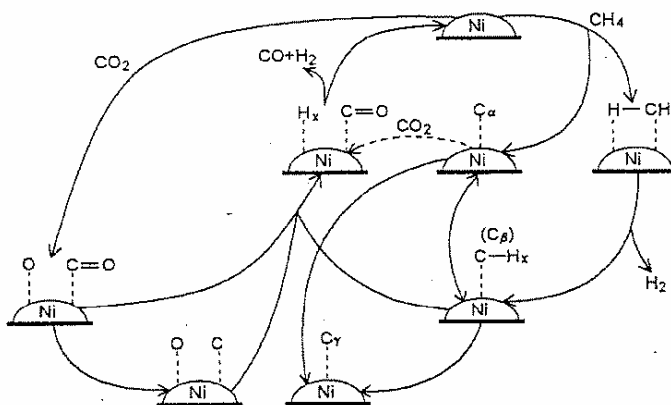


Figure 2.1 Patterns of activation and reaction of methane with carbon dioxide on the nickel catalyst.

2.1.1.2 Carbon formation on metal surfaces

In the CO₂ reforming of methane, carbon formation can occur via two possible pathways: CH₄ decomposition and CO disproportionation (the Boudouard reaction). Carbon formation by CH₄ decomposition is a structure-sensitive reaction. Specifically, the Ni(100) and Ni(110) surfaces are more active in the decomposition of CH₄ to carbon than the Ni(111) surface.



The CO disproportionation is an exothermic reaction favored at temperatures below 973 K.



Measurable rates of carbon deposition occur in the presence of cobalt, iron, and nickel catalysts at temperatures above 623 K. The form of carbon on metal surfaces generated during this reaction depends on the reaction conditions; amorphous and filamentous carbons predominate in the lower temperature range of 623–873 K, and a graphitic structure predominates at 973 K or higher temperatures. The diffusion and segregation of carbon are also dependent on the metal surface structure. For example, the carbon on Ni(110) can diffuse more readily into the bulk than that on Ni(100). Furthermore, the carbon adsorbed on the smaller metal particles diffuses with more difficulty than that on the larger particles. The structure-sensitivity of carbon formation provides the possibility for inhibition of the carbon deposition by modification of the catalyst surface structure [3].

2.1.1.3 Sintering of metal

Sintering is the process whereby at high temperature small metal particles grow into big ones, with consequent loss of metal area and activity. It has been widely studied, both experimentally and theoretically, because of its great nuisance value particularly in reactions that need somewhat high temperatures. Two mechanisms

have been considered: (i) whole particle migration and (ii) movement of single atom species governed by Ostwald ripening considerations. Both processes have been observed, but the former is thought to be more important for practical catalysts having rough surfaces. Mobility of intermediate species involved in catalyst preparation can be responsible for particle growth during drying and calcination. Sintering rate depends very much on the gas atmosphere; it is much faster under oxidizing than under reducing conditions. Once sintering has taken place, it is no easy task to reverse the process, which is thermodynamically up-hill, unless the metal-support interaction is stronger than that between the metal atoms, in which case sintering ought not to have occurred. It is usually therefore necessary to use a chemical driving force to disaggregate the metal, that is, to convert it via oxidation and reduction back to highly dispersed metal [59].

2.1.2 Catalyst for dry reforming

2.1.2.1 Support and catalyst preparation

Many preparation methods have been applied for the preparation of CeO₂–ZrO₂ solid solution for catalytic applications. These include the high-temperature firing or high-energy milling of a mixture of the oxides, sol–gel techniques, and conventional precipitation, and surfactant assisted templating routes.

2.1.2.1.1 Precipitation methods [60]

In this procedure, the solutions containing the metal salt and a salt of a compound that will be converted into the support are contacted under stirring with a base in order to precipitate as hydroxides and/or carbonate. After washing, these can be transformed to oxides by heating. Typical examples of industrial catalysts prepared by this procedure are Ni/Al₂O₃ and Cu-Zn oxide/alumina, both used in large scale productions: the first in the steam reforming process and the second in the methanol synthesis and in low temperature shift. The choice of the salts and/or alkali depends mainly on availability at a moderate cost, the solubility in the solvent (water), and, most important, on avoiding the introduction of compounds that can cause negative

effects in the final catalyst. Nitrate is inexpensive and particularly soluble in water, but calcination has to be controlled because of the exothermic evolution of nitrogen oxides. As for the base, Na^+ , K^+ , NH_4^+ hydroxides, carbonates and bicarbonates can be used as precipitating agents, although ammonium hydroxide is often preferred because of the absence of cation residue. By co-precipitation a uniform distribution on a molecular scale of the different active species in the final catalyst could be attained, at least in principle. Many variables have to be controlled: very important is an efficient mixing, the procedure and order of addition of the different solutions, the temperature, the ageing time of the precipitate (which may help filtration by transferring a gelatinous precipitate into a more crystalline one), the filtering and washing procedure (during washing the precipitate may peptize, i.e. redisperse into a colloidal gel difficult to filter). Precipitation is the preferred procedure for preparing supported catalysts with a metal loading higher than 10-15%.

Surfactant-assisted templating route, a modified co-precipitation assisted with the surfactant, can be used to prepare the solid solutions with high surface area and thermal stability, which favors the application of the solid solutions in the high temperature.

2.1.2.1.2 Impregnation methods

This procedure requires that the support is contacted with a certain amount of solution of the metal precursor, usually a salt, and then it is aged, usually for a short time, dried and calcined. According to the amount of solution used, two types of impregnation can be distinguished: one called incipient “incipient wetness” or “dryimpregnation” because the volume of the solution containing the precursor does not exceed the pore volume of the support. In the simplest way, the impregnating solution is sprayed on the support which is maintained under stirring and has been previously evacuated. By removing the air trapped in the inner pores, a deeper penetration of the solution is allowed and a consequent more uniform distribution of the metal precursor should be attained. In principle this method appears to be simple, economic (especially when using solutions of costly active components) and able to

give a reproducible metal loading which is however limited by the solubility of the metal precursor. However, when higher concentration of the metal are required, this limitation can be overcome by carrying out consecutive impregnation steps. The other type of impregnation, called “wet” or “soaking”, involves the use of an excess of solution with respect to the pore volume of the support. The system is left to age for a certain time under stirring, filtered and dried. This procedure is applied especially when a precursor-support interaction can be envisaged. Therefore, the concentration of the metal precursors on the support will depend not only on the concentration of the solution and on the pore volume of the support, but also on the type and/or concentration of adsorbing sites existing at the surface

2.1.2.1.3 Drying

After impregnation, the material undergoes a drying treatment which is generally performed at temperatures between 80 °C and 200 °C in order to eliminate the solvent used in the previous impregnation step. Different variables such as the rate of heating, final temperature and time of treatment, type of atmosphere, can influence the process and have to be selected according to the different systems. It has been pointed out that this step can affect, even severely, the results obtained during the impregnation procedure (in case of weak or no interaction between the metal precursor and the carrier surface) in terms of distribution of the active precursor. The significant factors which influence the process and make the redistribution of the metal compounds possible are different and complex: for instance, the rate of nucleation, rate of heating, degree of liquid saturation, viscosity, volume and forms of pores, distribution of pore size, etc. If the drying rate is very slow the evaporation of the solvent (usually water), which starts at the external surfaces, allows the diffusion of the salt into the liquid deeper in the pore resulting in an increase of concentration of the solution in the inner pore: after precipitation the metal precursor is mainly located at the bottom of the pore. On the contrary, too high drying rates will generate temperature gradients and will force the solution towards the outer layer of the particles, where the precipitation will occur. In order to obtain a uniform distribution, the rate of drying has to be higher than the rate of homogenization of the solution. In

practice the situation is more complicated because we are dealing with a complex porous system.

2.1.2.1.4 Calcination

This treatment consists of heating the catalysts in oxidizing atmosphere at a temperature usually as high as or a little higher than that encountered during reaction. Calcination has the purpose of decomposing the metal precursor with formation of an oxide and removal of gaseous products (usually water, CO_2) and the anions (Cl^- , NO_3^- , etc) which have been previously introduced. In the case of industrial production, calcination is useful for the removal of extraneous materials, like binders or lubricants, which have been used during the previous forming operations (extrusion, tableting, etc.). Besides decomposition during the calcinations are (i) a sintering of the precursor or of the formed oxide, and (ii) a reaction of the oxide with the support can occur. In fact, in case of alumina as the support, a calcination performed at temperatures around 500-600 °C, can give rise to reaction with divalent metal (Ni, Co, Cu) oxide with consequent formation on the surface of metal aluminates which are more stable than the oxides and so might require a higher temperature of reduction than that needed for the oxides. However, this is not a problem if the reduction temperature is not going to cause excessive sintering: in fact after reduction, the final catalysts will be well dispersed due to this textural effect. When dealing with bimetallic catalysts, a severe control of calcination temperature is required in order to avoid the formation of two separate oxides or segregation of one of the component.

2.1.2.1.5 Reduction

With this operation the metal oxide, or sometimes the metal precursor, is transformed into a metal by thermal treatment in hydrogen (or diluted hydrogen) flow. In some catalysts the reduction is performed in solution by chemical reagent such as formaldehyde or hydrazine. As in the previous thermal treatments, variables like the rate of heating, final temperature and time of reduction, hydrogen concentration and flow have to be carefully chosen depending on the type of metal, catalytic system and

reaction to be performed. The quality of the reduction gas or mixture is very important: water vapor has to be as low as possible because it can be detrimental for a high dispersion of the metal. For the same reason hydrogen flow has to be high enough to remove from the support the water formed during the reduction. Direct reduction of the metal precursor, for instance metal chlorides, is avoided although the latter are more easily reduced than the corresponding oxides: the hydrochloric acid would be very corrosive in the presence of small amounts of water vapor. Usually the catalysts are reduced to metals by the manufacture and stabilized before shipping, by oxidation of a thin film of metal which can be easily removed in the reactor. This stabilization is usually performed with a diluted oxidant mixture (1-2% O₂ in inert gas like N₂). A commonly used technique to study the reduction process is the temperature programmed reduction (TPR).

2.1.2.2 Catalyst characterization

2.1.2.2.1 Nitrogen adsorption/ desorption technique: BET [61]

Many solid and powder materials both natural and manufactured contain a certain void volume of empty space. This is distributed within the solid mass in the form of pores, cavities, and cracks of various shapes and sizes. The total sum of the void volume is called the porosity. The type and nature of porosity in natural materials depend on their formation while in man-made materials depend on their manufacturing and generally it can be controlled. Porosity strongly determines important physical properties of materials such as durability, mechanical strength, permeability, adsorption properties, etc. The knowledge of pore structure is an important step in characterizing materials, predicting their behavior. There are two main and important typologies of pores: closed and open pores. Closed pores are completely isolated from the external surface, not allowing the access of external fluids in neither liquid nor gaseous phase. Closed pores influence parameters like density, mechanical and thermal properties. Open pores are connected to the external surface and are therefore accessible to fluids, depending on the pore nature/size and the nature of fluid. Open pores can be further divided in dead-end or interconnected

pores. Further classification is related to the pore shape, whenever is possible to determine it.

The characterization of solids in terms of porosity consists in determining the following parameters:

(a) Pore size: pores are classified according to three main groups depending on the access size as shown in Table 2.1

Table 2.1 IUPAC Classification of pores

Pore Type	Pore Diameter (nm)
Micropores	less than 2 nm
Mesopores	between 2 and 50 nm
Macropores	larger than 50 nm

(b) Specific pore volume and porosity: the internal void space in a porous material can be measured. It is generally expressed as a void volume (in cc or ml) divided by a mass unit (g).

(c) Pore size distribution: it is generally represented as the relative abundance of the pore volume (as a percentage or a derivative) as a function of the pore size.

(d) Bulk density: bulk density (or envelope density) is calculated by the ratio between the dry sample mass and the external sample volume.

(e) Percentage porosity: the percentage porosity is represented by ratio between the total pore volume and the external (envelope) sample volume multiplied by 100.

(f) Specific surface area: the surface area of a solid material is the total surface of the sample that is in contact with the external environment. It is expressed as square meters per gram of dry sample. This parameter is strongly related to the pore size and the pore volume i.e. the larger the pore volume the larger the surface area and the smaller the pore size the higher the surface area. The surface area results from the contribution of the internal surface area of the pores plus the external surface area of

the solid or the particles (in case of powders). Whenever a significant porosity is present, the fraction of the external surface area to the total surface area is small.

Adsorption is defined as the concentration of gas molecules near the surface of a solid material. Adsorption is a physical phenomenon (usually called physisorption) that occurs at any environmental condition (pressure and temperature) but only at very low temperature it becomes measurable. Thus physisorption experiments are performed at very low temperature, usually at the boiling temperature of liquid nitrogen at atmospheric pressure.

Adsorption takes place because of the presence of an intrinsic surface energy. When a material is exposed to a gas, an attractive force acts between the exposed surface of the solid and the gas molecules. The result of these forces is characterized as physical (or Van der Waals) adsorption, in contrast to the stronger chemical attractions associated with chemisorption. The surface area of a solid includes both the external surface and the internal surface of the pores.

Due to the weak bonds involved between gas molecules and the surface (less than 15 KJ/mole), adsorption is a reversible phenomenon. Gas physisorption is considered non-selective, thus filling the surface step by step (or layer by layer) depending on the available solid surface and the relative pressure. Filling the first layer enables the measurement of the surface area of the material, because the amount of gas adsorbed when the mono-layer is saturated is proportional to the entire surface area of the sample. The complete adsorption/desorption analysis is called an adsorption isotherm. The six IUPAC standard adsorption isotherms are shown below, they differ because the systems demonstrate different gas/solid interactions.

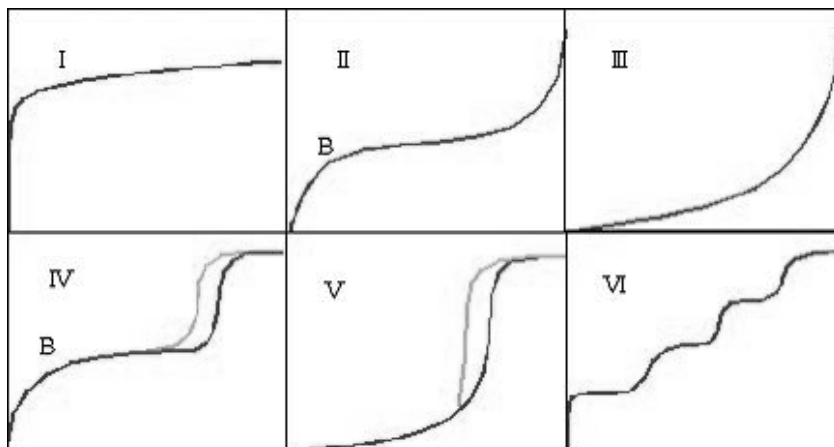


Figure 2.2 The IUPAC standard adsorption isotherms.

The Type I isotherm is typical of microporous solids and chemisorption isotherms. Type II is shown by finely divided non-porous solids. Type III and type V are typical of vapor adsorption (i.e. water vapor on hydrophobic materials). Type VI and V feature a hysteresis loop generated by the capillary condensation of the adsorbate in the mesopores of the solid. Finally, the rare type VI step-like isotherm is shown by nitrogen adsorbed on special carbon.

BET is a rule for the physical adsorption of gas molecules on a solid surface and serves as the basis for an important analysis technique for the measurement of the specific surface area of a material. In 1938, Stephen Brunauer, Paul Hugh Emmett, and Edward Teller published an article about the BET theory in a journal for the first time; “BET” consists of the first initials of their family names. The concept of the theory is an extension of the Langmuir theory, which is a theory for monolayer molecular adsorption, to multilayer adsorption with the following hypotheses: (a) gas molecules physically adsorb on a solid in layers infinitely; (b) there is no interaction between each adsorption layer; and (c) the Langmuir theory can be applied to each layer.

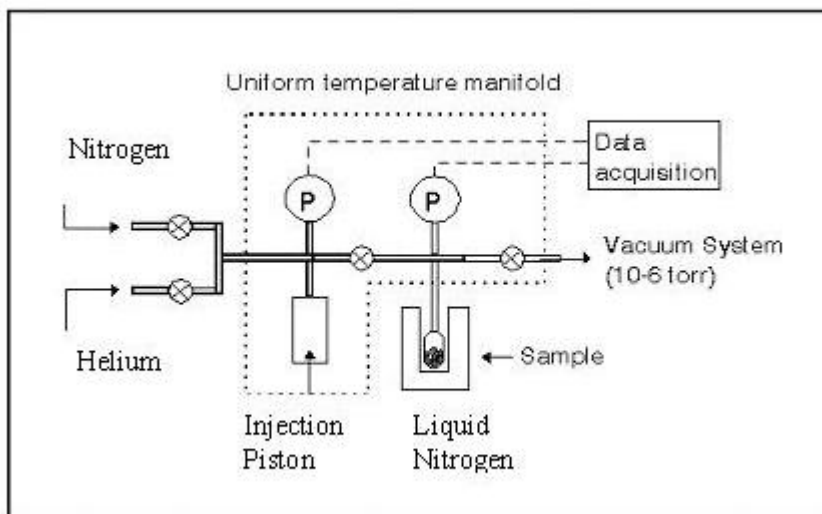


Figure 2.3 A schematic of the N₂ adsorption instrument.

2.1.2.2.2 Oxygen storage capacity (OSC)

The oxygen storage and release capacity is the ability of CeO₂-based materials to release and store oxygen according to the reaction: [62]

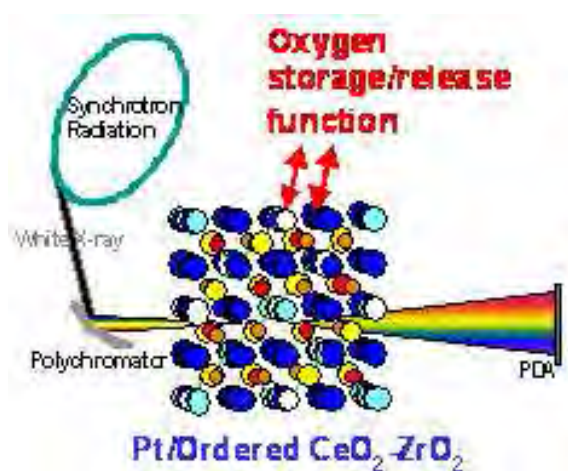
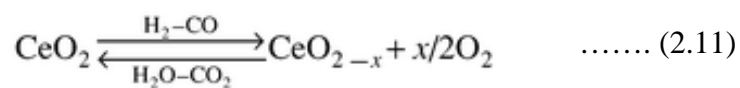


Figure 2.4 Oxygen storage and release.

Thermogravimetric Analyzer (TGA) measures weight changes in materials to determine composition, thermal stability and related phenomena. It operates from room temperature to 800 degree centigrade in many different atmospheres.

Differential Scanning Calorimeter (DSC) with modulated DSC capability can be used in the temperature range of 25 degrees centigrade to 800 degrees centigrade to measure the heat flow and temperatures associated with transitions. The material is subjected to a sinusoidal temperature ramp, superimposed on the linear temperature ramp in order to provide information about reversing and non reversing characteristics of the thermal events

2.1.2.2.3 Temperature programmed reduction (TPR)

This useful technique is mainly used for investigation and characterization of metal catalysts. In principle, during the TPR experiment, a reducing mixture (5% H₂/N₂) flows through a fixed amount of catalyst [B] (where the active metal is in its oxidic or other reducible form) contained in a reactor which is linearly heated. The amount of hydrogen consumed during the reaction is given by the difference of its concentration in the mixture before and after reduction and is measured by a TCD detector [A]. In order to obtain quantitative data, the gas mixture leaving the reactor passes through a cold trap [C] before going to the TCD detector, to remove H₂O or other reduction products and a proper calibration has to be performed, for instance by injecting known amounts of H₂ through a sampling valve [D]. The change in hydrogen concentration and temperature with time are recorded: a typical TPR profile shows one or more peaks for each different reduction process. In order to avoid artifacts in the TPR profile, care has to be taken to control such experimental parameters as gas flow rate, mass of sample, particle size, and heating rate. TPR experiments provide very useful information to decide the proper reduction conditions of the metal oxide precursor and to recognize the presence of different precursor phases, their oxidation state and their interaction with the support. So TPR patterns can be used to study and optimize catalyst pretreatment. In the industrial laboratories TPR is used as a quality control device to determine the efficacy of the preparation procedures. In case of bimetallic catalysts, TPR is very useful to characterize the state

of the metallic components, giving information on their mutual effect and on the factors which influence the formation of an alloy.

Temperature programmed reduction (TPR) with hydrogen is a widely used technique for the characterization of reducible solids and catalysts. In TPR, a reducible catalyst or catalyst precursor is exposed to a flow of a reducing gas mixture (typically a few vol.% of hydrogen in an inert gas) while the temperature is linearly increased. The rate of reduction is continuously followed by measuring the composition (H_2 content) of the reducing gas mixture at the outlet of the reactor. The experiment permits the determination of the total amount of hydrogen consumed, from which the degree of reduction and thus, the average oxidation state of the solid after reduction can be calculated [63].

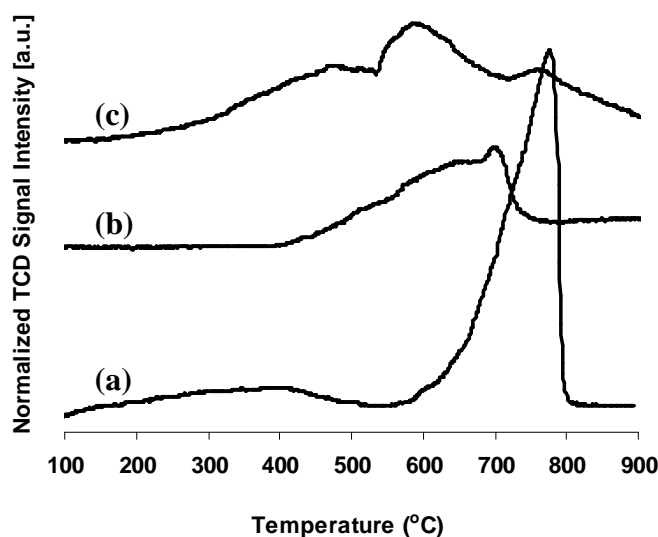


Figure 2.5 TPR spectra of of the ternary mixed oxide support and catalyst calcinated at 650 °C (a) CaO (b) CeZrCa (c) Ni/CeZrCa.

2.1.2.2.4 X-ray diffraction spectroscopy (XRD)

The X-ray diffraction pattern of a pure substance is, therefore, like a fingerprint of the substance. The powder diffraction method is thus ideally suited for characterization and identification of polycrystalline phases. An electron in an

alternating electromagnetic field will oscillate with the same frequency as the field. When an X-ray beam hits an atom, the electrons around the atom start to oscillate with the same frequency as the incoming beam. In almost all directions we will have destructive interference, that is, the combining waves are out of phase and there is no resultant energy leaving the solid sample. However the atoms in a crystal are arranged in a regular pattern, and in a very few directions we will have constructive interference. The waves will be in phase and there will be well defined X-ray beams leaving the sample at various directions. Hence, a diffracted beam may be described as a beam composed of a large number of scattered rays mutually reinforcing one another.

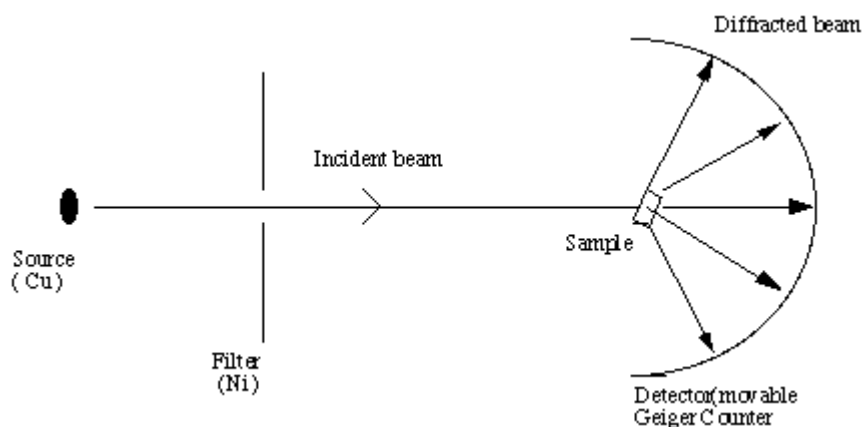


Figure 2.6 Schematic of an X-ray powder diffractometer.

The orientation and interplanar spacings of these planes are defined by the three integers h , k , l called indices. A given set of planes with indices h , k , l cut the a -axis of the unit cell in h sections, the b axis in k sections and the c axis in l sections. A zero indicates that the planes are parallel to the corresponding axis. e.g. the $2, 2, 0$ planes cut the a - and the b - axes in half, but are parallel to the c - axis. In X-ray diffraction work we normally distinguish between single crystal and polycrystalline or powder applications. The single crystal sample is a perfect (all unit cells aligned in a perfect extended pattern) crystal with a cross section of about 0.3 mm. The single crystal diffractometer and associated computer package is used mainly to elucidate the molecular structure of novel compounds, either natural products or man made

molecules. Powder diffraction is mainly used for “finger print identification” of various solid materials, e.g. asbestos, quartz. In powder or polycrystalline diffraction it is important to have a sample with a smooth plane surface. If possible, we normally grind the sample down to particles of about 0.002 mm to 0.005 mm cross section. The ideal sample is homogeneous and the crystallites are randomly distributed (we will later point out problems which will occur if the specimen deviates from this ideal state). The sample is pressed into a sample holder so that we have a smooth flat surface. Ideally we now have a random distribution of all possible h, k, l planes. Only crystallites having reflecting planes (h, k, l) parallel to the specimen surface will contribute to the reflected intensities. If we have a truly random sample, each possible reflection from a given set of h, k, l planes will have an equal number of crystallites contributing to it. We only have to rock the sample through the glancing angle THETA in order to produce all possible reflections.

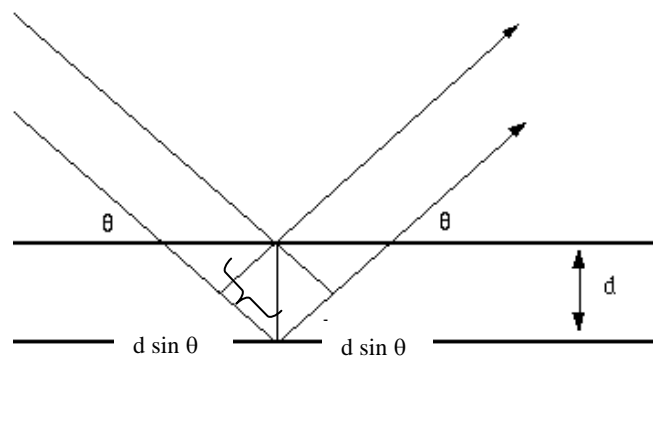


Figure 2.7 Reflection of x-rays from two planes of atoms in a solid. [64]

Using this method, Bragg’s law is able to determine the interplanar spacing of the samples, from diffraction peak according to Bragg angle.

$$n\lambda = 2d \sin \theta \quad \dots\dots (2.12)$$

Where the integer n is the order of the diffraction beam, λ is the wavelength, d is the distance between adjacent planes of atoms (the d -spacings), and θ is the angle of between the incident beam and these planes. [65]

2.1.2.2.5 Raman spectroscopy (RS)

Raman spectroscopy is a widely used technique for studying carbons and coke samples. One of the first attempts to explain the Raman spectra of graphite-like materials was published in 1970 by Tuinstra and Koenig. In a perfect single crystal of graphite only one Raman band is observed at 1575 cm^{-1} , which is called the G band or graphitic band. This band is due the in-plane bond-stretching motion of pairs of sp^2 carbons. This mode does not require the presence of six membered rings but occurs at all sp^2 sites, as it does in aromatic and olefinic molecules. In those cases the frequency always lies in the range of $1500\text{--}1630\text{ cm}^{-1}$. In amorphous graphite another major contribution in the Raman spectrum is observed around 1355 cm^{-1} : the D or disordered band. This is the “breathing” mode of the aromatic ring clusters in the graphite sheets. The smaller the size of the graphitic planes, the larger the Raman contribution in the 1355 cm^{-1} region will be. For purely graphitic cokes this interpretation appears to be straightforward, however, in many practical cases the structure of the carbon species is not purely graphitic, like in activated carbons or coked catalysts. Several researchers attempted to characterize these materials using a two-band, three-band, or four-band fitting of the Raman spectra. When there is significant line broadening of the Raman signal, as is often the case in these highly amorphous samples, peak fitting becomes very error-sensitive, and interpretation will be difficult. Because of this, and because we expect the coke to be quite illdefined, we did not attempt to deconvolute the coke contribution in the Raman spectra in this study. The total carbon contribution was calculated by integrating the Raman bands between 950 and 1750 cm^{-1} , yielding the total coke intensity.

Nowadays, Raman equipment is relatively cheap and very easy to operate. Of course this technique has its drawbacks, like problems with fluorescence, sensitivity or quantification. Fluorescence is a phenomenon that can completely obscure the Raman spectrum, and may be caused by organic impurities, basic surface OH groups, proton superpolarizability or reduced transition metal ions when resonantly excited. All these conditions may be present in the case of spent hydroprocessing catalysts. Fortunately, current technology has greatly improved the sensitivity of Raman spectrometers by using highly sensitive CCD cameras and high performance holographic notch filters.

However, quantitative Raman analysis is still a difficult task because the scattering cross-sections and the local morphology of many materials are not known, and may change as a function of analysis conditions like temperature and pressure. Moreover, Raman cross-sections of surface species, like ad-layers or adsorbates, may change due to interaction effects with the support. For heterogeneous, polydisperse materials, large errors may arise due to different particle sizes and morphologies. Consequently, care must be taken when interpreting absolute Raman intensities as a measure for the total amount of coke. We can however assume that within the particle, the morphology is more or less the same. Hence, relative differences in the particle, i.e. coke profiles, can be measured with reasonable accuracy [66].

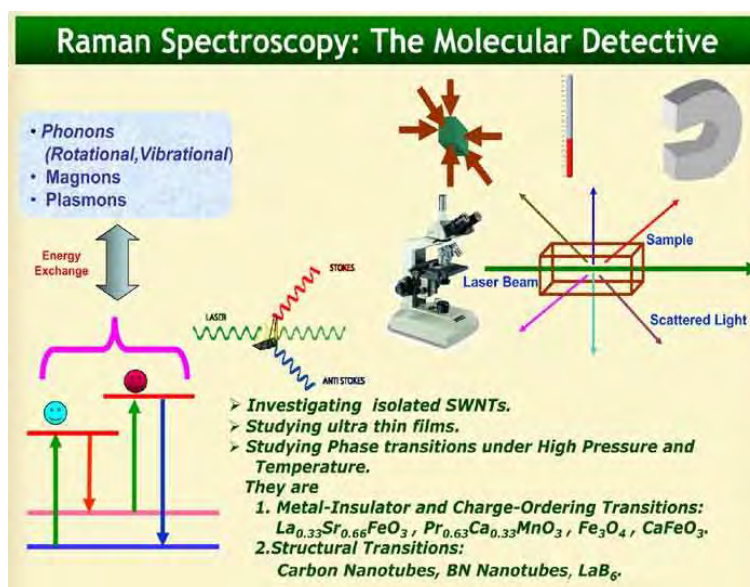


Figure 2.8 Raman spectroscopy

2.1.2.2.6 X-ray photoelectron spectroscopy (XPS)

X-ray photoelectron spectroscopy (XPS) is a surface sensitive spectroscopy technique that allows chemical identification of the elements in the top atomic layers of a sample by recording the binding energies of the electrons associated with these atoms. Furthermore, because the binding energies differ not only from chemical species to species, but also vary with the bonding conditions in which the element is

found, this technique also provides information on the actual compounds present on the surface. In essence, it probes the electronic structure of the surface. When used in combination with sputter depth profiling, in which ions are used to remove surface layers from a sample, XPS provides information about the binding energy spectra of a sample.

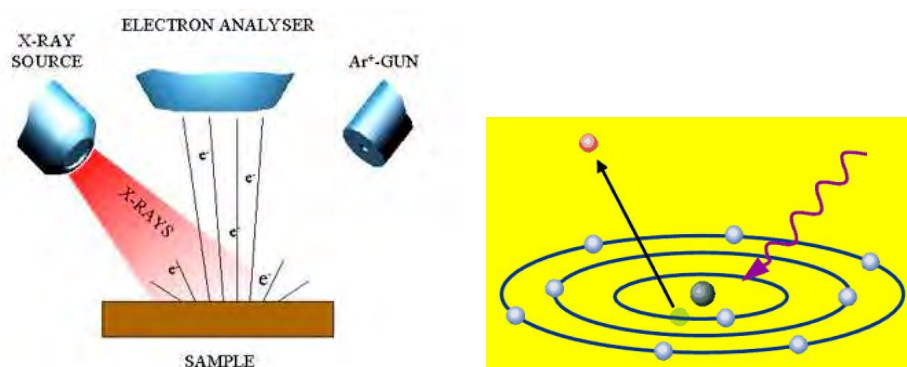


Figure 2.9 Concept of XPS technique

The information provided by XPS is complementary to the data obtained with other techniques, as it provides information about the true electronic structure of the surface. Binding energies are sensitive to local environments of atoms or ions in materials, information about which is not accessible through regular (EDS or WDS) spectroscopy techniques. XPS also known as Electron Spectroscopy for Chemical Analysis (ESCA), is a widely used technique for obtaining chemical information of various material surfaces. Core-level electrons are emitted from a surface after it has been irradiated with soft X-ray. The low kinetic energy (0 - 1500 eV) of emitted photoelectrons limit the depth from which it can emerge so that XPS is a very surface-sensitive technique and the sample depth is in the range of few nanometers. Photoelectrons are collected and analyzed by the instrument to produce a spectrum of emission intensity verse electron binding energy. In general, the binding energies of the photoelectrons are characteristic of the element from which they are emanated so that the spectra can be used for surface elemental analysis. Small shifts in the elemental binding energies provide information about the chemical state of the elements on the surface. Therefore, the high resolution XPS studies can provide the chemical state information of the surface [67].

2.2 Literature review

2.2.1 Ni/CeZrO₂ catalyst for dry reforming reaction

Among the supported metal catalysts for methane reforming, the nickel and the noble metal catalysts show quite promising catalytic activity. It has been reported that the supports markedly affect the activity and stability of the catalysts. Recently, there has been much interest in developing CeO₂ and CeZrO₂ supported catalysts for CO₂ reforming of CH₄.

Montoya et al. [13] had study Ni/ZrO₂ catalysts promoted with different amounts of CeO₂ (0, 1, 8 and 20 wt.%) which prepared by the sol–gel method. The catalysts were characterized after calcination at 800 °C and after reaction of CH₄ reforming with CO₂. Rietveld analysis reveals that the tetragonal ZrO₂ phase present in the catalysts is stabilized by the CeO₂, forming a solid solution, and avoiding transformation to the monoclinic phase. Ni²⁺ also competes with Ce⁴⁺ in the incorporation to t-ZrO₂. The t-ZrO₂ stability increases with CeO₂ concentration. The catalyst activity is increased with the CeO₂ content, although some degree of deactivation, due mainly to the sintering of the support, was not completely avoided by ceria addition. The deposition of graphitic carbon does not play an important role in the catalysts deactivation. The catalytic performance is related to the Ni surface dispersion and NiO reducibility, both promoted by CeO₂ incorporation. CeO₂ enhances the reverse water-gas shift reaction during dry reforming of methane over the studied catalysts.

Roh et al. [22] had prepared Ni/CeZrO₂ catalysts for carbon dioxide reforming of methane by co-precipitation/digestion method in a single step. The loading amount of Ni and the ratio of CeO₂ to ZrO₂ were systematically varied to optimize the co-precipitated Ni/CeZrO₂ catalysts. The prepared catalysts were characterized by various physico-chemical characterization techniques such as XRD, BET surface area, hydrogen chemisorption, SEM, TPR and XPS. It was found that 15% Ni (w/w) co-precipitated with Ce_{0.8}Zr_{0.2}O₂ having cubic phase gave synthesis gas with CH₄

conversion more than 97% at 800 °C and such activity was maintained without significant loss during the reaction for 100 h. On the contrary, Ni/CeZrO₂ having tetragonal phase (Ce_{0.2}Zr_{0.8}O₂) or mixed phase (Ce_{0.5}Zr_{0.5}O₂) deactivated during the reaction due to carbon formation. The enhanced catalytic activity and stability of the co-precipitated Ni/Ce_{0.8}Zr_{0.2}O₂ catalyst is attributed to a combination of the nanocrystalline nature of cubic Ce_{0.8}Zr_{0.2}O₂ support and the finely dispersed nano-sized NiO_x crystallites, resulting in the intimate contact between Ni and Ce_{0.8}Zr_{0.2}O₂ particles.

Terribile et al. [29] had investigated the preparation of high surface area, three-way catalysts (TWC)-like, ceria-zirconia mixed oxide. It is shown that under basic conditions cationic surfactants effectively incorporate into hydrous oxides of cerium and zirconium. The presence of cerium inhibits the action of alkyl-trimethylammonium salts as true templating agents and there is no formation of a regular pore structure. The elimination of surfactants upon calcination gives rise to the formation of high surface area, fluorite-structured CeO₂-ZrO₂ solid solution characterized by a fairly good compositional homogeneity. Surface areas in excess of 230 m²/g were obtained after calcination at 723 K, which drop to ca. 40 m²/g following treatment at 1173 K.

Kumar et al. [32] had studied the carbon dioxide reforming of methane (CDRM) to synthesis gas over various Ni-based catalysts. It is shown that the mixed oxide supports CeO₂-ZrO₂, CeO₂-Al₂O₃, and La₂O₃-Al₂O₃, prepared using surfactant, exhibit a high catalytic activity and stability for CDRM. Temperature program reduction (TPR) results demonstrate that the presence of CeO₂, ZrO₂, or La₂O₃ leads to the enhancement of the Ni reducibility compared to Al₂O₃, which is an important indicator of high activity and stability of these Ni catalysts for CDRM. Our thermodynamic calculations indicate that CeO₂ could react with CH₄ to produce synthesis gas, and then CO₂ might reoxidize CeO_{2-x} to its oxidation state. Furthermore, CeO₂ might help in gasification of deposited carbon to inhibit the carbon formation and therefore improve catalyst stability. The presence of alumina tends not to affect the stability of the catalyst as well.

Chen et al. [1] synthesized the impregnation Ni/Ce_{0.75}Zr_{0.25}O₂ and co-precipitated Ni/Ce_{0.75}Zr_{0.25}O₂ catalysts by preparing the support by the co-precipitation involving the surfactant or not. In the co-precipitated catalysts, Ni²⁺ entered the lattice of Ce_{0.75}Zr_{0.25}O₂ solid solution, which led to a better nickel dispersion and a stronger interaction between nickel species and the solid solution in comparison with the impregnated catalysts. With the surfactant assistance, the catalysts had larger surface area and pore volume than the ones without the surfactant. Among the prepared catalysts, the co-precipitated one with the surfactant assistance showed the highest activity in CH₄-CO₂ reforming. Under the conditions of 0.1 MPa, 1123 K, nCH₄ /nCO₂ = 1 and space velocity of 1.2 x 10⁴ h⁻¹, the CH₄ and CO₂ conversions were about 92% and 94% over the catalyst, respectively. It is revealed that the catalysts performance is related to the textural properties, the support activity, and the nickel dispersion and the interaction between nickel species and the support.

2.2.2 Ni/CeZrMO₂

Mei et al. [49] had prepared Ni-catalysts supported on CeO₂, ZrO₂, CeO₂-ZrO₂-Al₂O₃ and Al₂O₃ were prepared and characterized by means of X-ray diffraction (XRD), BET areas, H₂ temperature-programmed reduction (H₂-TPR), and X-ray photoelectron spectroscopy (XPS). Through the test of catalytic partial oxidation of methane (CPOM), Ni/CeO₂-ZrO₂-Al₂O₃, displayed the highest activity, which resulted from its largest BET area and best NiO dispersion. Furthermore, Ni/CeO₂-ZrO₂-Al₂O₃, maintained a long-time stability in CPOM, which was attributed to its best coking resistance among all the prepared catalysts.

Strobel et al. [68] had prepared the Pt/Ba catalysts for NO_x storage-reduction (NSR) supported on ceria/zirconia by two-nozzle flame spray pyrolysis. Emphasis was placed on the effect of the support composition on the thermal deterioration and the related behavior during NO_x storage and reduction. The as-prepared material consisted of intimately mixed agglomerates of BaCO₃ and Ce_xZr_{1-x}O₂ particles. Low thermal stability of BaCO₃ resulted in high NO_x storage capacity. The support

composition ($\text{Ce}_x\text{Zr}_{1-x}\text{O}_2$) strongly affected the NO_x reduction activity of Pt. Higher Ce content favored the formation of stable Pt oxides exhibiting lower reduction activity. Thermal deterioration was investigated in different atmospheres. At 800 °C, BaCO_3 transformed into inactive Ba zirconate and Ba cerate. At high Ce content, BaCO_3 was reformed when exposed to CO_2 at high temperatures, recovering its high NO_x storage capacity. During the high-temperature treatment, however, Pt strongly deactivated, resulting in a loss of the catalyst's NO_x reduction activity.

An et al. [69] had studied the doping effect of CaO and MgO on the microstructure and dynamic oxygen storage capacity (OSC) of $\text{Ce}_{0.67}\text{Zr}_{0.33}\text{O}_2$ was compared. XRD, Raman spectra and HRTEM observation confirmed that after MgO and CaO doping, more oxygen ion vacancies and lattice defect in the fluorite lattice were produced due to charge compensation and radius effect. On the other hand, improved phase thermal stability was obtained from doping. Results of dynamic OSC measurements showed that MgO and CaO doping enhance the dynamic OSC of $\text{Ce}_{0.67}\text{Zr}_{0.33}\text{O}_2$. But after redox treatment difference was found between the two dopants. The improved OSC of CaO doping was due to the proper ionic radius and effective modification of microstructure. The decreased OSC of MgO doped $\text{Ce}_{0.67}\text{Zr}_{0.33}\text{O}_2$ after redox treatment was due to the small solubility of Mg^{2+} in ceria lattice and collapse of the defective structure of Mg–Ce–Zr–O system.

Wang et al. [70] had investigated the catalytic behaviors of Pd (1.4 wt%) catalysts supported on $\text{CeO}_2\text{-ZrO}_2\text{-La}_2\text{O}_3$ mixed oxides with different Ce/Zr molar ratios for methanol decomposition. Nitrogen adsorption-desorption (BET), X-ray photoelectron spectroscopy (XPS), H_2 temperatureprogrammed reduction ($\text{H}_2\text{-TPR}$), X-ray diffraction (XRD) and Pd dispersion analysis were used for their characterization. Pd/ $\text{Ce}_{0.76}\text{Zr}_{0.18}\text{La}_{0.06}\text{O}_{1.97}$ catalyst showed the highest BET surface area, best Pd dispersion capability and strongest metal-support interaction. Moreover, XPS showed that there was lattice defect oxygen or mobile oxygen. According to the result of $\text{O}1s$ measurements the lattice defect oxygen or mobile oxygen helped to maintain Pd in a partly oxidized state and increased the activity for methanol decomposition. The Pd/ $\text{Ce}_{0.76}\text{Zr}_{0.18}\text{La}_{0.06}\text{O}_{1.97}$ catalyst exhibited the best activity. A

100% conversion of methanol was achieved at around 260 °C, which was about 20–40 °C lower than other catalysts.

Rossignol et al. [71] prepared $Zr_{0.1}(Ce_{1-x}Pr_x)_{0.9}O_2$ mixed oxides (x between 0 and 0.75) by coprecipitation (nitrates) or by the sol–gel route. Zirconium n-propoxide and cerium and/or praseodymium nitrates were used as precursors. “Sol–gel” oxides calcined at 900 °C were shown to be cubic with a fluorite-type structure. Coprecipitated oxides could not be obtained as solid solutions. The BET surface area of these samples rapidly decreases when $x \leq 0.50$. A Raman study confirmed that all oxides were cubic and evidenced the presence of oxygen vacancies. The optimum oxygen storage capacity (OSC) was obtained for $Zr_{0.1}(Ce_{0.5}Pr_{0.5})_{0.9}O_2$. It appears that the substitution of cerium by praseodymium in $Zr_{0.1}Ce_{0.9}O_2$ mixed oxides leads to a material with improved redox properties. The presence of vacancies, associated with Pr^{3+}/Pr^{4+} ions, is thought to be responsible for these enhanced OSC.

Wang et al. [72] prepared the nano-sized Ce–Zr–Sr ternary mixed oxide ($Ce_{0.67}Zr_{0.33}Sr_{0.03}O_{2.03}$) with a good thermal stability and high surface area up to 150.6 $m^2 g^{-1}$ using a reversed microemulsion method. The measurements of the dynamic oxygen storage capacity (DOSC) and H_2 -TPR showed that Sr-incorporation improved remarkably the DOSC of mixed oxide and low temperature activity when used as TWC support. As a result, the Pd-only TWC based on the Ce–Zr–Sr mixed oxide support exhibited the improved TWC performance with amplified amplitude of stoichiometric window.

Aneggi et al. [48] had studied the soot combustion behavior and the textural and structural characteristics of CeO_2 and a series of ceria-modified materials. It is shown that ceria doped with transition metals (Zr and Fe) and rare earth elements (La, Pr, Sm, Tb) results in more active catalysts with enhanced textural properties. ZrO_2 enhances the thermal stability and the oxygen storage capacity of pure ceria, resulting in better performance in soot oxidation. Remarkably, cerium–zirconium solid solution doped with rare earth does not achieve lower temperature of combustion, providing performances comparable to CeO_2 and CeO_2 – ZrO_2 . Cerium doped with Fe_2O_3

presents the better results as far as fresh samples are taken into account, but suffers from a net loss of activity after calcination. TGA experiments under N₂ atmosphere have confirmed the key role of oxygen storage capacity in soot oxidation.

Hu et al. [74] prepared Ce_{0.6}Zr_{0.3}RE_{0.1}O₂ (RE = Y, La, Pr and Tb) solid solutions by co-precipitation technique and characterized by a series of methods. XRD and FT-Raman results show that Ce_{0.6}Zr_{0.3}RE_{0.1}O₂ has cubic- fluorite structure. The different dopant ion radii bring different effect on the cell parameter of Ce_{0.6}Zr_{0.3}RE_{0.1}O₂. The X-ray photoelectron spectroscopy (XPS) results show that the binding energy of Ce 3d, Zr 3d, and O 1s for Ce_{0.6}Zr_{0.3}RE_{0.1}O₂ increases compared with that for Ce_{0.6}Zr_{0.4}O₂, indicating that dopant elements change chemistry environment of solid solutions which is available to improve redox performance. Compared with Pd/Ce_{0.6}Zr_{0.4}O₂, doping Y and La does not change air/fuel (A/F) characteristic of TWCs, but doping Pr and Tb widens A/F operating window and makes HC, CO and NO have higher conversion. The light-off temperature of Pd/Ce_{0.6}Zr_{0.3}La_{0.1}O₂ is corresponding to that of Pd/Ce_{0.6}Zr_{0.4}O₂. However, the light-off temperatures of Pd/Ce_{0.6}Zr_{0.3}RE_{0.1}O₂ (RE = Y, La, Pr and Tb) are lower than that of Pd/Ce_{0.6}Zr_{0.4}O₂ which keep much lower after high temperature treatments. Among Pd/Ce_{0.6}Zr_{0.3}RE_{0.1}O₂, Pd/Ce_{0.6}Zr_{0.3}Tb_{0.1}O₂ represent wider A/F operating window, higher conversion, lower light-off temperature and better high-temperature resistance.

2.2.3 Dry reforming with steam

Lemonidou et al. [35] had investigated the methane reforming by carbon dioxide over 5 wt.% Ni/CaO-Al₂O₃ catalyst. X-ray diffraction (XRD) and temperature-programmed reduction (TPR) techniques were applied to characterize the catalyst. The catalyst exhibited high activity and very good stability at stoichiometric methane and carbon dioxide feed. The addition of steam in the reacting mixture was tested and proved beneficial for the conversion of methane and the drastic decrease in carbon deposition. The kinetic behavior of the catalyst was investigated as a function of temperature and methane and carbon dioxide partial pressures. The apparent activation energies of the two reactants CH₄ and CO₂ were estimated 25.5 ± 2.0 and

23.6 ± 1.8 kcal/mol, respectively and that of CO was 24.6 ± 1.2 kcal/mol while hydrogen activation energy was estimated at 35.2 ± 3.2 kcal/mol. Partial pressure dependencies of the reaction rates were obtained at 630 °C. The increase of H₂ partial pressure resulted in an acceleration of the CO formation, while an increase in CO partial pressure demonstrated the inhibiting role in H₂ formation and the conversion of the reactants.

Koo et al. [41] had prepared Nano-sized Ni catalysts by using MgO-Al₂O₃ mixed oxides from hydrotalcite-like structure as a support. The property of support was controlled with various Mg/Al mixed ratio to enhance coke resistance in combined H₂O and CO₂ reforming of CH₄ (CSCRM) to produce synthesis gas (H₂/CO = 2) for gas to liquid (GTL). 12% Ni/MgO-Al₂O₃ catalyst with Mg/Al of 0.5 shows the highest activity in CSCRM due to high coke resistance, resulting from nano-sized Ni particles strongly interacting with the support.

Li et al. [45] had studied the CO₂ reforming of CH₄ with and without steam over a Ni/CeO₂-ZrO₂-Al₂O₃ catalyst. The catalytic performance, amount of carbon deposit and the EXAFS of the Ni *K*-edge of samples were measured. The results show that when the catalyst is used for CO₂ reforming of CH₄ without the addition of steam, the catalyst gradually deactivates, however, addition of a small amount of steam to the feed gas can significantly inhibits the deactivation, which is due to the great suppression of coke formation on the catalyst during the reaction. The EXAFS result showed that, maybe due to the penetration of more carbon atoms into the Ni lattice, the coordination number of the nearest Ni-Ni of the sample after the reaction without steam reduces more than that of samples after the reaction with a small amount of steam in the feed gas.

Roh et al. [34] had prepared Ni-CeO₂, Ni-ZrO₂ and Ni-Ce_{0.8}Zr_{0.2}O₂ catalysts by a co-precipitation method to develop catalysts suitable for synthesis gas production for gas to liquid (GTL) process. A conventional impregnation method was also employed to prepare Ni/CeO₂, Ni/ZrO₂ and Ni/Ce_{0.8}Zr_{0.2}O₂ catalysts to compare the impregnated catalysts with the co-precipitated ones. Ni content was fixed at 15% for

both cases. It has been confirmed that the co-precipitated Ni–CeO₂ and Ni–Ce_{0.8}Zr_{0.2}O₂ catalysts exhibited relatively high activity as well as stability, while the impregnated Ni/CeO₂ and Ni/Ce_{0.8}Zr_{0.2}O₂ catalysts slowly deactivated with time on stream at 800 °C. At the temperature range from 700 to 750 °C, co-precipitated Ni/Ce_{0.8}Zr_{0.2}O₂ catalyst showed higher CH₄ and CO₂ conversion than Ni/CeO₂ catalyst. The enhanced catalytic activity and stability of the co-precipitated Ni–Ce_{0.8}Zr_{0.2}O₂ catalyst is due to the combination of nano-crystalline nature of cubic Ce_{0.8}Zr_{0.2}O₂ support and finely dispersed nano-sized NiO crystallites resulting in intimate contact between Ni and support, better Ni dispersion, and enhanced oxygen transfer during the reaction.

CHAPTER III

EXPERIMENTAL

3.1 Chemicals, equipments and instruments

3.1.1 Materials

1. Cerium (III) nitrate hexahydrate $\text{Ce}(\text{NO}_3)_3 \cdot 6\text{H}_2\text{O}$, 99%: Aldrich
2. Zirconyl nitrate hydrate $\text{ZrO}(\text{NO}_3)_2 \cdot x\text{H}_2\text{O}$, 99.99%: Aldrich
3. Cetyltrimethyl ammonium bromide (CTAB) $\text{C}_{19}\text{H}_{42}\text{N} \cdot \text{Br}$: Aldrich
4. Ammonium hydroxide reagent ACS-Pure: Fisher
5. Nickel (II) nitrate hexahydrate $\text{Ni}(\text{NO}_3)_2 \cdot 6\text{H}_2\text{O}$, 99.999%: Aldrich
6. Aluminum (III) nitrate nonahydrate, $\text{Al}(\text{NO}_3)_3 \cdot 9\text{H}_2\text{O}$, 98+% ACS Reagent: Sigma-Aldrich
7. Barium (II) nitrate $\text{Ba}(\text{NO}_3)_2$, 99+% ACS Reagent: Sigma-Aldrich
8. Calcium (II) nitrate tetrahydrate $\text{Ca}(\text{NO}_3)_2$, Sigma-Ultra, minimum 99%: Sigma-Aldrich
9. Hafnium dinitrate oxide $\text{HfO}(\text{NO}_3)_2$, 99.9% (metal basis excluding Zr), $\text{Zr} < 0.1\%$, 10% w/v aqueous solution. Sigma-Ultra, minimum Calcium Nitrate Tetrahydrate $\text{Ca}(\text{NO}_3)_2$, Sigma-Ultra, minimum 99%: Sigma-Aldrich
10. Lanthanum (III) nitrate hexahydrate $\text{La}(\text{NO}_3)_3 \cdot 6\text{H}_2\text{O}$, 99.99%: Aldrich
11. Praseodimium (III) nitrate hexahydrate $\text{Pr}(\text{NO}_3)_3$, REO 99%: Alfa Aesar, A Johnson Matthey Company
12. Concentrated colloidal silica, SI830: SilcO₂ International, Inc
13. Samarium (III) nitrate hexahydrate $\text{Sm}(\text{NO}_3)_3 \cdot 6\text{H}_2\text{O}$, REO 99.99%: Alfa Aesar, A Johnson Matthey Company
14. Strontium (II) nitrate $\text{Sr}(\text{NO}_3)_2$, 99+% ACS Reagent: Sigma-Aldrich
15. Terbium (III) nitrate hydrate $\text{Tb}(\text{NO}_3)_3$, 99.9%, Packed under Ar: Alfa Aesar, A Johnson Matthey Company
16. Yttrium (III) nitrate hexahydrate, $\text{Y}(\text{NO}_3)_3 \cdot 6\text{H}_2\text{O}$, 99.99%: Aldrich

17. Liquid nitrogen: Praxair
18. Helium gas: Praxair
19. Nitrogen gas: Praxair
20. Hydrogen: nitrogen (5%:Balance): Praxair
21. Methane: carbon dioxide: nitrogen (40:40:20): Praxair

3.1.2 Equipments

1. Tube furnace: ZCP 386, Zesta Engineering, Ltd.
2. Digital mass flow controller:
3. Mass flow meter (GFM): GFM 171S, 0-500 mL/min, Aalborg
4. High pressure liquid chromatography Pump: Alltech 426
5. Syringe pump: Model 78000, Kd Scientific
6. Rotary evaporator: RII, Buchi
7. Vacuum pump: model 2025, Welch
8. Hydraulic compressor, model 3912, Carver

3.1.3 Instruments

1. Scanning electron microscope (SEM), JEOL model JSM-5600 with Energy dispersive spectrometer (EDS)
2. Surface and porosity: Micromeritics ASAP 2010
3. Thermogravimetric analysis/differential scanning calorimetry (TG/DSC): TG-DSC-111, Setaram
4. Temperature-programmed reduction (TPR): ChemBET 3000 TPR/TPD, Quantachrome
5. X-ray diffraction (XRD): Bruker D8 Discover with GADDS
6. Raman spectroscopy (RS): Renishaw inVia Raman

3.2 Experimental procedure

3.2.1 Binary mixed oxide catalyst preparation

3.2.1.1 Support preparation

3.2.1.1.1 Co-precipitation method

The CeO₂/ZrO₂ mixed oxide of a composition having 60:40 atom % was prepared by co-precipitation method. In a typical preparation experiment, appropriate amounts of Ce(NO₃)₃·6H₂O and ZrO(NO₃)₂·xH₂O salts were dissolved in 500 mL each of deionized water separately and were subsequently mixed together to form a clear mixture solution. Ammonium hydroxide was used as a precipitation agent. Ammonium hydroxide was slowly added over a period of 120 min until the pH of the solution was > 8.5 and the precipitation was complete. This caused the precipitation of hydrous cerium-zirconium oxide as a yellow solid which was filtered, washed and dried at 120 °C overnight and subsequently calcined at 650°C for 3 h.

3.2.1.1.2 Surfactant-assisted templating route

In order to prepare the Ce_{0.6}Zr_{0.4}O₂ mixed oxide support by surfactant-assisted templating route, appropriate quantities of Ce(NO₃)₃·6H₂O and ZrO(NO₃)₂·H₂O precursor salts were dissolved in deionized water. Separately, a calculated amount of cetyltrimethyl ammonium bromide (CTAB) was dissolved in deionized at 60 °C. The above two solutions were mixed together to obtain a resultant mixture solution. The molar ratio of [CTAB]/[Ce+Zr] was varied as 1.25, 0.8 and 0.5. Aqueous ammonia (25 vol.%) was gradually added to the aforementioned mixture solutions under vigorous stirring until precipitation was complete (pH 11.8). The addition of ammonia induced the precipitation of gelatinous yellow–brown colloidal slurry. The slurry was stirred for 60 min in a glass reactor, subsequently transferred into pyrex glass bottles, sealed and aged “*hydrothermally*” in autogenous pressure conditions for 5 days at 90 °C. After this time frame, the mixture was cooled and the resulting precipitate was

filtered and washed repeatedly with warm DI water. The resulting cakes were oven-dried at 120 °C overnight and finally calcined at 650 °C for 3 h in air environment.

3.2.1.2 Supported-nickel catalyst preparation

A nominal 5 wt.% Ni was loaded over the above prepared supports by standard wet impregnation method. In a typical impregnation 14.25 g of catalyst support was immersed in 127.75 ml of 0.1 M Ni(NO₃)₂ solution. The mixture was subjected to slow heating under constant stirring in a hot water bath, so as to remove the excess water; the dried powders thus obtained were calcined at 650 °C in air for 3h. The calcined catalysts were reduced *in situ* during the course of reaction in order to reduce the NiO species to metallic Ni species. The reduction was carried out at 710 °C for 3h in flowing 5% H₂/bal.N₂.

3.2.2 Ternary mixed oxide catalyst preparation

A portfolio of ternary oxide catalysts with a nominal composition of CeZrMO₂ (where ‘M’ = transition/ non-transition/ inner-transition. metal ion) were prepared by “*surfactant assisted templating route*” under basic conditions. The various dopant metal ions employed in the current study are Al, Ba, Ca, Hf, La, Pr, Sr, Sm, Tb, and Y. Nitrate precursors were employed to prepare all the above catalysts. In a typical preparation, calculated amounts of nitrate precursors of various metal ions, were dissolved separately in deionized water and mixed together. In a separate beaker, known amount of surfactant (CTAB) was dissolved in DI water at 60 °C. The above two solutions were mixed together to obtain a resultant mixture solution. The molar ratio of [CTAB]/[Ce+Zr+M] was kept constant at $\cong 0.5$. Aqueous ammonia (25 vol.%) was gradually added to the aforementioned mixture solutions under vigorous stirring until precipitation was complete (pH 11.8). The addition of ammonia induced the precipitation of gelatinous yellow–brown colloidal slurry. The slurry was stirred for 60 min in a glass reactor, subsequently transferred into pyrex glass bottles, sealed and aged “*hydrothermally*” in an air circulated oven for 5 days at 90 °C. After this time,

the mixture was cooled and the resulting precipitate was filtered and washed repeatedly with warm DI water. The resulting cakes were oven-dried at 120 °C for 12 h and finally calcined at 650 °C for 3 h in air environment. A nominal 5 wt.% Ni was loaded over the above prepared supports by standard wet impregnation method. In a typical impregnation 14.25 g of catalyst support was immersed in 127.75 ml of 0.1 M Ni(NO₃)₂ solution. The mixture was subjected to slow heating under constant stirring in a hot water bath, so as to remove the excess water; the dried powders thus obtained were calcined at 650 °C in air for 3h. The calcined catalysts were reduced *in situ* during the course of reaction in order to reduce the NiO species to metallic Ni species. The reduction was carried out at 710 °C for 3h in flowing 5% H₂/bal.N₂.

3.2.3 Catalyst Characterization

All of the catalysts were further characterized using different analytical techniques.

3.2.3.1 Surface area and pore size distribution analysis

The BET surface area and pore size distribution analyses for all catalysts were obtained by N₂ physisorption at liquid N₂ temperature using a Micromeritics ASAP 2010 apparatus. Prior to analysis, all the samples were degassed overnight at 180 °C under vacuum. Pore size distribution and average pore volume were analyzed using the desorption branch of the N₂-isotherm.

3.2.3.2 Oxygen storage properties: OSC

The dynamic oxygen storage/release capacity of the catalyst powders was measured using thermogravimetry under cyclic oxidative/reductive excursions. A known amount of sample was loaded into the TGA (Setaram TG/DSC111). The sample was subjected to reduction/oxidation cycles using the following reactive gas mixtures 5% H₂/N₂ and 5% O₂/N₂, respectively. Prior to every experiment, the catalyst sample was heated to 800 °C in inert atmosphere at a ramp rate of 15 °C/min and

maintained at 800 °C for 1h, after which the cyclic reduction/oxidation was carried out for 1h each. The flow rate was maintained constant at 40 cc/min. The weight loss during reduction and weight gained during oxidation were used to calculate the dynamic OSC of the catalyst powders. The change of weight for a ca. 0.5 g sample was monitored by thermogravimetry (TG) measurement under cyclic heat treatment in flowing air. This technique of OSC evaluation is essentially similar to that described previously [47].

3.2.3.3 X-ray diffraction spectroscopy: XRD

Powder XRD patterns were recorded on a Bruker Discover diffractometer using nickel-filtered Cu $K\alpha$ (0.154056 nm) as the radiation source. The intensity data were collected over a 2θ range of 10–90° with a step size of 0.02° using a counting time of 1 s per point. Crystalline phases were identified through comparison with the reference data from ICDD files. The average crystallite size was estimated with the help of Debye–Scherrer equation using the XRD data of all prominent lines.

3.2.3.4 Raman spectroscopy: RS

The Raman measurements were obtained on a Renishaw inVia Raman Microscope using a Ar⁺ laser (Spectra Physics) operating at 514.5 nm. The laser (10 mW at the laser) was focused onto a pelletized sample using a Leica 20X NPLAN objective (NA=0.40). The spectra were acquired using a 10 s detector acquisition time, and the spectra were accumulated to achieve sufficient signal-to-noise intensities. The spectra were baseline corrected using the Renishaw Wire V3.1 software provided with the instrument.

3.2.3.5 Temperature-programmed reduction: TPR

H₂-TPR of various catalyst samples was performed on a Quantachrome ChemBET 3000 unit equipped with a thermal conductivity detector (TCD). Prior to TPR measurements, the samples were degassed at 150 °C in an inert atmosphere (N₂

UHP grade) for 4h. The TPR experiments were performed between ambient to 1000 °C at a heating rate of 15 °C/min. Approximately 5 vol.% H₂ in N₂ bal., was used for reduction at the flow rate of 45 mL/min (STP). The total reactive gas consumption during TPR analysis was measured.

3.2.3.6 X-ray photoelectron spectroscopy: XPS

Spectrometer using Al K α (1487 eV) radiation as the excitation source. Charging of the catalyst samples was corrected by setting the binding energy of the adventitious carbon (C 1s) at 285 eV [46]. The XPS analysis was performed at ambient temperature and at pressures typically of the order of $<10^{-9}$ torr. Pass energies of 192 and 48 eV were used for survey scan and narrow scan measurements, respectively. All binding energies quoted in this study were measured within a precision of ± 0.1 eV. The quantitative surface atomic composition was determined by standard methods.

3.2.4 Activity evaluation

Activity evaluation studies were carried out in a packed bed tubular reactor (PBTR) (1/2" I.D.) made of Inconel 625. The reactor was placed vertically inside a programmable tubular furnace (Zesta, Mississauga, ON, Canada), which was heated electrically. The catalyst bed temperature was measured by means of a sliding thermocouple dipped inside the catalyst bed. The catalyst particles were sieved to ~ 0.3 mm size and mixed with 0.3 mm sized quartz sand (inert diluent) to make a catalyst bed height of ~7.8 cm. Prior to each run, the catalyst bed was pre-reduced at 710 °C for 3h using a reducing gas mixture of 5% H₂ bal. N₂ (100 cm³/min). The catalyst pretreatment involved the partial reduction of nickel oxide (NiO) to metallic nickel species (Ni), enough care was exercised to avoid over-reduction and sintering of metallic 'Ni' species. All the gases were regulated through precalibrated mass (gas) flow controllers with a digital readout unit (Aalborg Instruments, Orangeburg, NY, USA). The feed gas was composed of CH₄:CO₂:N₂ (1:1:0.5). The stoichiometric amount of water was used in the case of steam-assisted CO₂ reforming runs, the water

feed rate was regulated through a motorized syringe pump (Kd science, Holliston, MA, USA). The activity evaluation tests were performed at two different temperatures, namely 800 and 700 °C. In order to approach plug flow conditions and minimize backmixing and channeling, certain operating criteria as prescribed in our previous publications were used [32, 33]. Accordingly, the ratio of catalyst bed length to catalyst particle size (L/D_p) was 100, and the ratio of the inside diameter of the reactor to particle size (D/D_p) was 21. The product reformat stream coming from the reactor was passed through a series of heat exchangers and ice cooled knockout trap to condense water, after which, the product gases were analyzed with an online GC/TCD (Agilent 6890 N, Mississauga, ON, Canada.) equipped with Hayesep Q and Molecular Sieve A columns.

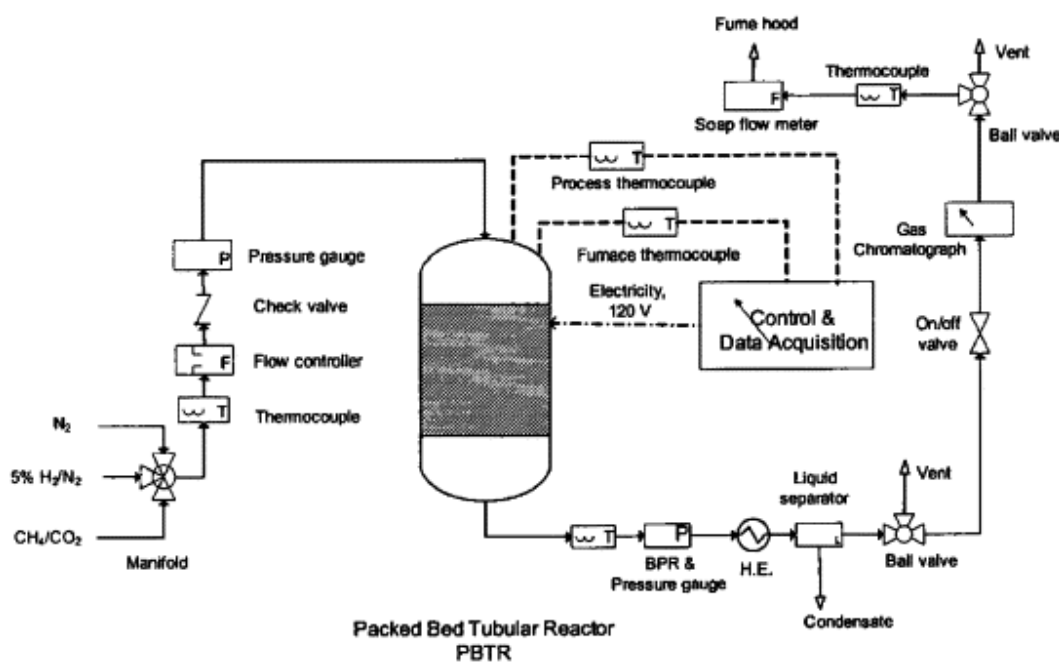
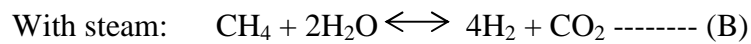
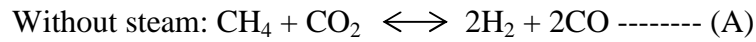


Figure 3.1 Schematic diagram of the experimental setup for the CO₂ dry reforming of methane, CDRM, using packed bed tubular reactor, PBTR. [33]

3.2.4.1 Equations used for calculating conversion, selectivity and yield.

The conversions of CH₄ and CO₂, yield and selectivity of H₂ are defined as follows:



Without steam

$$\% \text{ CH}_4 \text{ conversion} = \frac{(\text{CH}_4 \text{ in}) - (\text{CH}_4 \text{ out})}{\text{CH}_4 \text{ in}} \times 100 \text{ ----- (3.1)}$$

$$\% \text{ CO}_2 \text{ conversion} = \frac{(\text{CO}_2 \text{ in}) - (\text{CO}_2 \text{ out})}{(\text{CO}_2 \text{ in})} \times 100 \text{ ----- (3.2)}$$

$$\% \text{ H}_2 \text{ yield} = \left(\frac{\text{H}_2 \text{ out}}{\text{CH}_4 \text{ in}} \right) \times 100 \times 0.5 \text{ ----- (3.3)}$$

$$\% \text{ H}_2 \text{ selectivity} = \left(\frac{\text{H}_2 \text{ out}}{2 * [(\text{CH}_4 \text{ in}) - (\text{CH}_4 \text{ out})]} \right) \times 100 \text{ ----- (3.4)}$$

With steam

$$\% \text{ CH}_4 \text{ conversion}_A = \left(\frac{\text{CH}_4 \text{ used in A}}{\text{CH}_4 \text{ in}} \right) \times 100 \text{ ----- (3.5)}$$

$$\% \text{ CH}_4 \text{ conversion}_B = \left(\frac{\text{CH}_4 \text{ in} - \text{CH}_4 \text{ used in A} - \text{CH}_4 \text{ retained}}{\text{CH}_4 \text{ in}} \right) \times 100 \text{ ----- (3.6)}$$

$$\% \text{ CH}_4 \text{ conversion}_{\text{total}} = \% \text{ CH}_4 \text{ conversion}_A + \% \text{ CH}_4 \text{ conversion}_B \quad \text{----- (3.7)}$$

$$\% \text{ CO}_2 \text{ conversion} = \left(\frac{\text{CO}_2 \text{ used in A}}{\text{CO}_2 \text{ in}} \right) \times 100 \quad \text{----- (3.8)}$$

$$\% \text{ H}_2 \text{ selectivity} = \left(\frac{\text{H}_2 \text{ out}}{\text{H}_2 \text{ from A} + \text{H}_2 \text{ from B}} \right) \times 100 \quad \text{----- (3.9)}$$

3.2.5 Carbon deposition evaluation

At the end of each experimental run, the catalyst was cool down in inert atmosphere using flowing UHP N₂ gas. The total amount of carbon formed during the course of reaction was evaluated by standard weighing method.

3.2.6 Long-term stability test of 5%Ni/CeZrMO₂

The long-term stability test of Ni/CeZrCaO₂ and Ni/CeZrYO₂ was studied on dry reforming, with and without steam using the same condition as the catalytic reaction test in section 3.2.4

The research objectives of the Chapter IV section 4.1 of the present thesis are:

1. To study the influence of preparation method on the resultant catalytic activity for a typical dry reforming reaction.
2. To study the effect of different surfactant/metal molar ratios ([CTAB]/[Ce+Zr] = 0.5, 0.8, 1.25) on the resultant catalytic activity for typical dry reforming reaction in the absence and presence of steam.
3. To study the influence of operating temperature (700-800 °C) to the resultant catalytic activity for a typical dry reforming reaction.
4. To study the influence of different steam/methane molar ratio on the resultant catalytic activity for dry reforming reaction in the presence of steam.

The research objectives of the Chapter IV section 4.2 of the present thesis are:

1. To study the role of the individual dopant metal ion on the resultant catalytic activity for typical dry reforming reaction.
2. To study the influence of operating temperature (500-800 °C) on the resultant catalytic activity for steam-assisted dry reforming reaction..
3. To study the influence of different steam/methane molar ratios on the resultant catalytic activity for steam-assisted dry reforming reaction
4. To establish the thermal and textural stability of the best catalyst by performing a long-term time-on-stream (TOS) run.

CHAPTER IV

RESULTS AND DISCUSSION

4.1 Binary mixed oxide catalysts

4.1.1 Characteristics of the supports and catalysts

4.1.1.1 BET surface area and oxygen storage capacity

The textural characteristics of the supports as well as that of catalysts prepared by co-precipitation and surfactant-assisted templating route are summarized in Table 4.1.

Table 4.1 Characteristics of supports and catalysts after calcination at 650°C for 3 h.

Sample	Acronym	CTAB/ [Ce+Zr] Molar ratio	BET SA (m ² g ⁻¹)	Pore Volume (cc g ⁻¹)	Avg. Pore Diameter (Å)	Pore Vol/ BET SSA (10 ⁻⁹ m)	OSC (μ. Mol O/g cat.)	Avg. Crystallite Size (nm) [⊥]
Ce _{0.6} Zr _{0.4} : CP	CZ	n/a	178.9	0.23	38.7	1.28	1218.75	4.0
5%Ni/Ce _{0.6} Zr _{0.4} : WI	NCZ	n/a	136.1	0.19	42.2	1.39	1843.75	3.8
Ce _{0.6} Zr _{0.4} : SA	CZ(1.25)	1.25	201.0	0.26	40.8	1.28	1093.75	4.6
5%Ni/Ce _{0.6} Zr _{0.4} : WI	NCZ(1.25)	1.25	184.5	0.23	41.0	1.25	1812.50	4.1
Ce _{0.6} Zr _{0.4} : SA	CZ(0.8)	0.8	203.2	0.35	56.6	1.72	1031.25	4.3
5%Ni/Ce _{0.6} Zr _{0.4} : WI	NCZ(0.8)	0.8	169.3	0.27	52.7	1.59	1781.25	4.2
Ce _{0.6} Zr _{0.4} : SA	CZ(0.5)	0.5	232.0	0.38	51.0	1.63	937.50	4.2
5%Ni/Ce _{0.6} Zr _{0.4} : WI	NCZ(0.5)	0.5	215.1	0.32	51.3	1.49	1625.50	3.2

CP = Co-precipitation route; WI = Wet impregnation route; SA = Surfactant Assisted route; [⊥] Pure CeO₂ = 7.3 nm; Pure NiO = 19.0 nm;

The influence of surfactant concentration on the textural characteristics of the resultant supports was also investigated in the current study. $\text{Ce}_{0.6}\text{Zr}_{0.4}\text{O}_2$ supports with varying CTAB/[Ce+Zr] molar ratios of 1.25, 0.8 and 0.5 were prepared in the current study. For the sake of brevity, the supports and the corresponding catalysts employed in the present investigation are abbreviated as detailed in Table 4.1. From Table 4.1, it is observed that the supports and catalysts prepared by surfactant assisted route exhibit larger specific surface area and pore volume, when compared to the support and catalyst prepared by co-precipitation method. Similar results were reported by Terribile et al. [29], for which the larger surface areas were obtained as a result of the interaction of hydrous mixed metal hydroxide gel with cationic surfactants under basic conditions. At $\text{pH} \geq 11.0$, the surface hydroxyl protons (CeZr-OH^+) are exchanged by the cetyltrimethylammonium cation ($(\text{C}_{16}\text{H}_{33})\text{N}^+(\text{CH}_3)_3$), resulting in the incorporation of the surfactant cations into hydrous ceria-zirconia mixed oxide gel. This incorporation decreases the interfacial energy and eventually decreases the surface tension of water that exists in the hydrous support pores. As a result, the degree of shrinkage and pore collapse that would occur in the hydrous support during drying and calcination is reduced, which consequently, imparts higher surface area to the sample. Within the limits of the surfactant/metal molar ratios used, the $\text{CeZrO}_2(0.5)$ and $5\%\text{Ni/CeZrO}_2(0.5)$ exhibit higher surface area and pore volume when compared to $\text{CeZrO}_2(1.25)$ and $5\%\text{Ni/CeZrO}_2(1.25)$, respectively (Table 4.1). Based on the above findings, it can be seen that, in general, decreasing the CTAB/[Ce+Zr] molar ratio from 1.25 to 0.5, leads to improvement in the textural characteristics of the resultant supports. A suitable explanation for the above observations can be provided by considering the following three case scenarios: (1) $\text{CTAB} < \text{CMC}$; (2) $\text{CTAB} \sim \text{CMC}$; and (3) $\text{CTAB} > \text{CMC}$ where CMC is the critical micelle concentration. When $\text{CTAB} < \text{CMC}$, the metal precursor is bound by CTAB molecules, which prevent the metal particles from agglomeration, resulting in smaller particle sizes. When $\text{CTAB} \sim \text{CMC}$, the CTAB micelles are formed, which are present mainly on the surface of metal particles, and impart stronger interparticle repulsion; the bigger particles could collapse into smaller particles in order to minimize the surface tension. When $\text{CTAB} > \text{CMC}$, free micelles of CTAB can be formed. At high concentration of CTAB, excess CTAB molecules are encapsulated by the particles

and then reside inside the particles as bound molecules or mixed micelles. These interior CTAB micelles increase the internal electrostatic repulsion to result in a few expanded particles [75].

Upon impregnation of the supports obtained by surfactant assisted and co-precipitation routes, with a nominal 5%Ni, a loss in the surface area and pore volume results as can be seen in Table 4.1. This is a general phenomenon observed in the case of supported catalysts when an active component is impregnated over its surface. The observed decrease is mainly due to penetration of the dispersed nickel oxide into the pores of the support, thereby narrowing its pore diameter and blocking some of the pores [32].

The oxygen storage capacity (OSC) is the ability of the catalysts to undergo cyclic reduction/oxidation depending on the surrounding ambience. The OSC experiments were performed in a thermogravimetric analyzer (TGA), under cyclic reductive and oxidative excursions at 800 °C. In a typical experiment, a known amount of sample was subjected to cyclic reduction/oxidation by switching the reactive gas mixture from 5% H_2 /bal. N_2 to 5% O_2 /bal. N_2 respectively. The weight loss during reduction cycle and weight gained during oxidation cycle was monitored by TGA and was used to calculate the OSC of the support powders. The OSC measurements obtained for various supports investigated in the current study are shown in Table 4.1. The catalyst supports prepared by co-precipitation route and surfactant-assisted templating route with varying surfactant/metal ion molar ratios exhibit variable OSC functionality, which implies that they differ in their redox properties. Supports with higher OSC values, will possess highly facile $\text{Ce}^{4+} \leftrightarrow \text{Ce}^{3+}$ redox couple compared to the ones with lower OSC values. The OSC of the support obtained by co-precipitation route is higher than the OSC of supports obtained by surfactant assisted route. Within the family of supports obtained by surfactant assisted route, it is observed that the OSC increases with increasing surfactant/metal molar ratios. Previous literature reports suggest that the OSC values are independent of their specific surface area measurements [76].

4.1.1.2 X-ray diffraction

The XRD patterns of NiO, CeO₂, Ce-ZrO₂ and 5%Ni/CeZrO₂ comparing to 5%Ni/CeZrO₂ prepared by co-precipitation method are shown in Figure 4.1.

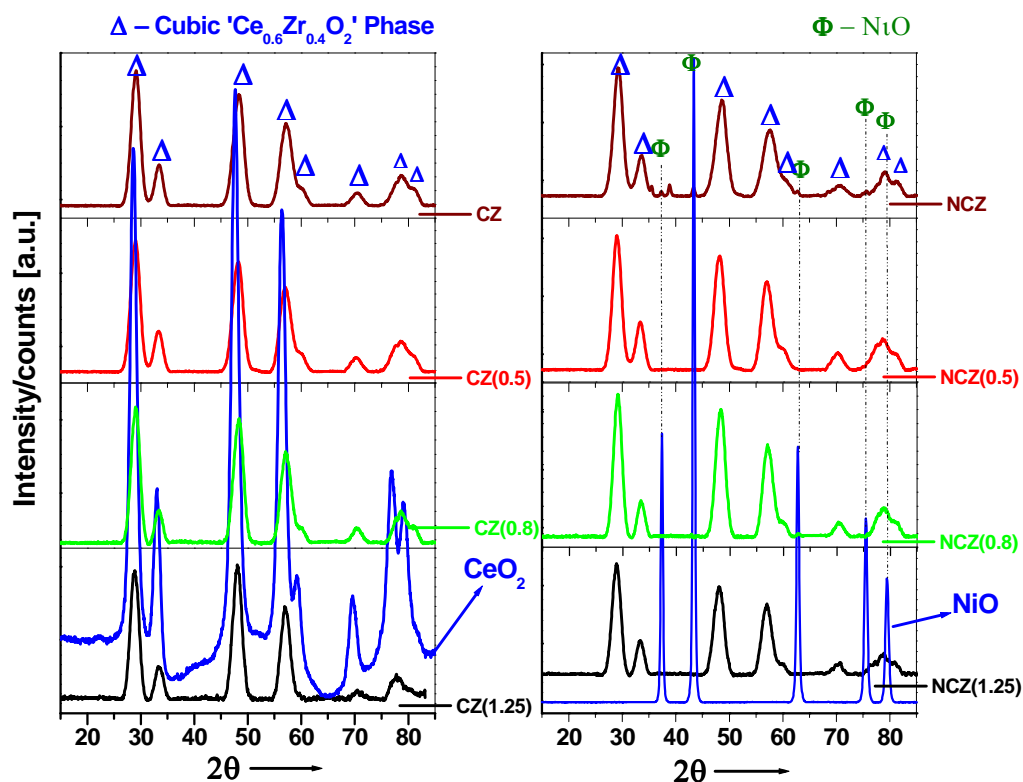


Figure 4.1 X-ray diffraction patterns of titled Ce_{0.6}Zr_{0.4}O₂ supports and 5Ni/Ce_{0.6}Zr_{0.4}O₂ catalysts

The typical XRD patterns of various samples (CeZrO₂, CeZrO₂(0.5), CeZrO₂(0.8), CeZrO₂(1.25), 5%Ni/CeZrO₂, 5%Ni/CeZrO₂(0.5), 5%Ni/CeZrO₂(0.8), and 5%Ni/CeZrO₂(1.25)) are shown in Figure 4.1 along with the XRD profiles of pure ceria and nickel oxide samples. The diffraction patterns observed show the existence of a single phase cubic fluorite-type structure for all the CeZrO₂ supports similar to what is observed in the case of pure ceria sample. A distinct shift towards higher two theta values could be noted in the case of ceria-zirconia samples ($2\theta \sim 29.0^\circ$), when compared with pure CeO₂ ($2\theta = 28.65^\circ$). The shift in the peak positions can be attributed to the substitution of the smaller Zr⁴⁺ ions (0.84 Å) in place of Ce⁴⁺

ions (0.97 \AA) in the cubic fluorite lattice resulting in the formation of solid solution with structural distortion [96]. The XRD pattern of pure NiO was used to indicate the presence/absence of crystalline NiO features in the Ni-impregnated catalyst samples (Figure 4.1). The XRD patterns of catalysts obtained by surfactant route are similar to diffraction patterns of the supports, signifying the presence of single phase cubic fluorite CeZrO_2 solid solution and absence of any crystalline NiO structures. In the case of Ni impregnated ceria-zirconia sample ($5\% \text{Ni/CeZrO}_2$) prepared by coprecipitation method, diffraction patterns of crystalline NiO could be noted indicating that the nickel oxide species was not dispersed homogeneously on the support, resulting in the formation of crystalline bulk NiO structure. On the contrary, no crystalline NiO could be noted in the samples prepared by SA route [$5\% \text{Ni/CeZrO}_2$ (1.25), $5\% \text{Ni/CeZrO}_2(0.8)$ and $5\% \text{Ni/CeZrO}_2(0.5)$]. The fact that NiO crystallites were not observed in the above samples indicates that the surfactant assisted route imparts special characteristics to the support resulting in the better dispersion of active NiO species.

Using Debye-Scherrer equation, average crystallite size was calculated for all the samples prepared in this study. In the case of CeZrO_2 support obtained by coprecipitation method, the average size of crystallite was $\sim 4 \text{ nm}$, which is smaller than the average crystallite size observed in the CeZrO_2 supports obtained by surfactant route. Among the CeZrO_2 supports prepared by surfactant route, the average crystallite size decreased slightly with decreasing CTAB/[Ce+Zr] ratio. The average crystallite size of pure CeO_2 sample was found to be $\sim 7.3 \text{ nm}$, which is bigger, compared to those of CeZrO_2 supports prepared in this study. The formation of solid solution between Ce and Zr retards the crystallite growth thus paving the way for the formation of thermodynamically more stable phase(s), as observed in the current study. It should be remembered that the particle size estimates of CeZrO_2 solid solutions are subject to uncertainties attributed to the compositional non-uniformity. When using Debye-Scherrer equation, one assumes that the particle size effects are the only source of peak broadening. However, if compositional non-uniformity occurs in the particles, the particle size will be underestimated [96]. The XRD peaks of pure NiO have prominent and sharp features, indicate the presence of larger crystallite in the sample (Table 4.1). The crystallite size of the Ni-impregnated catalyst samples

varied in the range of 3.2 – 4.2 nm, with 5%Ni/CeZrO₂(0.5) exhibiting smallest crystallite size (3.2 nm). On the whole the current preparation routes namely co-precipitation and surfactant assisted routes offer better control over the particle/crystallite size and yield smaller crystallites.

4.1.1.3 Raman spectroscopy

The Raman spectroscopic characterization was performed in order to get valuable information on both M–O bond arrangement and lattice defects. In contrast to XRD results, which yield information related to the cation sublattice, Raman spectroscopy of these fluorite type oxide structures are dominated by oxygen lattice vibrations, which are sensitive to the crystal symmetry, thus being a potential tool to obtain additional structural information.

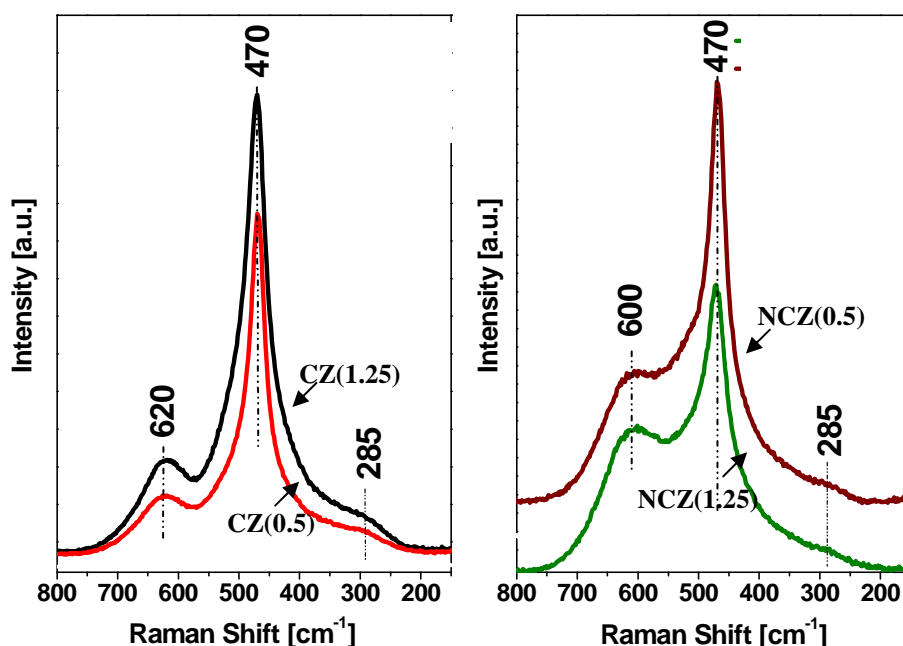


Figure 4.2 Raman spectra of titled Ce_{0.6}Zr_{0.4}O₂ supports and 5%Ni/Ce_{0.6}Zr_{0.4}O₂ catalysts.

The Raman spectra of $\text{CeZrO}_2(0.5)$, $\text{CeZrO}_2(1.25)$, $5\% \text{Ni/CeZrO}_2(0.5)$ and $5\% \text{Ni/CeZrO}_2(1.25)$ are shown in Figure 4.2. The Raman spectra of the samples shown in Figure 4.2 show an intense sharp feature at 470 cm^{-1} and two broad features at 620 cm^{-1} and 285 cm^{-1} . The band at 470 cm^{-1} corresponds to the triply degenerate F_{2g} mode and can be viewed as a symmetric breathing mode of the oxygen atoms around cerium ions [16]. The weak band observed near 600 cm^{-1} corresponds to a non-degenerate longitudinal optical (LO) mode of CeO_2 . Normally, this mode should not be observed by RS; however, the presence of some defects can involve the relaxation of the selection rules. In particular, this band has been linked to oxygen vacancies in the CeO_2 lattice. The intensity of the 600 cm^{-1} band is proportional to the number of oxygen vacancies formed. The substitution of smaller Zr^{4+} ions in place of Ce^{4+} ions causes the displacement of the O atoms from their ideal fluorite lattice positions, resulting in the appearance of a weak band at 285 cm^{-1} [96]. The relative intensities of the band at 600 and 470 cm^{-1} (I_{600}/I_{470}) were calculated and compared in order to get a comparative estimate of the oxygen vacancy (V_δ) concentration in the selected samples. In the case of $\text{CeZrO}_2(1.25)$ and $\text{CeZrO}_2(0.5)$, the ratio (I_{600}/I_{470}) is found to be 0.25 and 0.2 respectively, while in the case of $5\% \text{Ni/CeZrO}_2(1.25)$ and $5\% \text{Ni/CeZrO}_2(0.5)$ it is found to be 0.625 and 0.4 respectively. As noted above, the relative intensity measurements (I_{600}/I_{470}) provide valuable information, on the density of oxygen vacancies formed in a given sample, the higher the relative intensity of the 600 cm^{-1} band, higher would be the V_δ concentration in the given sample. From the I_{600}/I_{470} values, it is clear that V_δ concentration is higher in the $\text{CeZrO}_2(1.25)$ and $5\% \text{Ni/CeZrO}_2(1.25)$ samples when compared to $\text{CeZrO}_2(0.5)$ and $5\% \text{Ni/CeZrO}_2(0.5)$ samples. Within the limits of the surfactant ratios used in this study, it can be concluded that the V_δ concentration decreases with decreasing CTAB/[Ce+Zr] ratio employed.

4.1.1.4 Temperature program reduction

The reducibility of the supports as well as that of catalysts prepared in the current study, were studied by TPR technique in the temperature range from ambient to 1050 °C using 5% H_2 /bal. N_2 as the reactive gas. For reference purposes, TPR profiles of pure NiO and CeO_2 are included in Figure 4.3. The H_2 uptake as a function of TCD response vs. temperature is plotted in Figure 4.3.

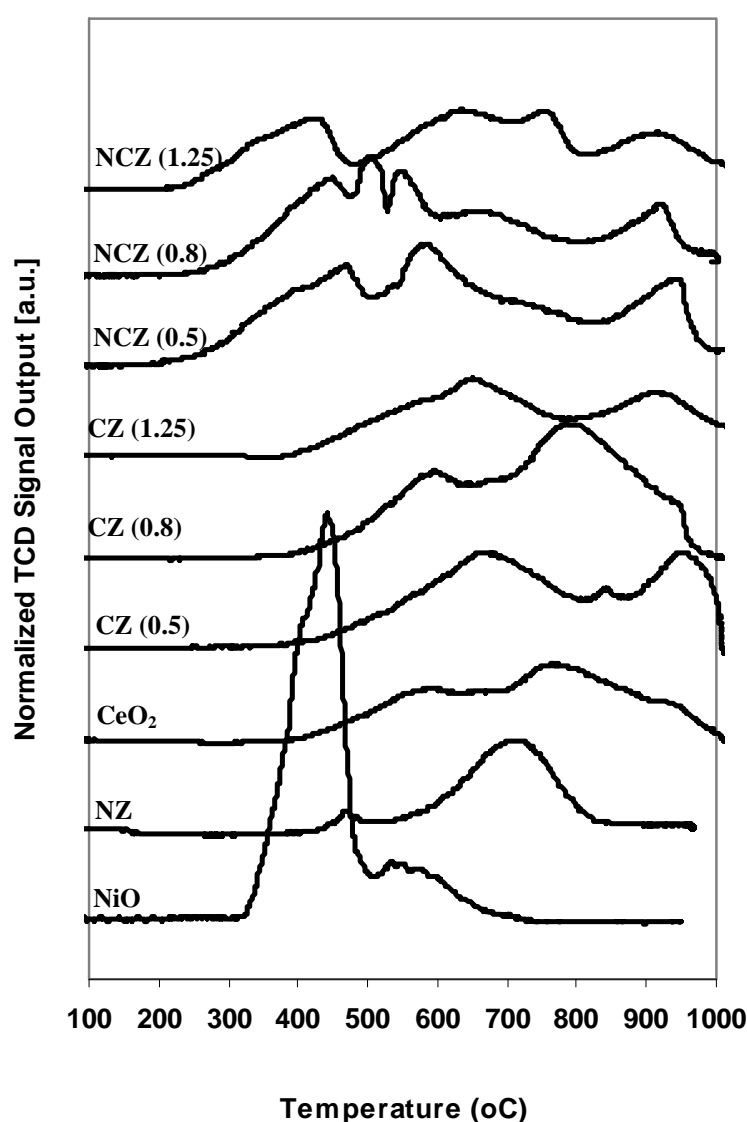


Figure 4.3 TPR profiles of the supports and catalysts with various CTAB ratios (1.25, 0.8 and 0.5) calcined at 650 °C.

Pure NiO shows a sharp reduction peak at about 440 °C, which can be attributed to the transformation of Ni²⁺ to Ni⁰ species. In the case of pure CeO₂, the one at the lower temperature (T_{max} ~ 600 °C) was ascribed to the reduction of the surface oxygen species, and the other two broad peaks at higher temperatures (T_{max} ~780 and 950°C) were due to the reduction of bulk oxygen species [97]. The higher mobility of the surface oxygen ions helps in the removal of lattice oxygen during the reduction process. The coordinately unsaturated surface capping oxygen ions can be easily removed in the low temperature region. However, bulk oxygen requires to be transported to the surface before their reduction. Consequently, the bulk reduction takes place at a higher temperature compared to the surface reduction. The bulk reduction begins only after the complete reduction of the surface sites [97]. Pure ZrO₂ does not show any sign of reduction below 900 °C, due to its refractory nature [15]. For Ni/ZrO₂, reduction peaks at about 475 °C and 700 °C are assigned to free and complex NiO species, respectively. By similar reasoning, ceria and ceria-zirconia solid solutions exhibit two distinct reduction zones; the former at lower temperatures pertains to surface shell reduction, while the later at higher temperatures pertains to the bulk reduction. In the case of all CeZrO₂, the reduction of CeO₂ occurs at higher temperatures, compared to that in the case of pure CeO₂. This result indicates that Zr incorporation into the CeO₂ make CeZrO₂ more stable.

In the case of 5%Ni/CeZrO₂ series catalysts, a reduction peak at about 440 °C is associated with the reduction of NiO to Ni and the other peaks at the higher temperature are associated with the surface and bulk reduction of Ce⁺⁴ to Ce⁺³ species. The low temperature reduction peak corresponding to CeZrO₂ of all the 5%Ni/CeZrO₂ catalysts shifted to the lower temperature than CeZrO₂ itself indicating that Ni incorporation into the CeZrO₂ makes CeO₂ more reducible, which helps produce mobile oxygen during the reforming reaction. This result agrees with the report of Dong et al [15]. A comparison among the reduction profiles of catalysts prepared from supports of variable CTAB/[Ce+Zr] molar ratio reveal that, in the case of 5%Ni/CeZrO₂(0.5) the reduction of NiO occurs at higher temperatures, compared to that in the case of 5%Ni/CeZrO₂(1.25). From our earlier investigations [32, 33] it was observed that reducibility of the NiO species plays a direct role on the resultant

catalytic activity. A comparison among the catalysts prepared by surfactant assisted and co-precipitation routes revealed that, the catalysts obtained by the former exhibit higher reducibility (i.e. lower T_{max}) compared to the later.

4.1.1.5 X-ray photoelectron spectroscopy

XPS analysis was performed in order to understand the nature of interactions between the various surface species and to get information on their oxidation state and relative surface composition. Accordingly, the measured electron binding energies (eV) of O1s, Zr3d, Ce3d, and Ni2p photoelectron peaks and the corresponding surface atomic composition are presented in Table 4.2.

Table 4.2 XPS characterization

Support/ Catalyst	CTAB/ [Ce+Zr] Molar ratio	Acronym	Binding Energy (eV)				Surface atomic composition		
			O1s	Zr3d	Ce3d	Ni2p	Zr %	Ce %	Ni %
$Ce_{0.6}Zr_{0.4}O_2$	1.25	CZ(1.25)	530.6	182.7	883.5	-	59.2	40.8	-
$Ce_{0.6}Zr_{0.4}O_2$	0.5	CZ(0.5)	530.8	182.9	883.8	-	62.2	37.8	-
5%Ni/ $Ce_{0.6}Zr_{0.4}O_2$	1.25	NCZ(1.25)	530.8	182.8	883.7	856.9	55.0	31.0	14.0
5%Ni/ $Ce_{0.6}Zr_{0.4}O_2$	0.5	NCZ(0.5)	531.0	183	884.0	856.8	60.9	32.8	6.3

In the current study, only a few representative samples e.g., $CeZrO_2(0.5)$, $CeZrO_2(1.25)$, 5%Ni/ $CeZrO_2(0.5)$ and 5%Ni/ $CeZrO_2(1.25)$ were characterized by XPS. The corresponding O1s, Ce3d, and Zr3d peaks of the selected/representative samples are shown in Figure 4.4. It is apparent from Figure 4.4(a) that the Ce3d spectra are complicated and made up of many individual overlapping peaks. By following the notation of Burroughs et. al. [51], each individual spectrum was split into two basing on their spin orbital level. Accordingly, two sets of spin-orbital multiplets with symbols u and v corresponding to the features of $3d_{3/2}$ and $3d_{5/2}$ levels respectively were assigned. In brief, the features v , v'' , v''' and u , u'' , u''' correspond to cerium in +4 oxidation state, while the features v_0 , v' and u_0 , u' correspond to cerium in +3 oxidation state. Looking at Figure 4.4(a), it is apparent that all the samples investigated by XPS in the current study, give rise to similar type of Ce3d XPS features. A more closer look at the Ce3d binding energies (B.E.) reveal that the

CeZrO₂(0.5) and 5%Ni/CeZrO₂(0.5) samples exhibit slighter higher B.E. values ~ 0.1 eV compared to that of the CeZrO₂(1.25) and 5%Ni/CeZrO₂(1.25) samples (Table 4.2). The three main features of 3d_{5/2} at ca. 883.5 (*v*), 890.0 (*v''*) and 899.5 (*v'''*) and three prominent features of 3d_{3/2} at ca. 902.5 (*u*), 912.8 (*u''*) and 917.5 (*u'''*) were observed indicating the presence of cerium in +4 oxidation state. The presence of Ce³⁺ was established from the appearance of *v'* and *u'* feature in the Ce3d spectra at ~ 887.5 and ~ 908.5 respectively. Thus, from the above finding, it can concluded that both the supports and catalysts samples, are composed of surface cerium species in both +4/+3 oxidation states, however the Ce(IV) species are predominant.

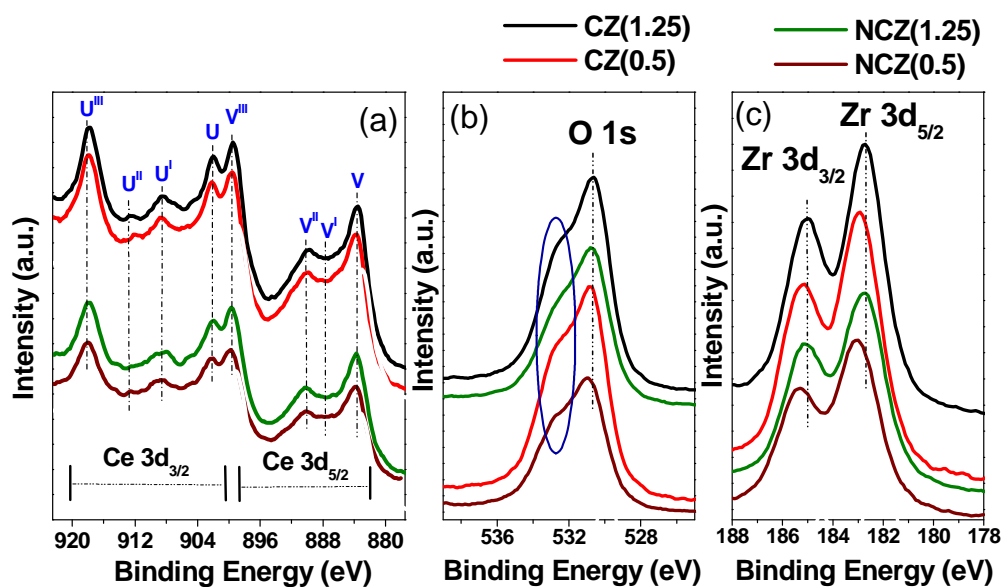


Figure 4.4 XPS spectra of supports and catalysts with various CTAB ratios (1.25 and 0.5): (a) Ce3d, (b) Zr3d, and (c) O1s

Figure 4.4 (b) shows the O1s photoelectron peaks of the selected support and selected catalyst samples investigated in the current study. The O1s peaks, shown in Figure 4.4 (b), are in turn composed of two peaks due to the nonequivalence of the surface oxygen chemical environments. The main feature at 530.6 – 531 eV corresponds to the surface lattice oxygen of CeZr-O solid solution, where both cerium and zirconium are present in their highest +4 oxidation state. As per the literature, the oxygen ions in pure CeO₂ and ZrO₂ exhibit intense peaks at 528.6 - 530.1 and 530.0

eV, respectively [96]. The broad hump like feature (indicated by blue colored circle) in Figure 4.4 (b) corresponds to the formation of Ce(III) related surface defects, where oxygen occupies additional lattice sites, resulting in the emergence of an O1s peak at ~2.0 - 2.2 eV higher binding energy [98]. Figure 4.4 (c) shows the Zr3d photoelectron peaks of the selected support and selected catalyst samples investigated in the current study. The corresponding B.E. values are shown in Table 4.2. As can be noted from Table 4.2, the B.E. values are in the range of 182.7 – 183.0 eV, which agree well with earlier literature reports and correspond to Zr in +4 oxidation state [99]. Galtayrie et al. [100], who studied ceria-zirconia solid solutions of varying composition, reported a B.E. of Zr3d_{5/2} of 181.7 -181.8 eV. The relatively higher B.E. values obtained in the current study can be attributed to the specific preparation route employed, which imparts special textural, morphological, physico-chemical, and surface characteristics to the resultant material. The Ni2p_{3/2} peak (850-870 eV) not shown here, was used for chemical state identification and quantification purposes. In the case of 5%Ni/CeZrO₂(1.25) and 5%Ni/CeZrO₂(0.5), the Ni2p_{3/2} peak B.E. values were recorded at 856.9 and 856.8 respectively. The above observed B.E. values agree well with those reported for NiO and Ni(NO₃)₂, where Ni is present in its highest oxidation state i.e., Ni(II) [101].

The surface atomic compositions of the selected supports and catalysts, as determined by XPS are presented in Table 4.2. From Table 4.2, it is evident that the surface atomic composition varied with varying surfactant/metal molar ratio. The surface cerium content of 5%Ni/CeZrO₂(1.25) was lower than that of 5%Ni/CeZrO₂(0.5) and on the contrary the surface nickel content of 5%Ni/CeZrO₂(1.25) was higher than that of 5%Ni/CeZrO₂(0.5). In addition, the surface atomic compositions (Table 4.2) among different supports and catalysts were found to be far away from their bulk composition, as expected. The trends on the characteristics observed among the samples studied here, provide valuable information on the nature of the surface active sites thereby providing the necessary information used to explain their resultant catalytic activities.

4.1.2 Catalytic performance

4.1.2.1 Effect of preparation method and CTAB/[Ce+Zr] molar ratio on catalyst performance for typical dry reforming of CH₄

In order to study the influence of the preparation method on the catalytic activity, the co-precipitated catalysts and surfactant-assisted templating route catalysts were evaluated in a PBTR at 800 °C at atmospheric pressure and gas hourly space velocity (GHSV) of 37,500 ml/h.g. The results obtained are presented in Figure 4.5. All the catalysts prepared by surfactant templating route were found to be catalytically active dry reforming of CH₄ with CH₄ conversions (~85%) for up to the 8h time on stream used for the current study. In contrast, the activity of the co-precipitated catalyst started to deteriorate within 1h TOS. The above finding indicate that the surfactant is essential in order to obtain a thermally, texturally, morphologically stable catalyst. A comparison of the catalysts prepared with different surfactant/metal molar ratios indicates that the amount of surfactant employed plays a role in the resultant activity. The catalysts with CTAB/[Ce+Zr] molar ratio of 1.25 is slightly better than the ratio of 0.8, which in turn, is better than the CTAB/[Ce+Zr] of 0.5. In the case of 5%Ni/CeZrO₂(0.5), the activity is found to be stable at ~ 80% CH₄ conversion, which is ~ 5% lower than that of 5%Ni/CeZrO₂(1.25). Pengpanich et al. [23] also reported that the catalytic activity was more dependent on structure and redox properties than the BET surface area. The reducing of chemicals and waste disposal cost in the preparation process is the benefit of this study, the catalyst with CTAB ratio of 0.5 was interested. The H₂/CO ratios obtained from these reactions with any of all catalysts are about 1, implying that only dry reforming reaction was performed.

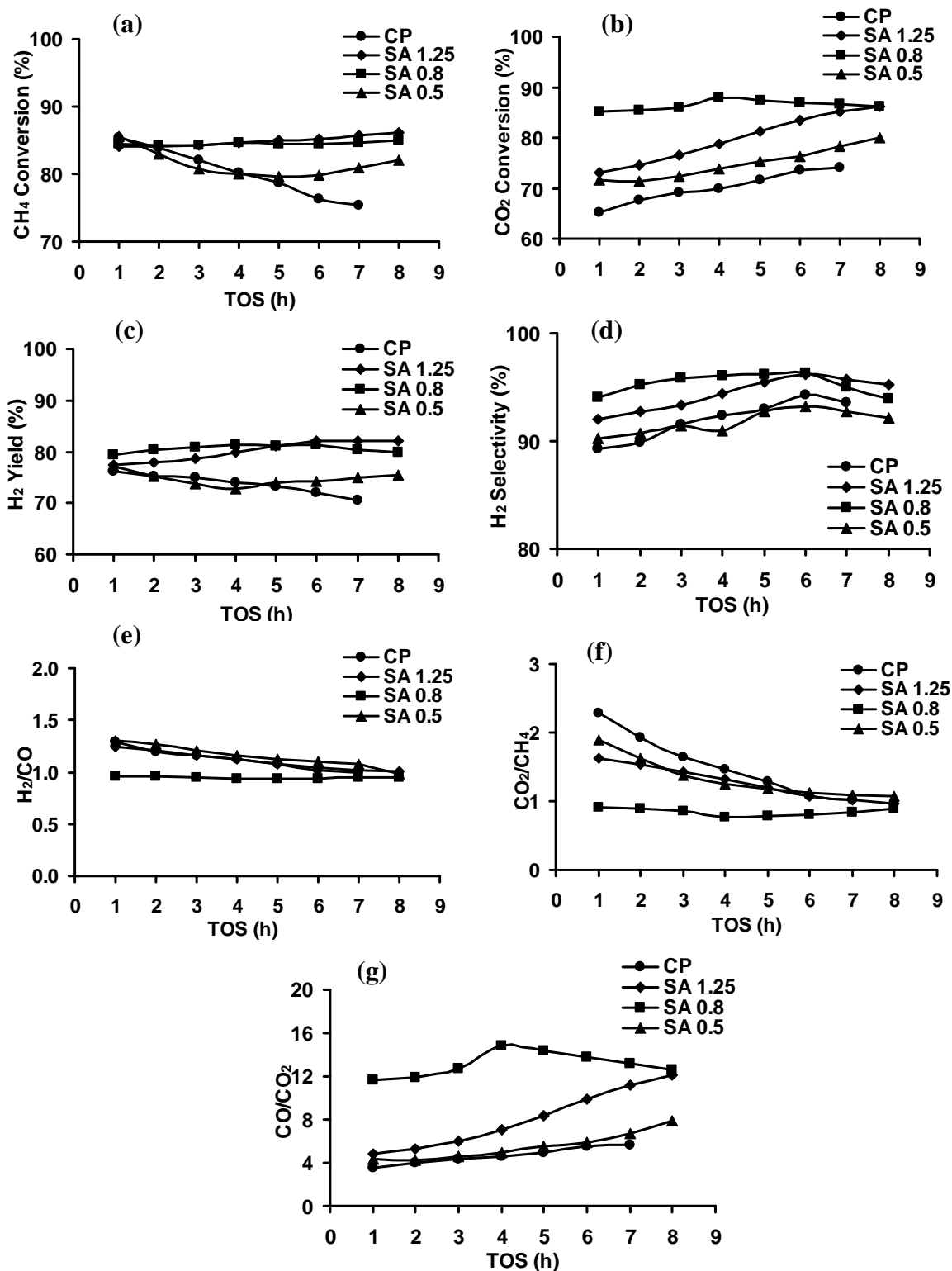


Figure 4.5 Performance evaluation of titled 5%Ni/Ce_{0.6}Zr_{0.4}O₂ catalysts for dry reforming reaction: (a) CH₄ conversion, (b) CO₂ conversion, (c) H₂ yield, (d) H₂ selectivity, (e) H/CO ratio, (f) CO₂/CH₄ ratio, and (g) CO/CO₂ ratio.

4.1.2.2 Effect of steam/methane ratio on the resultant catalytic activity

Li et al. [45] reported that the addition of small amount of steam to the dry reforming feed gas can significantly inhibit the catalyst deactivation, due to coking/carbon formation on the catalyst surface. The steam/methane ratio plays an important role in the overall steam assisted dry reforming process. Generally higher steam/methane ratios yield higher conversions, but excess steam over that required by the reaction stoichiometry is energetically unfavorable, and also dilutes the feed gas. On the contrary, the use of lower steam/methane ratios leads to a carbon deposition problem [37]. In this study, the influence of steam/methane ratio on the catalyst performance was investigated by varying the steam/methane ratios to $\text{H}_2\text{O}/\text{CH}_4 = 1$ and 0.625. The results obtained over 5%Ni/CeZrO₂(1.25) catalyst are showed in Figure 4.6.

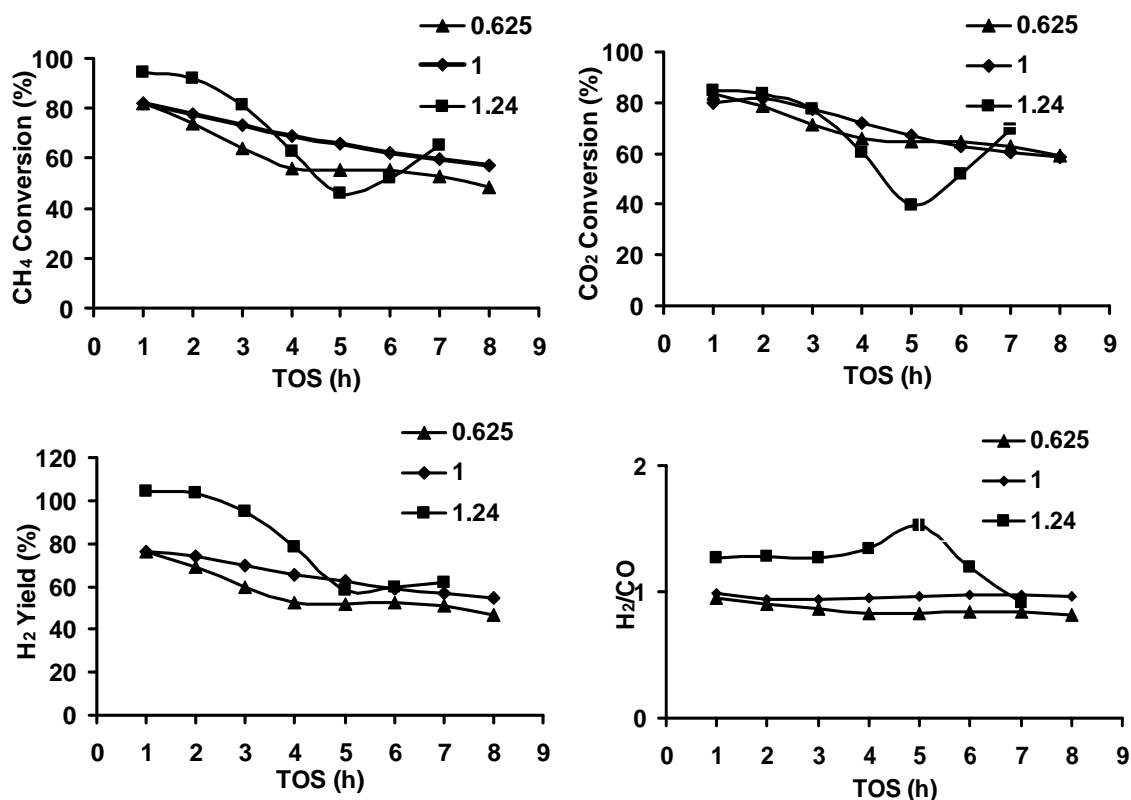


Figure 4.6 Influence of steam/methane ratio on the catalytic activity of titled 5Ni/Ce_{0.6}Zr_{0.4}O₂ CTAB 1.25 catalyst for dry reforming reaction at 800 °C in the presence of steam:—▲— $\text{H}_2\text{O}:\text{CH}_4:\text{CO}_2 = 0.625:1:1$ —◆— $\text{H}_2\text{O}:\text{CH}_4:\text{CO}_2:\text{N}_2 = 1:1:1$ and—■— $\text{H}_2\text{O}:\text{CH}_4:\text{CO}_2 = 1.24:1:1$.

The results indicate that the feed composed of stoichiometric amount of steam and methane ($\text{H}_2\text{O}:\text{CH}_4:\text{CO}_2 = 1:1:1$) yields relatively better results, than the feed with less or more than stoichiometric amount of steam ($\text{H}_2\text{O}:\text{CH}_4:\text{CO}_2 = 0.625:1:1$ or $1.24:1:1$). Therefore, subsequent tests involving steam were performed using the stoichiometric feed ratio ($\text{H}_2\text{O}:\text{CH}_4:\text{CO}_2 = 1:1:1$).

4.1.2.3. Effect of the addition of steam on the performance of NCZ catalysts for dry reforming of CH_4

In order to find out whether steam plays a similar role on the activity of other catalysts, the catalysts were screened under identical operating conditions (temperature: $800\text{ }^\circ\text{C}$; $\text{H}_2\text{O}:\text{CH}_4:\text{CO}_2 = 1:1:1$) over $5\%\text{Ni}/\text{CeZrO}_2(1.25)$, $5\%\text{Ni}/\text{CeZrO}_2(0.8)$ and $5\%\text{Ni}/\text{CeZrO}_2(0.5)$. The results obtained are shown in Figure 4.7.

The addition of the stoichiometric amount of steam to the typical dry reforming feed gas mixture not only resulted in the decrease in CH_4 and CO_2 conversions and overall activity, but also promoted deactivation. The CO_2 reforming reaction was predominant under the experiment conditions employed in the current study, while the steam reforming reaction was negligible. The above observation is confirmed by the obtained H_2/CO ratios which were ~ 1 . The addition of steam to the dry reforming feed gas induced the water-gas shift reaction ($\text{H}_2\text{O} + \text{CO} \rightleftharpoons \text{H}_2 + \text{CO}_2$) which resulted in the decrease of CO/CO_2 ratio in the product stream. These results are in good agreement with those reported by Raju et al. [43]. Thus, the obtained results indicate poor performance of the above tested catalysts for the CO_2 reforming of CH_4 reaction in the presence of steam.

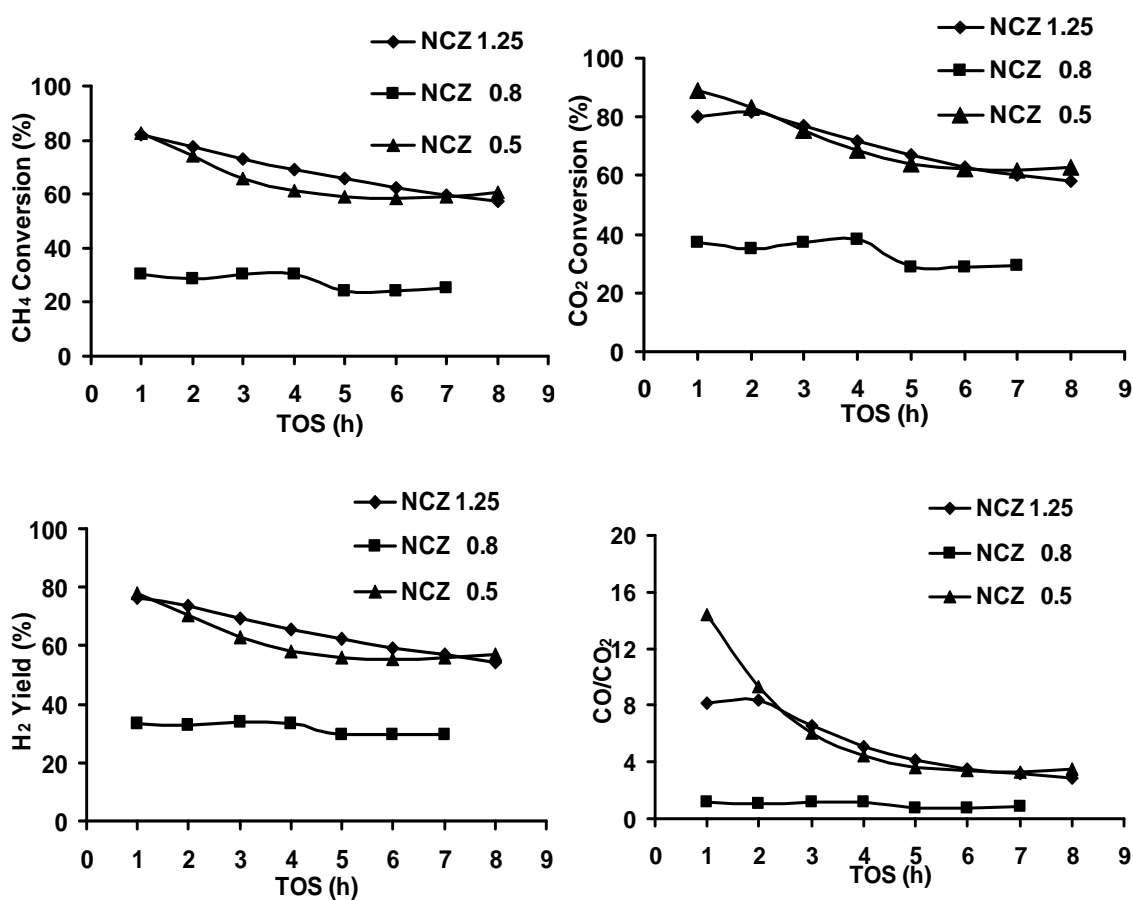


Figure 4.7 Screening of titled 5%Ni/Ce_{0.6}Zr_{0.4}O₂ catalysts for dry reforming reaction at 800 °C in the presence of steam (H₂O:CH₄:CO₂ = 1:1:1).

4.1.2.4 Effect of temperature on catalytic activity for typical dry reforming of CH₄

The influence of operating temperature on the catalytic performance over 5%Ni/CeZrO₂(1.25) catalyst for dry reforming reaction were studied by reducing the temperature from 800 °C to 700 °C and the results obtained are compared in Figure 4.8.

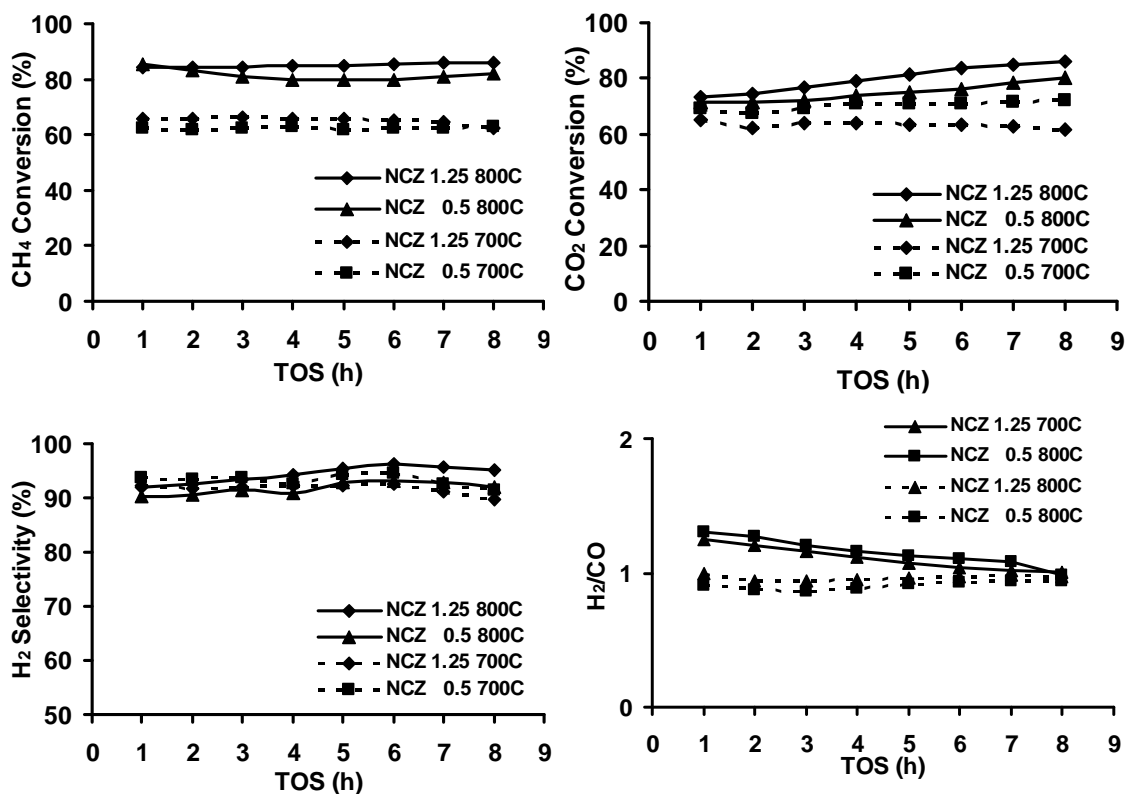


Figure 4.8 Influence of temperature on the catalytic activity of titled 5%Ni/CeZrO₂ (CTAB 0.5 and 1.25) catalyst for dry reforming reaction

As expected, the figure reveals a decline in catalytic activity at lower operating temperatures due to the endothermic nature of the reaction. On the whole, the performance of the 5%Ni/CeZrO₂(1.25) catalyst is found to be stable even at 700 °C operating temperature. On the basis of these results, it appears that it possible to employ 5%Ni/CeZrO₂ catalyst obtained by surfactant assisted route with higher CTAB/[Ce+Zr] molar ratio (1.25) even at an operating temperature as low as ~700 °C.

4.1.3 Carbon deposition results

The amount of carbon formation in the reaction at 700 and 800 °C was measured and the results are shown in Table 4.3

Table 4.3 The amount of carbon deposition in the reaction

Sample	Temp. (°C)	Steam	Carbon deposition (g/g cat.h)
Ni/CeZr co-ppt	800	W/O*	1.95
Ni/CeZr 1.25	800	W/O	1.90
Ni/CeZr 1.25	800	W/S**	0.81
Ni/CeZr 1.25	700	W/O	1.92
Ni/CeZr 1.25	700	W/S	0.26
Ni/CeZr 0.5	800	W/O	2.42
Ni/CeZr 0.5	800	W/S	0.53
Ni/CeZr 0.5	700	W/O	0.61
Ni/CeZr 0.5	700	W/S	0.28

*W/O = without steam, **W/S = with steam

There are a lot of carbons occurred in the reaction using catalysts prepared by co-precipitation method and surfactant-assisted templating route with CTAB ratio of 1.25 and 0.5 at 700 and 800 °C in the absence of steam. After the addition of steam in the feed gas, the carbon formation rates were significantly decreased. It indicates that the addition of steam in the feed gas can suppress carbon formation. The deposited carbon may be removed through gasification with steam [$\text{H}_2\text{O} + \text{C} (\text{s}) \rightarrow \text{CO} + \text{H}_2$] or carbon dioxide [$\text{CO}_2 + \text{C} (\text{s}) \rightarrow 2\text{CO}$] [37, 45].

4.1.4 The structure-activity relationships (SAR) of the catalysts

The results show a marked difference in activity and stability between the catalysts where the supports are prepared through the surfactant-assisted templating route and the one prepared by co-precipitation. It also shows a marked difference in activity and stability between the catalysts prepared by surfactant-assisted templating route but using different CTAB/(Ce+Zr) ratios. Also, the use of steam to assist the dry reforming process produced differences in terms of activity and stability. In order to elucidate the circumstances surrounding these differences, we have used the characterization results in conjunction with the activity/stability results to establish structure-activity relationships (SAR) for each catalyst system. This represents the correlation of the observed catalytic activity for dry reforming of CH₄ with the inherent textural, physico-chemical, and surface characteristics of the catalyst. These correlations are shown in Figure 4.9.

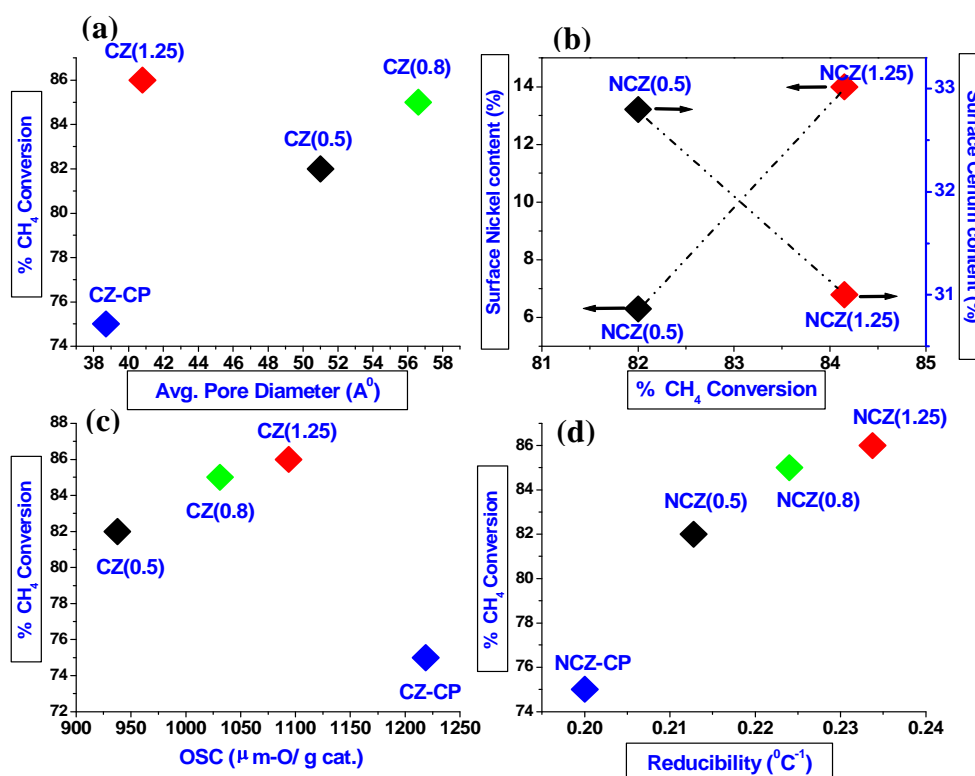


Figure 4.9 Structure/activity correlation plots for dry reforming of CH₄ reaction: (a) Activity vs. average pore diameter; (b) Surface cerium/nickel content vs. activity, (C) Activity vs. reducibility, and (D) Activity vs. OSC.

Figure 4.9 represents the various structure-activity correlation (SARs) plots generated in this study. The following parameters, namely, (1) oxygen storage capacity (OSC), (2) pore size, (3) surface cerium/nickel content, and (4) reducibility were used to establish the structure-activity relationships (SARs). The OSC values were obtained from thermo-gravimetric experiments as described earlier (Table 4.1) while the average pore diameter was obtained from the desorption branch of N₂-isotherm. On the other hand, the surface cerium/nickel content values were obtained from the wide survey scans of XPS analysis (Table 4.2), and the reducibility values were obtained from the TPR measurements (Figure 4.3), more specifically the T_{max} values pertaining to the reduction of NiO to Ni were used for calculating reducibility (where reducibility = $1/T_{\text{max}} * 100$). As the initial activity of all the catalysts for the typical dry reforming reaction were identical (figure 4.5), activity (% CH₄ conversion) observed at 8h operation was used to establish the structure/activity relationship (SARs).

Figure 4.9(a) presents the correlation plot of activity vs average pore diameter. As revealed from the plot, it is very explicit that pore size plays a significant role on the resultant activity. Wider pores allow easy access of reactant molecules to the active sites and also allow for the easy desorption of the product molecules thereby decreasing the contact time and enhancing the activity. The CeZrO₂(0.8) support (~ 56.6 Å) exhibits pores, which are ~5 Å wider than the pores of CZ(0.5) support (~ 51 Å), and ~18 Å wider than the pores of CeZrO₂(CP) support (~ 51 Å), leading to an increment in activity by ~ 3 mol.% and ~ 10 mol.% respectively. The CeZrO₂(1.25) support with average pore diameter ~ 40.8 Å appears to be an outlier in the current plot. The correlation between surface cerium/nickel contents vs. catalyst activity is plotted in figure 4.9(b). As is evident from figure 4.9(b), the catalyst performance improves with increasing surface nickel content and decreasing surface cerium content, respectively. The reason is that nickel is the active component and forms an integral part of the active sites. Thus, a higher surface nickel content implies a higher active site density per unit surface area. Hence, the improvement or enhancement in activity and stability with surface nickel content. The other aspect is that of surface cerium content. As cerium is the redox component in the catalyst formulation, it is generally accepted that bulk cerium plays a vital role in regulating

the bulk-to-surface oxygen transport functionalities (OTC) and oxygen buffer capacity (OBC). Accordingly, a catalyst formulation with higher bulk cerium content (\cong lower surface cerium content) will possess higher OTC/OBC and will yield better activity/stability. The relationship between catalyst reducibility and activity is presented in figure 4.9(c). As expected the activity trends show a linear relationship with the reducibility, which means that highly reducible catalysts perform better because their redox ability is enhanced. Among the various catalysts tested, the reducibility trend observed was $5\%Ni/CeZrO_2(1.25) > 5\%Ni/CeZrO_2(0.8) > 5\%Ni/CeZrO_2(0.5) > 5\%Ni/CeZrO_2(CP)$, which is also the trend of their relative catalytic performance. Figure 4.9(d) represents the correlation plot of activity vs. OSC. An increase in OSC leads to an improvement in the resultant catalytic activity; however, there is an outlier in this plot too. Among the different catalyst supports tested, $CeZrO_2(CP)$ exhibits unusually higher OSC; however, the performance of the catalyst prepared using the above support is unsatisfactory. As noted in the figures 4.9 (a-d), there are a few outliers. The presence of these outliers throws light on the complex nature of the heterogeneous catalyst used for dry reforming reaction. It is very important to mention here that although there were many concrete correlations between the observed catalytic activity and most of the characteristics, it would be best to consider that a right combination of many relevant characteristics is responsible for the resultant catalyst activity, and that the percentage contribution from each characteristic is not necessarily the same. Based on our results, it is observed that if any of the desired characteristics in a catalyst is absent, it leads to poor performance or deactivation of the catalyst. From the present investigation, it is quite apparent that reasonable OSC, reasonable surface area, reasonable pore size, high reducibility, lower surface cerium content (redox component) and higher surface nickel content (active component) lead to excellent catalytic activity for dry reforming process. An example is $5\%Ni/CeZrO_2(1.25)$ which exhibits excellent performance in dry reforming reaction. The superior performance of the above catalyst can be explained in terms of high reducibility, higher surface nickel content, lower surface cerium content, and reasonably higher surface area and OSC.

4.2 Ternary mixed oxide catalyst

4.2.1 Characteristics of the supports and catalysts

4.2.1.1 BET surface area

The textural characteristics of a few selected ternary mixed oxide supports and nickel-impregnated catalysts are summarized in Table 4.4. To emphasize the role played by the third metal ion, the textural characteristics of the CeZrO₂ binary oxide support (CTAB/[Ce+Zr] = 0.5) and the corresponding Ni-impregnated catalyst are also shown in Table 4.4.

Table 4.4 Textural characteristics of ternary mixed oxide supports and catalysts calcined at 650°C for 3 h.

Sample	BET SA (m ² g ⁻¹)	PV (cc g ⁻¹)	Avg.Pore Diameter (Å)	PV*/ BET SA** (10 ⁻⁹ m)
Ce _{0.6} Zr _{0.4} O ₂	232.0	0.38	51.0	1.63
5%Ni/Ce _{0.6} Zr _{0.4} O ₂	215.1	0.32	51.3	1.49
CeZrCaO ₂	145.5	0.26	53.8	1.75
5%Ni/CeZrCaO ₂	103.8	0.19	57.7	1.83
CeZrPrO ₂	174.8	0.27	46.0	1.53
5%Ni/CeZrPrO ₂	123.2	0.21	52.9	1.66
CeZrSmO ₂	182.1	0.26	42.6	1.42

*PV= Pore Volume, **SA = Surface area

From table 4.4, it was found that CeZrO₂ binary oxide support and corresponding 5%Ni/CeZrO₂ catalyst samples have larger BET surface area and pore volume, when compare to that of any ternary mixed support or catalyst characterized in this study. Similar findings were reported by Mikulova et al. [53] and Rossignol et

al. [71], who reported that addition of small amounts of Pr to CeZrO₂ oxides yields very similar BET area as that of CeZrO₂ binary oxide, while increasing the Pr content in the CeZrO₂ system results in decrease in the BET surface area, which was attributed to the formation and segregation of Pr₆O₁₁ phase. An et al. [69] also reported that the BET surface area of CeZrO₂ was slightly decreased after doping with Ca. Ca²⁺ has larger ionic radius (0.111 nm) than Ce⁴⁺ (0.097 nm), and may thus, expand the lattice. The cell expansion/shrink caused by doping may produce some defects in the lattice. In another study, Atribak et al. [80] reported that the CeZrYO₂ ternary series presents more or less constant BET values comparable with CeZrO₂. The results further suggested that the BET area depends on the synthesis conditions and Zr⁴⁺ addition and not on yttrium loading. Interestingly, the BET surface area values observed in the current study are reasonably higher than that reported in literature [53, 71, 69, 81], which can be attributed to the unique preparation route employed.

4.2.1.2 Oxygen storage capacity (OSC)

The OSC experiments were performed using TGA and the results are shown in Table 4.5.

Table 4.5 Oxygen storage capacity of ternary mixed oxide supports calcined at 650°C for 3 h.

Sample	OSC (μ.mol-O/g cat.)
CeZrO ₂	937.50
CeZrAlO ₂	1000.0
CeZrBaO ₂	906.2
CeZrCaO ₂	1156.2
CeZrHfO ₂	875.0
CeZrLaO ₂	1093.7
CeZrPrO ₂	968.7
CeZrSmO ₂	1156.2
CeZrSrO ₂	1500.0
CeZrTbO ₂	750.0
CeZrYO ₂	1031.2

The OSC values of CeZrO₂ doped with Al, Ca, La, Pr, Sm, Sr, and Y are higher than that of binary oxide CeZrO₂, indicating that the doping with any of the above rare earth metal ions enhances the OSC, due to the generation of additional oxygen vacancies. Similar results have been reported by Li et al, [47] in the case of CeZrO₂ binary oxide doped with Y³⁺ and La³⁺, who attributed the increase in OSC to the generation of additional oxygen vacancies due to the incorporation of Y³⁺ and La³⁺ ions into the CeZrO₂ lattice. In another study, Rossignol et al., [71] and Mikulova et al., [53] reported that Pr addition induces an increase of the OSC due to the creation of anionic vacancies, due to the replacement of Ce cation with substituting Pr cation, which also possesses a highly facile Pr³⁺/Pr⁴⁺ redox couple. In the case of Sr doping, Wang et al. [72] reported that the OSC of Pd/CeZrO₂ catalyst was improved by doping with Sr, which in turn improves the interaction between Pd and Ce, and promotes the reducibility and thermal stability of catalysts. On the contrary, CeZrO₂ doped with Ba, Hf, and Tb exhibit lower OSC values. A few literature reports state that the redox (OSC) properties of a given sample are independent of their BET surface areas [76].

4.2.1.3 X-ray diffraction

The XRD patterns of CeO_2 , CeZrO_2 and CeZrMO_2 are shown in Figure 4.10

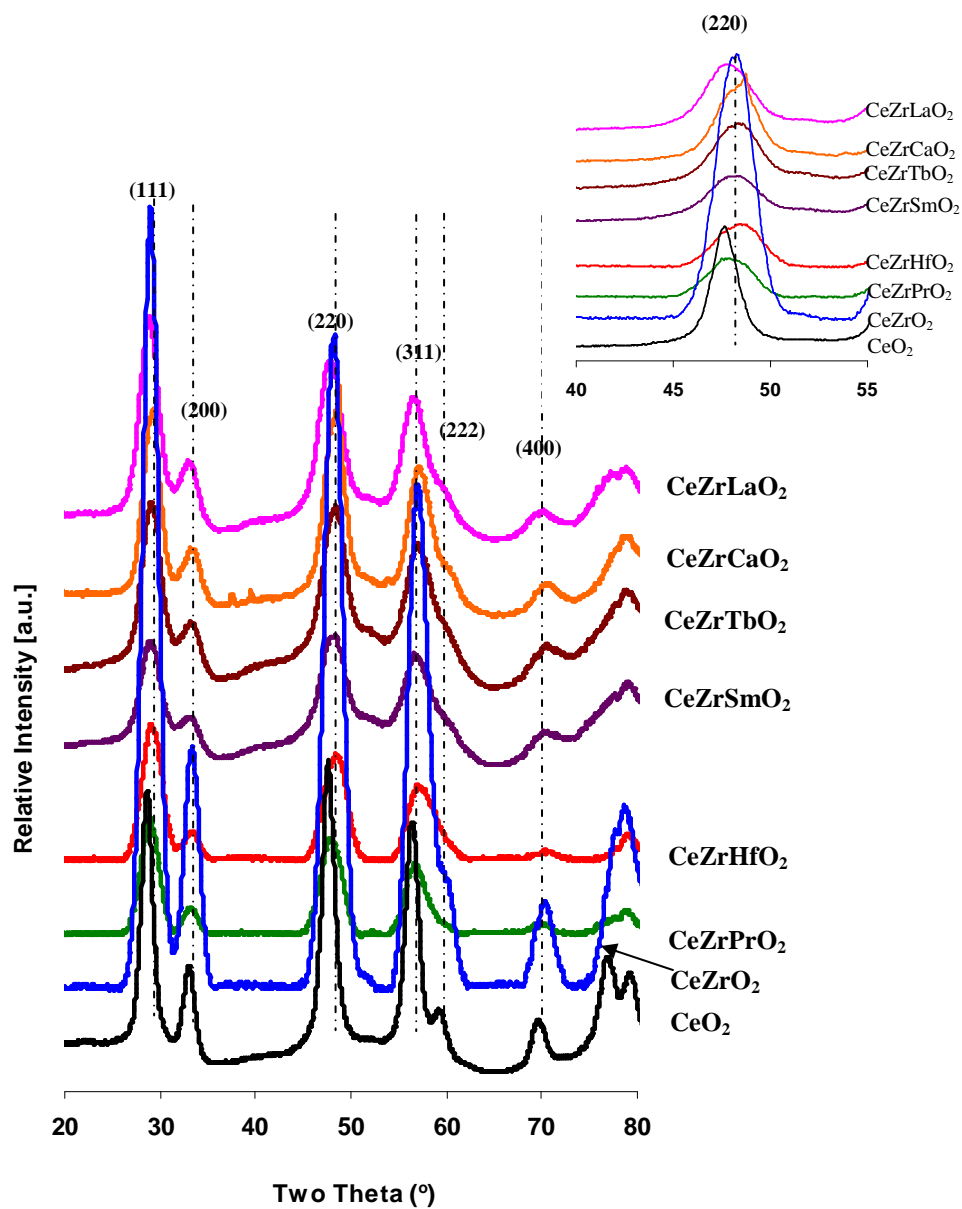


Figure 4.10 X-ray diffractograms of the ternary mixed oxide supports calcined at 650 °C.

From Figure 4.10, it can be seen that all the ternary mixed oxide supports analyzed in the current study, exhibit exactly similar XRD pattern as exhibited by the CeZrO_2 binary oxides, indicating the presence of cubic crystal structure. All the diffraction patterns show the characteristic peaks for fluorite-type structures. The phase segregation of the doped metal oxides such as ZrO_2 , CaO , La_2O_3 , HfO_2 , Pr_2O_3 , Sm_2O_3 and Tb_2O_3 was not detected, indicating that Zr^{4+} and doped metal ions have been incorporated into the CeO_2 lattice and formed a solid solution with the fluorite structure. Interestingly, the addition of dopant ions does not alter the crystal structure of CeZrO_2 . The dopant metal ion having larger ionic radii than that of Ce^{4+} will expand the lattice and the diffraction peaks will shift to the lower two-theta values. On the other hand, the dopant metal ion with smaller ionic radii than that of Ce^{4+} (0.97 Å) will shrink the lattice and the diffraction peaks will shift to the higher two-theta values. In comparison with CeZrO_2 , the diffraction peaks of doped CeZrO_2 do not shift markedly due to the ionic radius of dopants (Ca^{2+} 0.111, Sm^{3+} 0.108, Pr^{4+} 0.99, and Tb^{4+} 0.88 nm) correspond to that of Ce^{4+} (0.097 nm). The diffraction peaks of CeZrLaO_2 shift to the higher degree due to the largest ionic radius of La^{3+} (0.118 nm). Similar findings were reported by Hu et al. [73] for the $\text{Ce}_{0.6}\text{Zr}_{0.3}\text{La}_{0.1}\text{O}_2$ solid solution.

4.2.1.4 Raman spectroscopy

The Raman spectra of some ternary mixed oxide supports are shown in Figure 4.11.

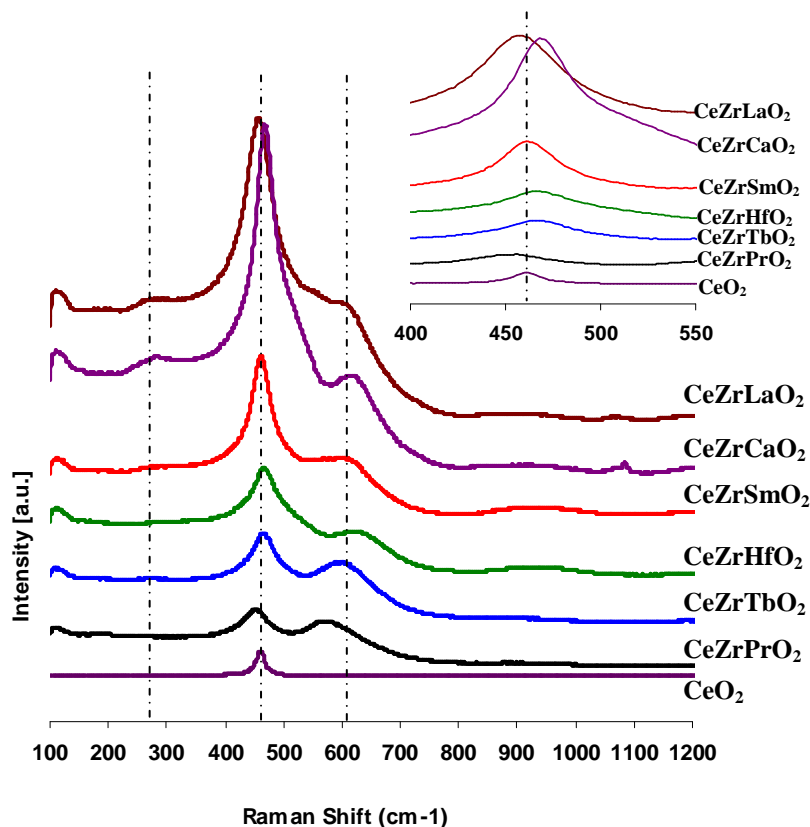


Figure 4.11 Raman spectra of the ternary mixed oxide supports.

The Raman spectra of all CeZrMO_2 supports further support XRD result because there is a single sharp intense absorption peak in the range of $460\text{--}470\text{ cm}^{-1}$ was attributed to the T_{2g} Raman active mode of a cubic fluorite structured materials [71, 74, 78]. After doping La^{3+} ion with larger ion radius, the lattice parameter increase and the T_{2g} band centered at low frequency due to cell expand which is consistent with the increased cell parameter observed by XRD. While doping Sm^{4+} or Pr^{4+} , whose ion radius correspond to that of Ce^{4+} the T_{2g} bands do not shift. Tb^{4+} or Hf^{4+} whose ion radius are smaller than that of Ce^{4+} , the lattice parameters decreased and the T_{2g} band centered at high frequency due to cell shrink. [69, 74] The minor peaks were observed at about $580\text{--}620\text{ cm}^{-1}$ which was attributed to the presence of oxygen vacancies. This would suggest that the solid can possess relatively high oxygen mobility. In addition, the peak at 285 cm^{-1} was observed in these supports,

which should be attributed to the displacement of the oxygen atoms from their ideal fluorite lattice positions.

4.2.1.5 Temperature program reduction

The reducibility of the supports and catalysts were studied by TPR under H_2 flow in the range from 25 to 1100 °C. The H_2 response as a function of temperature is illustrated in Figure 4.12 and 4.13.

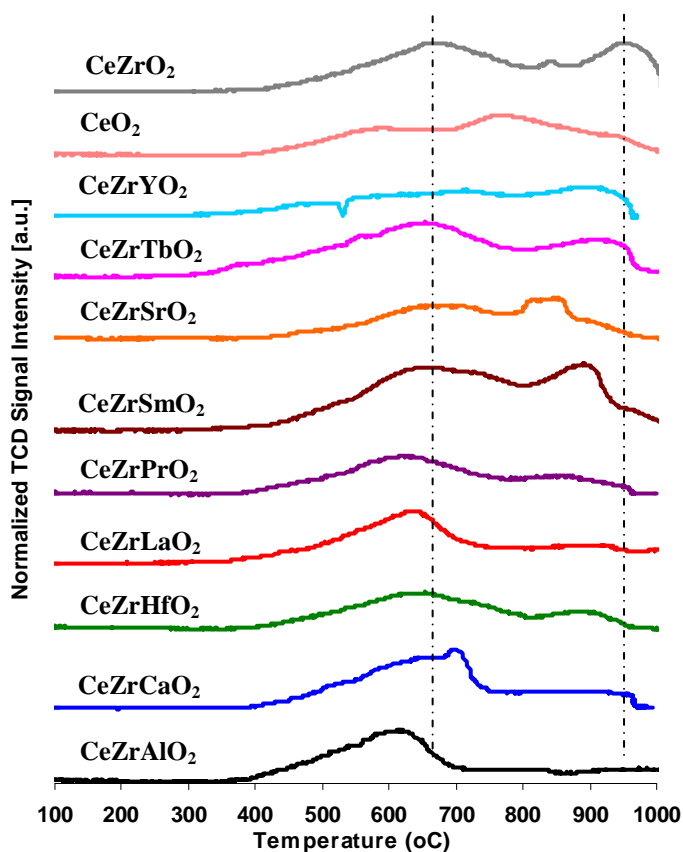


Figure 4.12 TPR profiles of the ternary mixed oxide supports.

From Figure 4.12, the TPR profiles of $CeZrMO_2$ are almost the same as that of $CeZrO_2$, indicating that the homogeneous mixed oxides were formed after the third metals doping. This result is well consistent with the XRD result mentioned above. Almost $CeZrMO_2$ supports showed two reduction peaks. The one reduction peak at

low temperature was ascribed to the reduction of the surface oxygen species of CeO_2 , and the other broad peak at higher temperature was ascribed to the bulk of oxygen species of CeO_2 . Pure ZrO_2 does not show any reduction peak below $900\text{ }^\circ\text{C}$. Therefore, the reduction peak of CeZrMO_2 may be ascribed to the reduction of highly dispersed CeO_2 in Ce-ZrO_2 solid solution. In addition, we can see that both of surface and bulk reduction peaks of doped CeZrO_2 supports shift to lower temperature after the addition some metal such as Y, Pr, Tb, La, and Al, indicating that the addition of these metals increases the reducibility of CeZrO_2 solid solution. These results agree with the result of Kang et al. [81]. They reported that Pr and Tb doped CeZrO_2 has the better OSC property than CeMO_2 , ZrMO_2 (where $M = \text{Pr}$ and Tb), and CeZrO_2 . Wu et al. [82] also reported that the high temperature reduction peaks of CeZrPrO_2 and CeZrYO_2 shifts to the lower temperature comparing to CeZrO_2 . The redox reaction between Pr^{4+} and Pr^{3+} ions is easier than that between Ce^{4+} and Ce^{3+} . Therefore, the migration of bulk oxygen species in CeZrPrO_2 is accelerated. In case of CeZrYO_2 , every two Y^{3+} ions hold the positions of Ce^{4+} ions in CeZrYO_2 , one oxygen vacancy is formed subsequently. The increasing oxygen vacancies are propitious to the migration of the lattice oxygen species, and the redox property of solid solutions is improved. In addition, Markaryan et al. [83] and Atribak et al. [80] also reported that the addition of Y_2O_3 could lead to higher oxygen mobility and therefore the bulk reduction peak shifted down comparing to CeZrO_2 .

In case of Sr, Sm, and Hf doped CeZrO_2 , the reduction peak at high temperature shift to lower temperature, indicating that the reduction of oxygen in bulk CeO_2 was easier. On the other hand, both of surface and bulk reduction peaks of Ca doped CeZrO_2 shift to higher temperature comparing to CeZrO_2 , resulting from the strong interaction between metal ions in the mixed oxide.

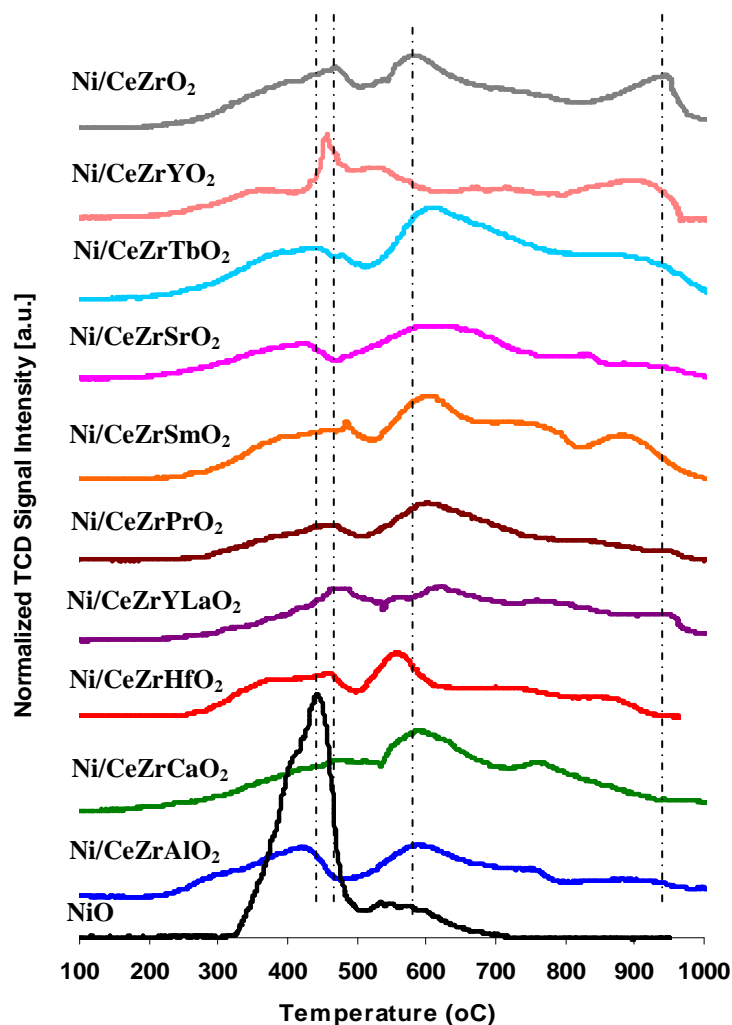


Figure 4.13 TPR profiles of Ni-based catalysts supported on ternary mixed oxide.

From Figure 4.13, the 5%Ni/CeZrMO₂ catalysts exhibited a reduction peak at about 440 °C is associated with the reduction of NiO to Ni⁰ and other peaks at the higher temperature are associated with the reduction of Ce⁺⁴ to Ce⁺³ were obtained. In addition, the peak corresponding to 5%Ni/CeZrMO₂ for almost of the Ni-based catalysts shifted to the lower temperature, indicating that Ni incorporation into the CeZrO₂ makes ceria more reducible, which helps produce mobile oxygen during the reforming reaction. This result agrees with the report of Dong et al [15]. In case of 5%Ni/CeZrHfO₂, the reduction peak, about 350 °C, of NiO shifted to the lower temperature, indicating that Hf introduction makes NiO more reducible. The other peak at about 550 °C was assigned to the reduction of HfO₂.

4.1.1.6 X-ray photoelectron spectroscopy

In order to study the effect of doping elements on surface properties of CeZrMO_2 solid solution, the XPS analysis was performed. The binding energy data for Ce3d, Zr3d, O1s, and C1s are shown in Figure 4.14

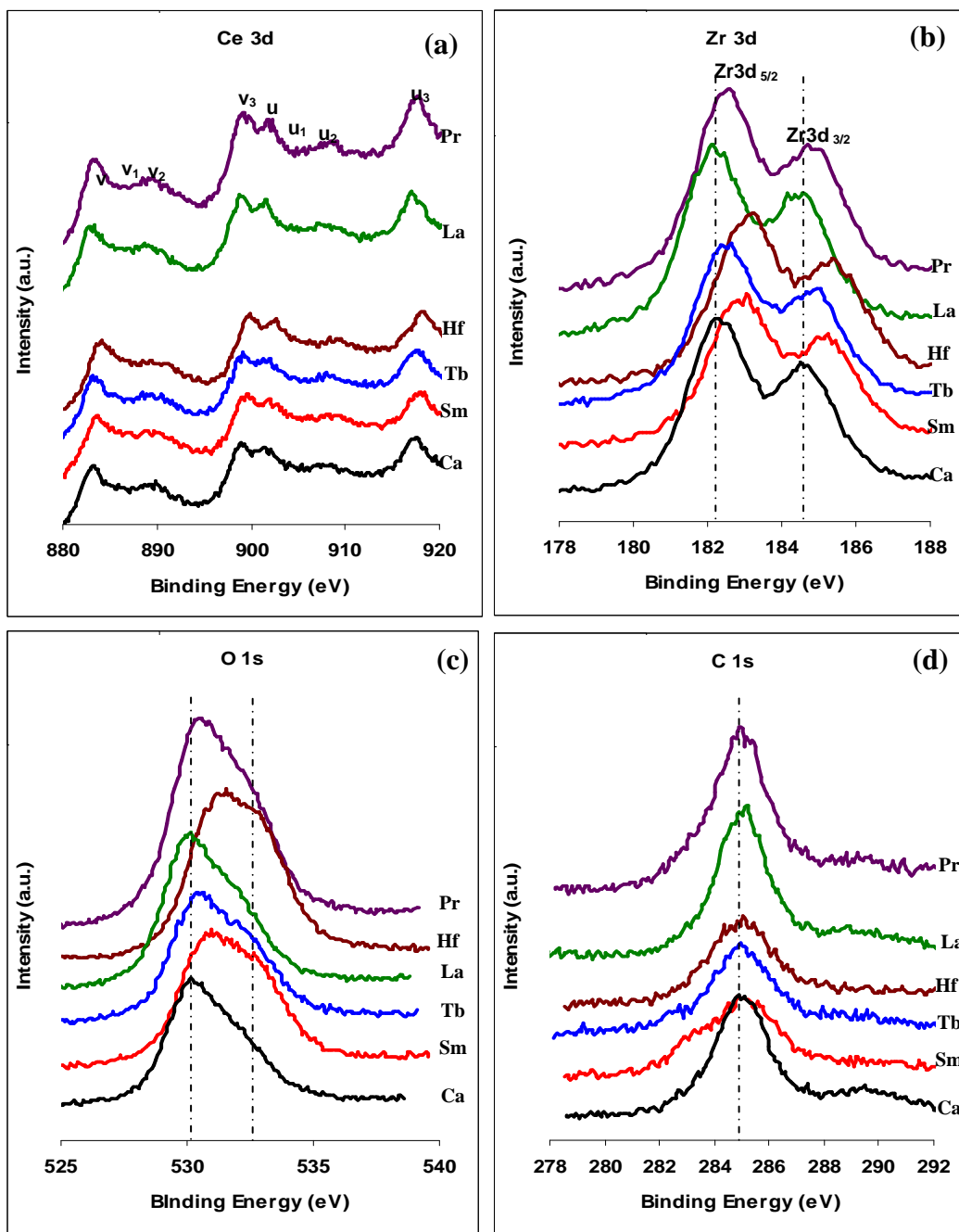


Figure 4.14 XPS spectra of CeZrMO_2 for (a) Ce3d, (b) Zr3d, (c) O1s, and (d) C1s.

As shown in Figure 4.14 (a), all the supports exhibited the similar spectra. The curves of Ce3d spectra are composed of eight speaks corresponding to four pairs of spin-orbit doublets, u and v correspond to the features of $3d_{3/2}$ and $3d_{5/2}$, respectively. The Ce3d spectrum correspond to three main features of $3d_{5/2}$ at about 882.58-883.55 eV (v_1), 888.23-888.58 eV (v_2) and 899.55-898.63 eV (v_3) arise from $Ce^{4+}3d_{5/2}$ and three features of $3d_{3/2}$ at about 900.58-901.95 eV (u_1), 907.15-908.35 eV (u_2) and 916.75-917.55 eV (u_3) arise from $Ce^{4+}3d_{3/2}$. The six peaks correspond to unique photoelectron features of Ce^{4+} state [49,62]. The specific Ce^{3+} features are present at approximately 884.18-885.95 eV (v_1) and 904.23-905.56 eV (u_1) in the Ce3d region, and these signals are considered as fingerprints indicating the existence of Ce^{+3} ion. The low intensity peaks of v_1 and u_1 indicated that Ce mainly existed in the form of Ce^{4+} on the surface of samples. Fig. 4.14 (b) shows the binding energy of the Zr3d photoelectron peaks at about 182.08-183.06 eV and 184.38-185.26 eV for Zr $3d_{5/2}$ and Zr $3d_{3/2}$ lines, respectively. The binding energies of Zr $3d_{5/2}$ and Zr $3d_{3/2}$ lines in pure ZrO $_2$ are 182.2 and 184.6 eV, respectively, indicating that ZrO $_2$ with an oxidation state of 4+ presence on the surface [52]. Figure 4.14 (c) shows the O1s spectra of the samples. There are two O1s peaks at about about 529.93-531.25 eV and 531.03-532.55 eV. The signal at lower binding energy was assigned to surface lattice oxygen represents the O1s ionization for oxygen associated with CeZrMO $_2$ mixed oxides, while the signal at higher binding energy to adsorbed oxygen species such as O $^-$, O $_2^{2-}$, and O $^{2-}$ of adsorbed molecular oxygen, water or -OH species [52, 86]. It can be seen that Pr, Tb, Hf and Sm doped samples showed the higher adsorbed oxygen amount than that of La and Ca doped samples, which implies these dopants can increase the amount of adsorbed oxygen on the surface of CeZrMO $_2$ solid solution. Fig. 4.14 (d) shows the binding energy of the C1s photoelectron peaks. The predominant peak at about 285 eV, used as standard for BE calibration, is due to the presence of C-C bonds on surface [84].

The binding energy data for Ca2p, Hf4f, La3d, Pr3d, Sm3d, and Tb4d are shown in Figure 4.15

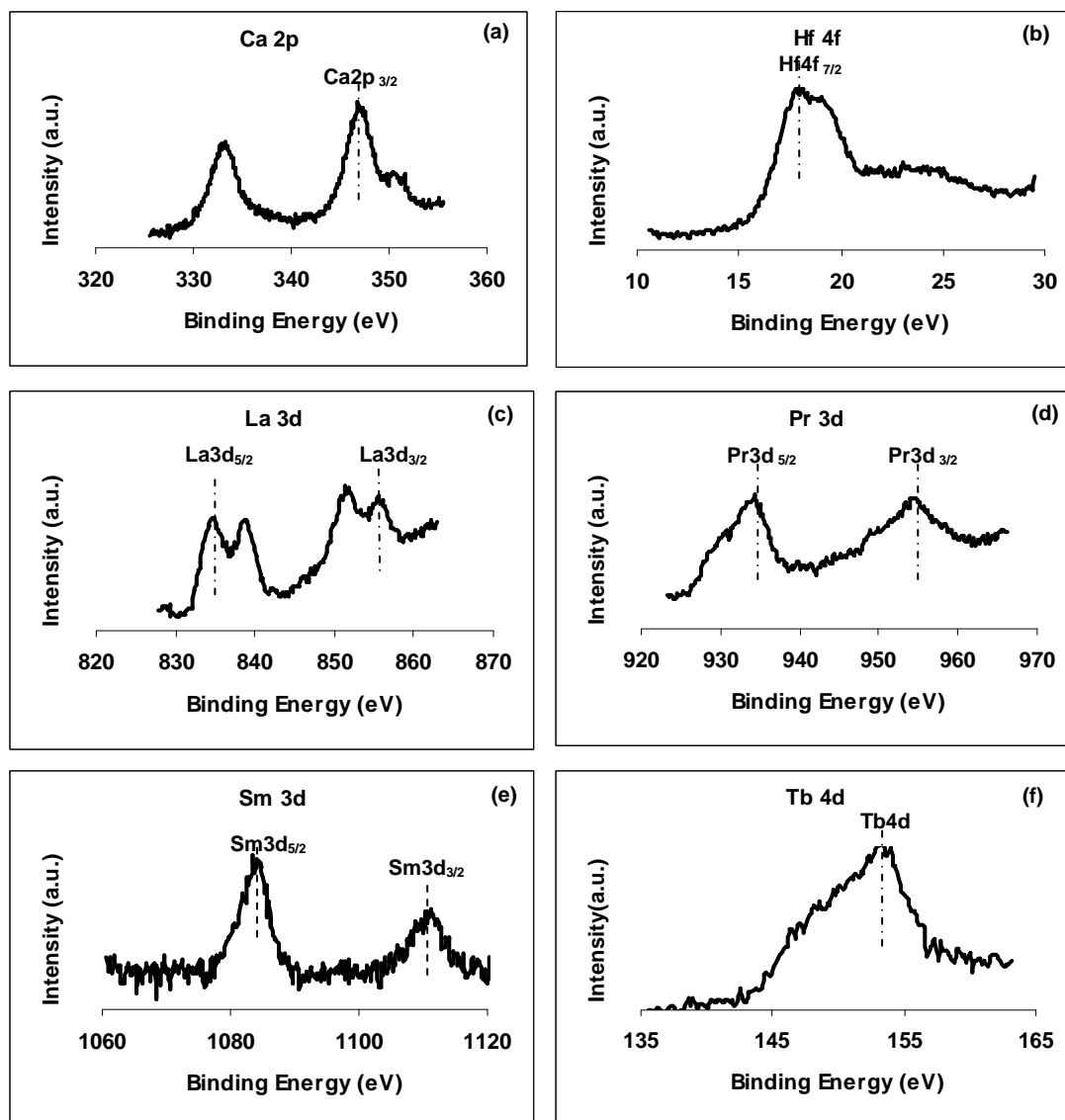
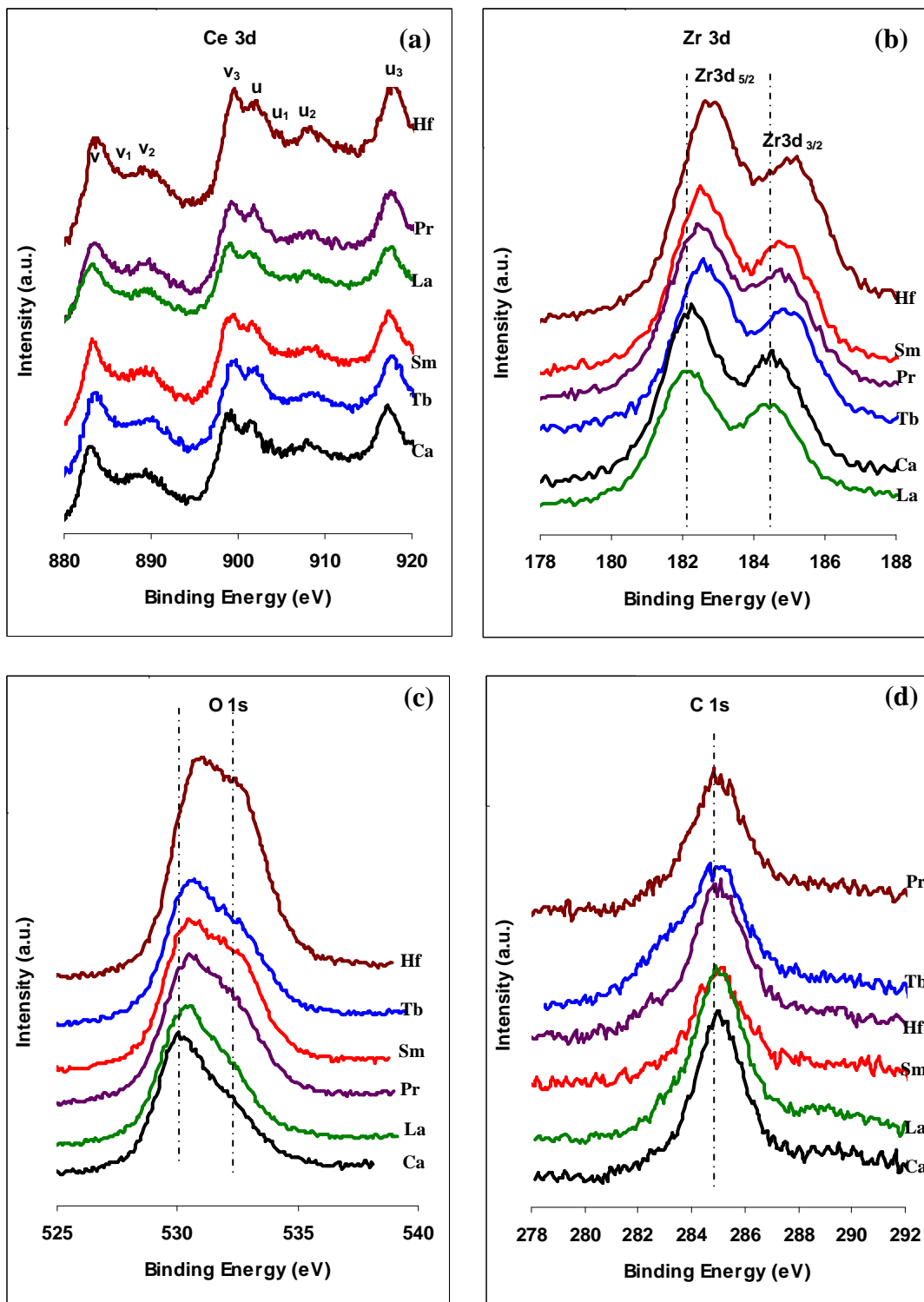


Figure 4.15 XPS spectra of CeZrMO₂ for (a) Ca2p, (b) Hf4f, (c) La3d, (d) Pr3d, (e) Sm3d and (f) Tb4d.

Figure 4.15 (a) shows the binding energy of the Ca2p photoelectron peaks at about 346.78 eV for Ca2p_{3/2} lines, indicating the presence of Ca²⁺ on the surface of catalysts [39]. According to the results of Grosvanor et al. [85], they reported that the Hf4f_{7/2} binding energy for HfO₂ is 16.7 eV. Figure 4.15 (b) shows the binding energy of the Hf4f at about 838.43 for Hf4f_{7/2}, indicating the presence of Hf⁴⁺ on the surface of catalysts. Figure 4.15 (c) shows the binding energy of the La3d photoelectron peaks at about 838.43 for Zr3d_{5/2} and 855.23 eV for Zr3d_{3/2}, indicating the presence of La³⁺ on the surface of catalysts. This similar result also reported by Perkins et al. [86]. They assigned the photoelectron peak at 837.9±0.3 eV for La3d_{5/2} and 854.8±0.4 eV for La3d_{3/2}. The Pr3d spectra are shown in Figure 4.15 (d), two sets of spin-orbit multiples are observed at the binding energies of about 953.40 and 934.0 eV, which represent the 3d_{3/2} and 3d_{5/2} of Pr, respectively. According to the results of Narula et al., Matsumura et al., Sarma and Rao which reported by He et al. [87], they assign the signals at about 933.9, 953.5, and 966.4 eV to Pr⁴⁺ and the signals at about 929.5, 949.8, and 973.2 eV to Pr³⁺. The low intensity peaks of Pr³⁺ indicated that Pr mainly existed in the form of Pr⁴⁺ on the surface of samples. From the results of Grosvanor et al. [88], the two Sm3d peaks were assigned as 1080 eV for Sm3d_{5/2} and 1110 eV for Sm3d_{3/2}. Fig. 4.15 (e) shows the binding energy of the Sm3d at about 1110.36 eV for Zr3d_{5/2} and 1083.56 eV for Zr3d_{3/2}, indicating the presence of Sm³⁺ on the surface of catalysts. The signals at 149.3 eV were assigned to the characteristic feature of Tb³⁺ and the signals at 156.9 and 164.5 eV to Tb⁴⁺ [52]. Figure 4.15 (f) shows the Tb4d spectra of the doped sample. It can be seen that Tb are mainly present in Tb⁴⁺ oxidation state on the surface at the binding energy 152.75 eV. This result is agreed with the result of Jia et al [89].

The binding energy data for Ce3d, Zr3d, O1s, C1s, and Ni2p of 55Ni/CeZrMO₂ was shown in Figure 4.16.



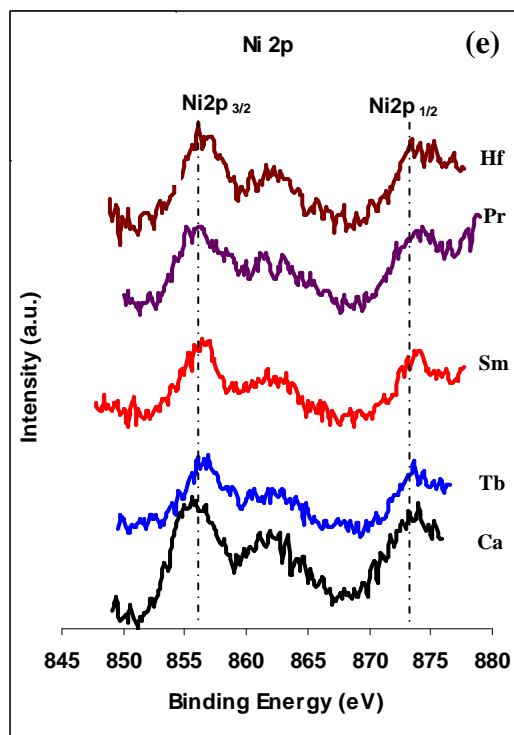


Figure 4.16 XPS spectra of CeZrMO₂ for (a) Ce3d, (b) Zr3d, (c) O1s, (d) C1s, and (e) Ni2p.

As shown in Figures 4.16 (a), 4.16 (b), 4.16 (c) and 4.16 (d), all the catalysts exhibited the similar spectra as the supports. The Ce⁴⁺ and Zr⁴⁺ are mainly existed on the surface of samples. Figure 4.16 (c) shows the O1s spectra of the samples. The surface lattice oxygen and adsorbed oxygen were showed in O1s spectra of all catalysts, which imply that these dopants can increase the amount of adsorbed oxygen on the surface of 5%Ni/CeZrMO₂ solid solution. The C1s photoelectron peaks at 285 eV were used as standard for BE calibration. Fig. 4.16 (e) shows the binding energy of the Ni2p photoelectron peaks at about 855.17-856.13 eV for Ni2p_{3/2} lines, indicating the presence of Ni²⁺ (BE=855 eV) on the surface of catalysts [39].

The binding energy data for Ca2p, Hf4f, La3d, Pr3d, Sm3d, and Tb4d are shown in Figure 4.17

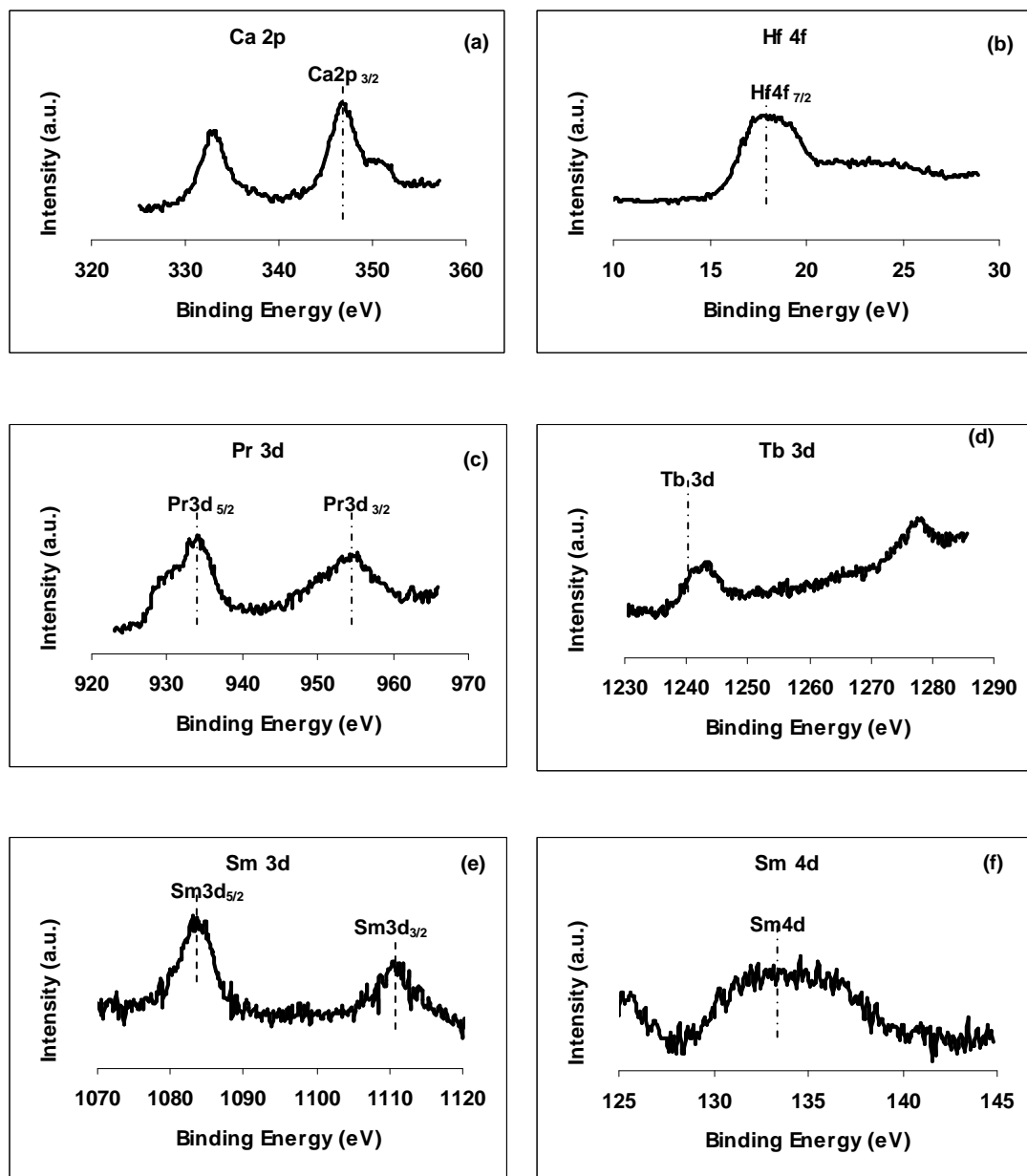


Figure 4.17 XPS spectra of Ni/CeZrMO₂ for (a) Ca2p, (b) Hf4f, (c) Pr3d, (d) Tb3d, (e) Sm3d and (f) Sm4d.

Figures 4.17 (a), 4.17 (b), 4.17 (c) show the binding energy of the Ca2p, Hf4f, and Pr3d photoelectron peaks, which indicating Ca²⁺, Hf⁴⁺, Pr⁴⁺, and Tb⁴⁺ were presented on the surface of the catalysts. These results were similar as the results of the supports.

According to the results of Fan et al. [52], the Tb3d peaks were assigned as 1241.6 eV correspond to the characteristic feature of Tb³⁺ Figure 4.17 (d) shows Tb3d spectra at the binding energy 1241.7 eV, indicating that Tb³⁺ was presented on the surface of the catalyst.

Figures 4.17 (e) and 4.16 (f) shows the binding energy of the Sm3d and Sm4d. According to the results of Ohno et al. [90], the Sm4d peak at the binding energy 125-142 eV was assigned for Sm³⁺. This result confirms the presence of Sm³⁺ on the surface of catalysts as the result from Sm3d spectra.

4.2.2 Catalytic performance

4.2.2.1 Effect of doped metals on catalytic performance of 5%Ni/CeZrMO₂ for typical dry reforming of CH₄

The screening of the various 5%Ni/CeZrMO₂ (M = Al, Ba, Ca, Hf, La, Pr, Sm, Sr, Tb, and Y) catalyst formulations was carried out for dry reforming of methane at 800 °C. The comparative results thus obtained are shown in Figure 4.18

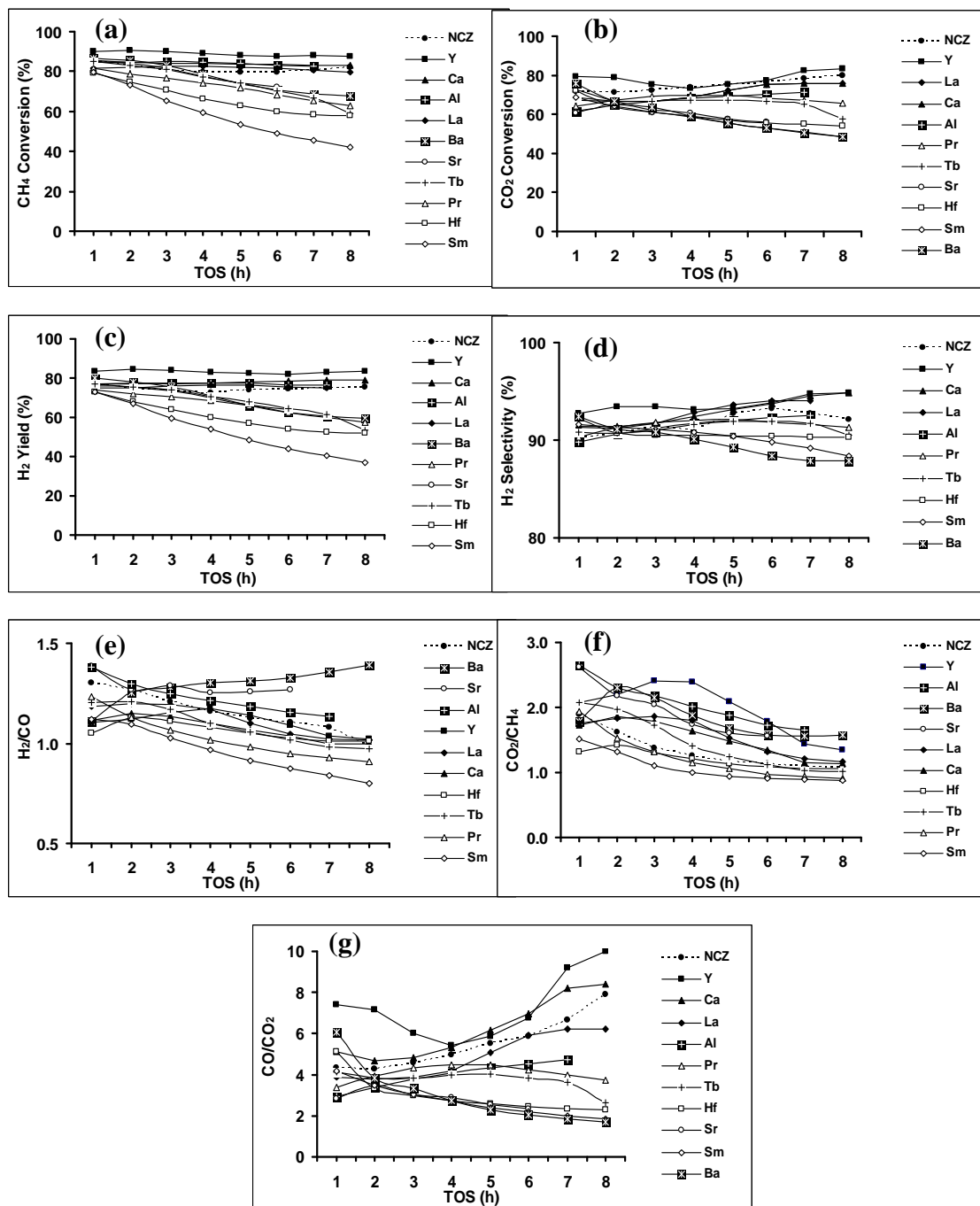


Figure 4.18 Performance evaluation of titled 5%Ni/CeZrMO₂ catalysts for dry reforming reaction: (a) CH₄ conversion, (b) CO₂ conversion, (c) H₂ yield, (d) H₂ selectivity, (e) H₂/CO ratio, (f) CO₂/CH₄ ratio, and (g) CO/CO₂ ratio.

Figures 4.18 (a) and 4.18 (b) show a plot of CH₄ and CO₂ conversion versus time on stream. It was found that 5%Ni/CeZrO₂ doped with Y, Ca and Al exhibited the higher CH₄ conversion than that of 5%Ni/CeZrO₂ binary mixed oxide support, whereas La doped catalyst showed corresponded performance to 5%Ni/CeZrO₂. These catalysts exhibited remarkably high activity (CH₄ conversion > 80%) and stability during the reaction time. This is attributed to their higher OSC value, and easy reducibility. The high OSC value is supported by the O1s spectra of 5%Ni/CeZrMO₂, indicating the surface lattice oxygen and adsorbed oxygen, which implies these doped metals can increase the amount of adsorbed oxygen on the surface. The CO₂ conversions using these catalysts were lower than CH₄ conversions, indicating that coking on catalyst was low. The similar result also reported by Wu et al. [82], they found that Y³⁺ doped CeZrO₂ showed higher activity and thermal stability than that of CeZrO₂ on dry reforming of methane. Doped Y³⁺ exhibited higher content of surface oxygen species which is due to oxygen vacancies or/and structure distortion resulted from the doping. Moreover, Y³⁺ doping also promoted the easier migration of bulk lattice oxygen. Pompeo et al. [91] reported that 5%Ni/CeZrAlO₂ catalyst showed the better methane reforming activity and stability than in the case of 5%Ni/CeO₂, 5%Ni/ZrO₂, and 5%Ni/Al₂O₃. CeZrAlO₂ mixed oxide support improved the Ni dispersion, the metal particle reducibility, and metal support interaction that prevent deactivation by sintering. Wang et al. [70] reported that Pd/CeZrLaO₂ showed the best activity in catalytic methanol decomposition to H₂ and CO which is attributed to their high surface area, oxygen mobility, Pd dispersion and strong metal-support interaction. For the Ca²⁺ doping, Yue et al. [92] reported that the addition of Ca to Pd/CeZrAlO₂ catalyst can promote the low temperature activity in methane combustion. Ca doping can improve reduction properties and thermal stability of the active PdO resulting from excellent Pd dispersion. H₂ yield and selectivity of the best four catalysts were higher than 75% and 90%, respectively. These catalysts exhibited the H₂/CO ratio about 1, indicating that only dry reforming was performed.

4.2.2.2 Effect of the addition of steam on the performance of 5%Ni/CeZrMO₂ catalysts for dry reforming of CH₄

The effect of steam on dry reforming reaction over 5%Ni/CeZrMO₂ was investigated at 800 °C with steam feed flow rate 0.03 cc/ min. The result are shown in Figure 4.19

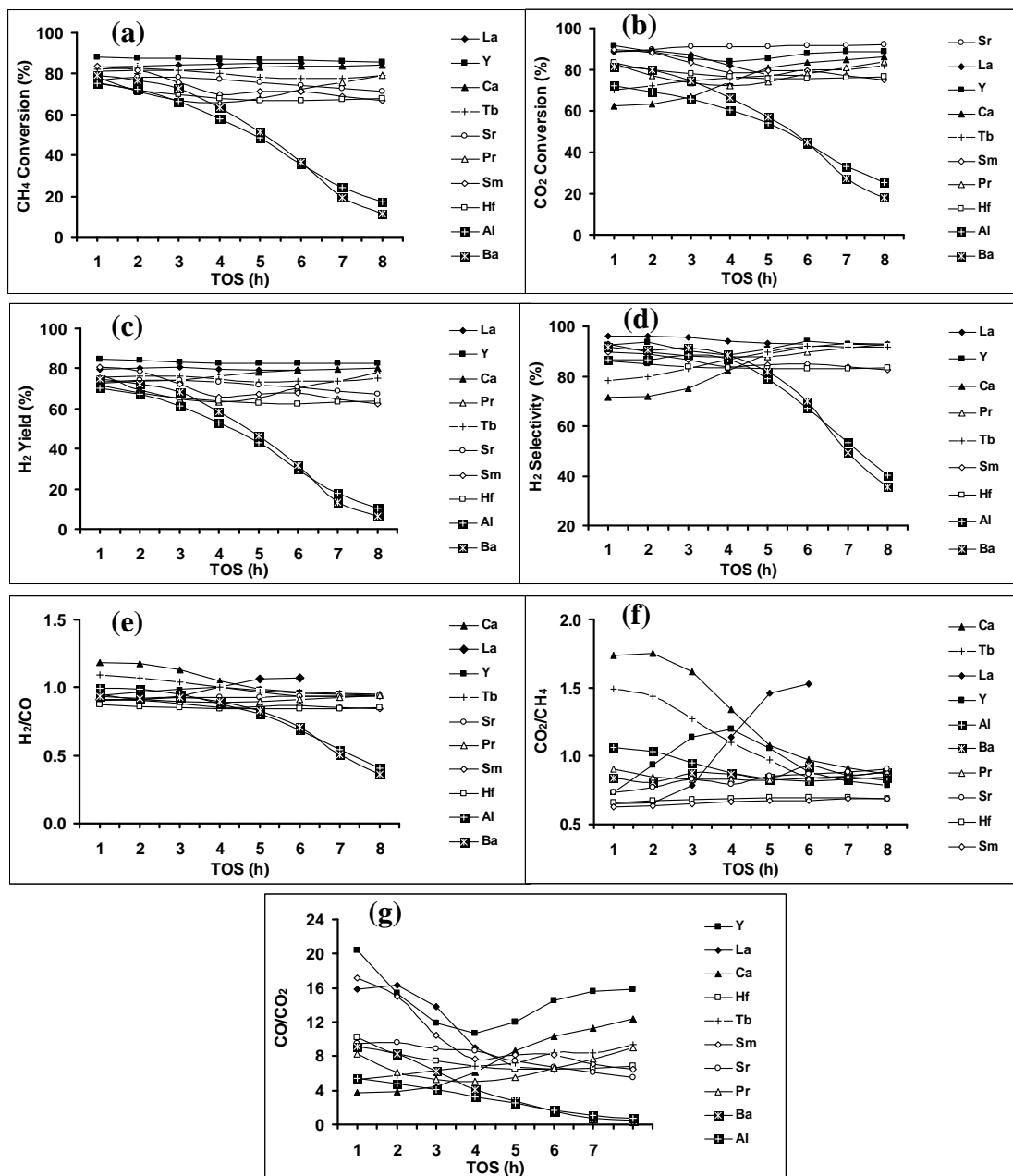


Figure 4.19 Effect of steam content (0.03 cc/min) on dry reforming reaction using 5%Ni/CeZrMO₂ for (a) CH₄ conversion, (b) CO₂ conversion, (c) H₂ yield, (d) H₂ selectivity, (e) H₂/CO ratio, (f) CO₂/CH₄ ratio, and (g) CO/CO₂ ratio.

Figure 4.19 show the catalytic performance of doped 5%Ni/CeZrO₂ in the presence of steam. It was found that 5%Ni/CeZrO₂ doped with Y, Ca and La still are the best three among all the other catalysts tested in the current study, in terms of higher CH₄ conversion and H₂ yield. After the addition of steam, 5%Ni/CeZrAlO₂ catalyst's performance deteriorates, when compared to its performance in the absence of steam. Accordingly to Pompeo et al. [91] sintering is the main cause of catalyst deactivation and occurs at high temperature operating conditions. As mentioned by Ferretti et al. in 1990, water vapor/steam in the feed leads to a marked decrease in the metal surface area especially in the case of Ni-impregnated catalysts. H₂ yield and selectivity of the three best catalysts were higher than 80% and 90%, respectively. These catalysts exhibit a H₂/CO ratio ≤ 1 , indicating that dry reforming is not the only reaction occurring under the stated reaction conditions, but water gas shift (WGS) reaction is also taking place parallelly. The evidence for the occurrence of WGS comes from the marked decrease in the resultant CO/CO₂ ratio of the product reformat stream with time. The above results are in good agreement with the data reported by Raju et al. [43]. Moreover, 5%Ni/CeZrO₂ doped with Tb, Pr, Sr, Sm and Hf also exhibit good stability during the course of 8 h test runs, however with lower CH₄ conversions, as compared to the three best formulations.

After the addition of steam in the feed gas, the carbon deposition rates were significantly decreased. It indicates that the addition of steam in the feed gas can suppress carbon formation. The deposited carbon may be removed through gasification with steam [$\text{H}_2\text{O} + \text{C} (\text{s}) \rightarrow \text{CO} + \text{H}_2$] or carbon dioxide [$\text{CO}_2 + \text{C} (\text{s}) \rightarrow 2\text{CO}$] [37, 45].

4.2.2.3 Effect of temperature on catalytic performance of 5%Ni/CeZrMO₂ for dry reforming of CH₄

One important limitation for making the dry reforming of CH₄ a commercially viable reaction using conventional reactors is due to thermodynamics, which limits reactants conversion. Nevertheless, methane (and carbon dioxide) conversion might be increased if both products of the reaction could be selectively removed from the reaction system. A palladium membrane reactor is an engineering device that offers the possibility to do this, achieving either higher methane conversion than a conventional process at a fixed temperature, or the same methane conversion but at lower temperature with the consequent energy saving. In fact, it combines the separation properties of membranes with the typical characteristics of catalytic reactions: by selectively removing hydrogen from the reaction mixture, the conversion of CH₄ was increased for dry reforming of CH₄. The intermetallic diffusion is an important limitation when use palladium membrane reactor supported on stainless steel at high temperature (> 400 °C). In order to improve the conversion of the reaction by using palladium membrane, the temperature of dry reforming reaction should be low as much as possible. In this study, the influence of operating temperature on the catalytic performance over 5%Ni/CeZrMO₂ doped with Ca, La, and Y (the three best formulations) were studied by lowering the temperature from 800 °C to 500 °C and the results thus obtained are shown in Figure 4.20.

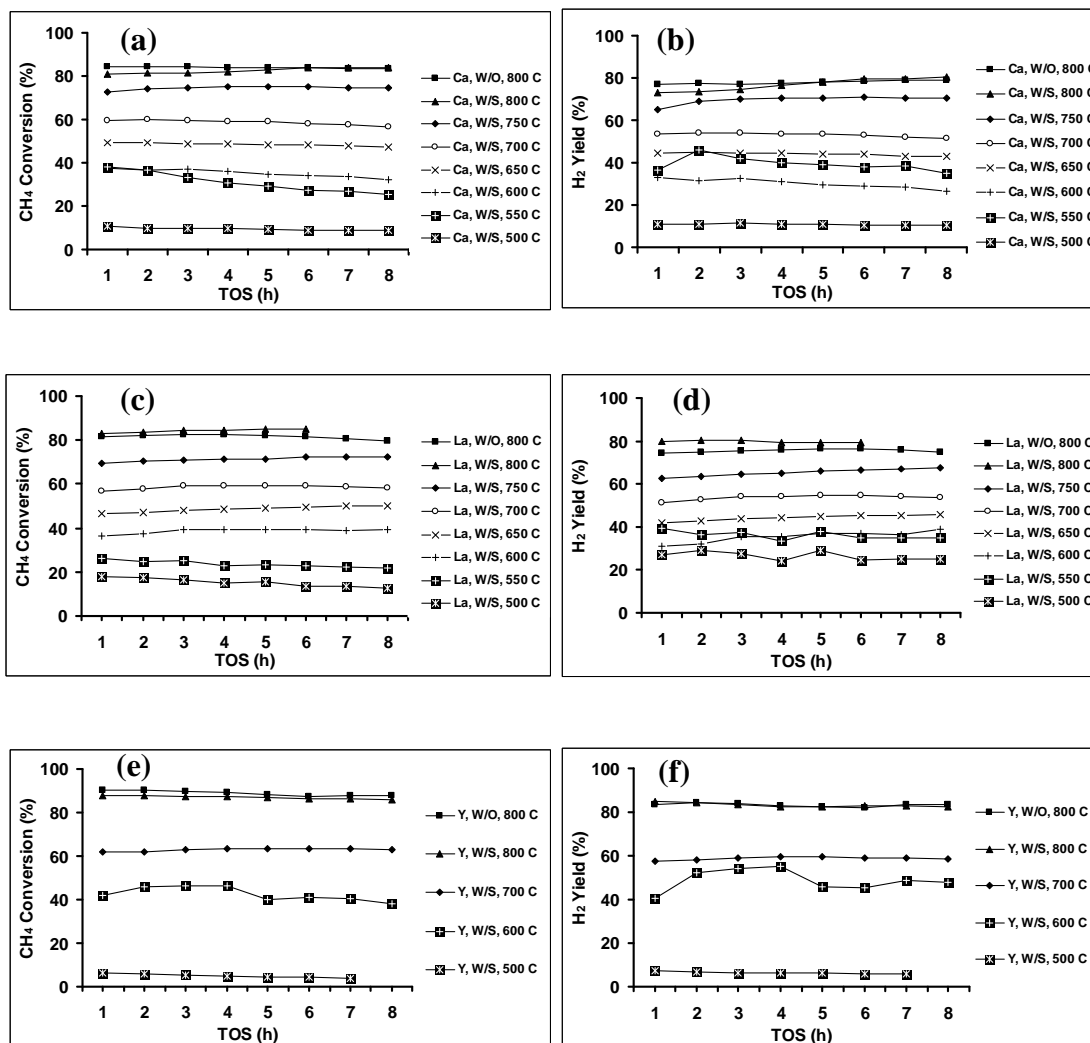


Figure 4.20 Effect of temperature on dry reforming reaction using 5%Ni/CeZrMO₂ at steam 0.03 cc/ min for (a-b) CH₄ conversion, and H₂ yield of 5%Ni/CeZrCaO₂ (c-d) CH₄ conversion, and H₂ yield of 5%Ni/CeZrLaO₂ (e-f) CH₄ conversion, and H₂ yield of 5%Ni/CeZrYO₂.

Figure 4.20 shows the stability of 5%Ni/CeZrO₂ doped Ca, La, and Y catalysts for steam-assisted dry reforming reaction at lower operating temperatures. It was found that the CH₄ and H₂ yield of all catalyst decreased with decreasing the operating temperature. Dry reforming is an endothermic reaction, and so higher reaction temperatures favor higher conversion. However, the trend observed (CH₄ conversion and H₂ yield) imply that there could be a marginal deactivation taking place during the course of reaction, which can be more pronounced at t lower operating temperatures. The above findings indicate that Ca, La, and Y dopants enhance the stability of 5%Ni/CeZrO₂ catalyst and facilitate the low temperature operation. The main cause for the low temperature activity could be due to the increased migration of bulk lattice and surface oxygen species. The above results are in good agreement with the data reported by Wu et al. [82]. From the current studies it is observed that, when steam was added to the dry reforming feed, the carbon deposition on the catalyst surface reduced drastically and no coke was noted at 550 and 500 °C. Very similar results were reported by Choudhary et al. [39]. At this low temperature, palladium membrane can use to improve the conversion of the reaction.

4.2.3 Long-term stability test

4.2.3.1 Long-term stability test of 5%Ni/CeZrCaO₂

The long-term stability test over 5%Ni/CeZrCaO₂ catalyst was investigated for dry reforming reaction at 800 °C for 100 h and the results thus obtained are shown in Figure 4.21.

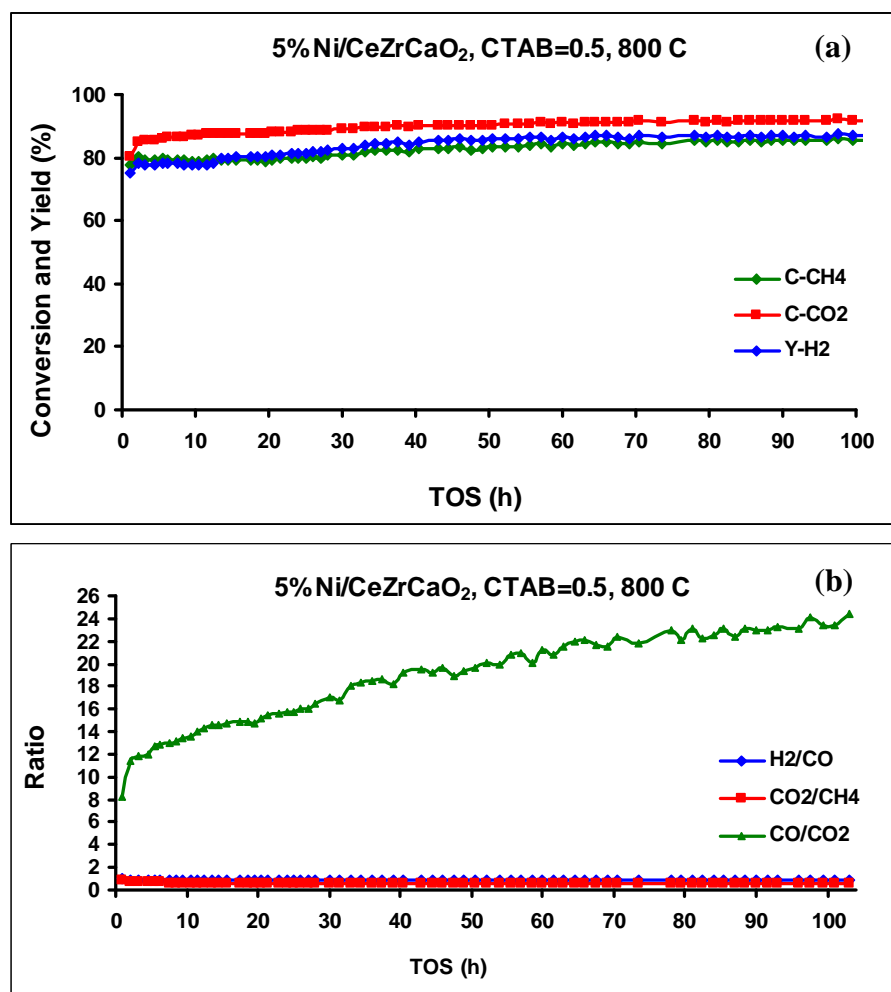


Figure 4.21 The long-term stability of 5%Ni/CeZrCaO₂ on dry reforming reaction at 800 °C, without steam for 100 h for (a) CH₄, CO₂ conversion, and H₂ yield, (b) ratio.

Figure 4.21 it is clear that, within the limits of the current study, the 5%Ni/CeZrCaO₂ catalyst exhibits exceptional stability for dry reforming reaction. Interestingly the CH₄ and CO₂ conversions and H₂ yield increased during the course

of 100 h test run. The catalyst's performance was stable with no signs of deactivation with the limits of the current run. The out put H_2/CO ratio was close to 1, indicating that only dry reforming reaction was taking place. The above results unequivocally imply that 5%Ni/CeZrCaO₂ is a highly promising catalyst for dry reforming reaction both in the absence and presence of steam.

4.2.3.2 Long-term stability test of 5%Ni/CeZrYO₂

The long-term stability test over 5%Ni/CeZrYO₂ was performed for dry reforming reaction at 800 °C, without steam for 25 h duration. The results are shown in Figure 4.22.

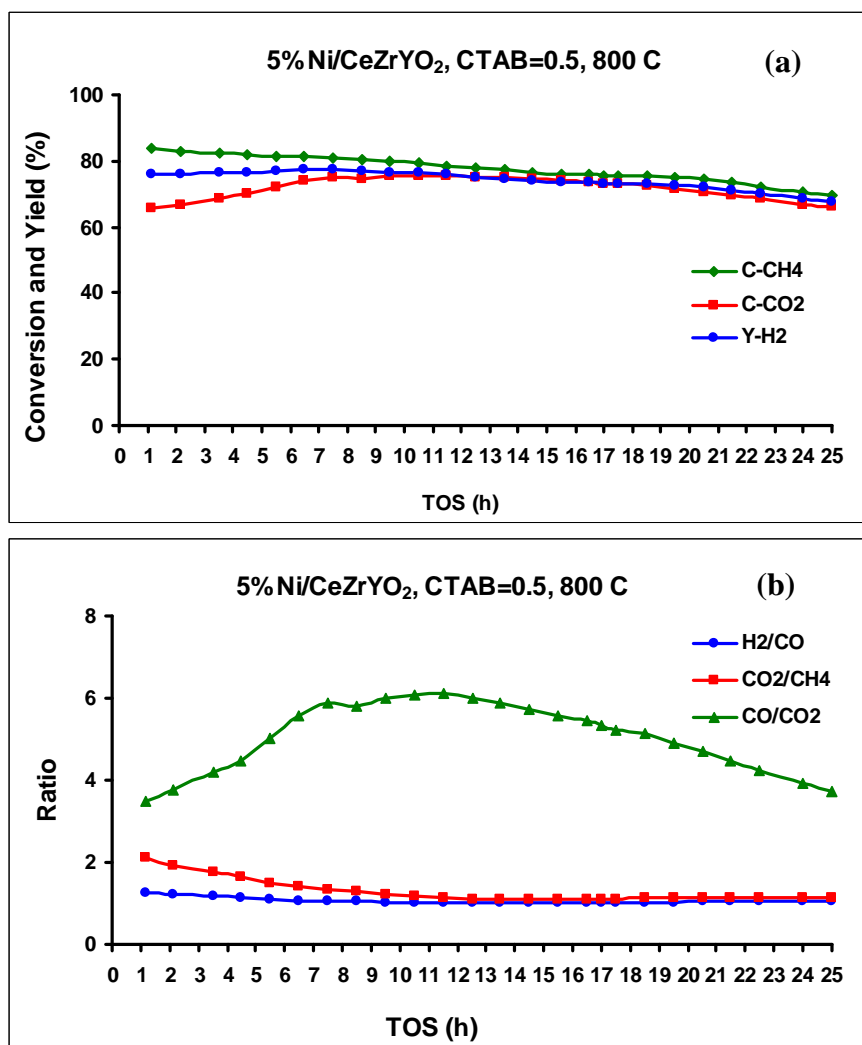


Figure 4.22 The long-term stability of 5%Ni/CeZrYO₂ for typical dry reforming reaction at 800 °C for 25 h for (a) CH₄, CO₂ conversion, and H₂ yield, (b) ratio.

Figure 4.22 shows the stability of 5%Ni/CeZrYO₂ catalysts on dry reforming. It was found that the CH₄ conversion and H₂ yield were high at the beginning and decreased after 8 h TOS. The CO₂ conversion increased and then decreased. The catalyst exhibited the H₂/CO ratio about 1, indicating that only dry reforming process was occurring under the chosen experimental conditions. The deactivation of the catalyst may be due to the carbon deposition or the sintering of the metal.

4.2.3.3 Long-term stability test of 5%Ni/CeZrCaO₂ in the presence of steam

The long-term stability test of 5%Ni/CeZrCaO₂ catalyst was studied at 500 °C in the presence of steam (flow rate = 0.03 cc/min). The results are shown in Figure 4.23.

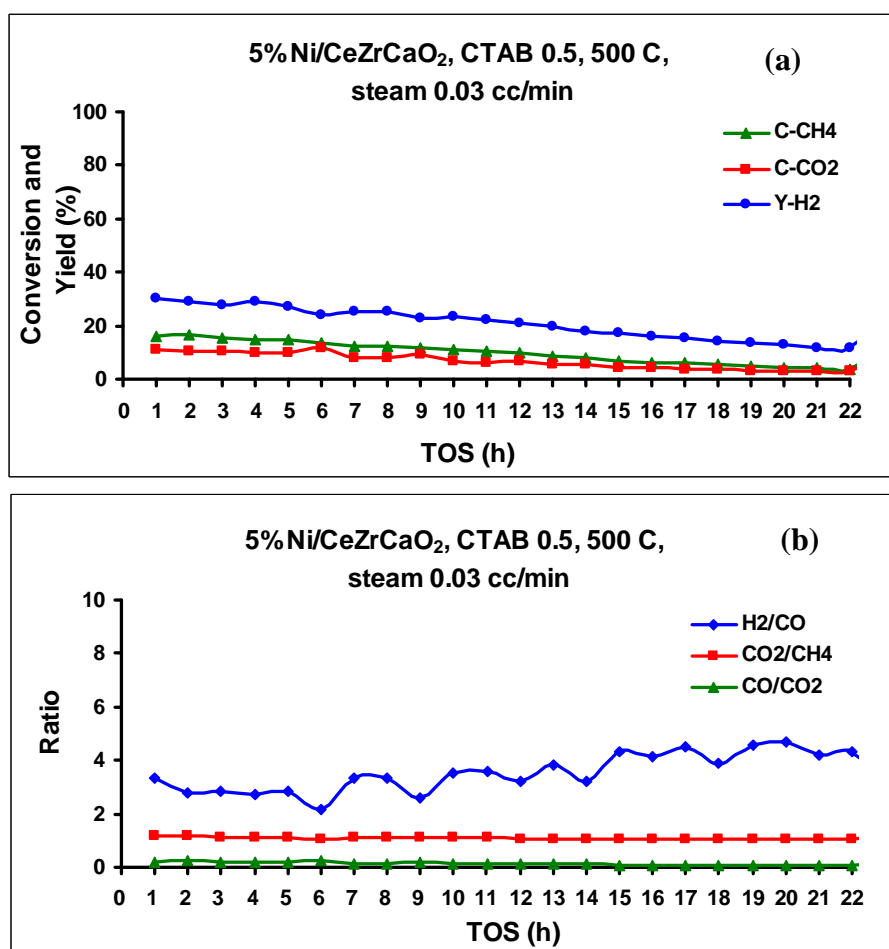


Figure 4.23 The long-term stability of 5%Ni/CeZrYO₂ on dry reforming reaction at 800 °C, steam 0.03 cc/ min for 25 h for (a) CH₄, CO₂ Conversion, and H₂ yield, (b) ratio.

From the Figure 4.23, it is observed that the CH₄, CO₂ conversions and H₂ yield values are reasonably higher initially; however decrease after 8 h TOS. The evidence for the occurrence of water-gas shift reaction comes from the following results (1) the decrease in the CO/CO₂ ratio and (2) the increase in H₂/CO ratio of product stream. The deactivation of the catalyst could be due to the effect of steam which induces sintering of the metal particles. The steam content is another important factor to obtain the high conversion and yield. The excess steam would promote the water-gas shift reaction and could change the designated H₂/CO ratio.

4.2.4 The structure-activity relationships (SAR) of the catalysts

The structure-activity relationships (SAR) for each ternary mixed oxide catalysts are shown in Figures 4.24 and 4.25.

Figure 4.25 shows the relationship between catalyst reducibility and activity of the catalysts. The highly reducible catalysts perform better because their redox ability is enhanced, except Al doped catalysts. Among the various catalysts tested, the reducibility trend observed was 5%Ni/CeZrYO₂ > 5%Ni/CeZrLaO₂ > 5%Ni/CeZrCaO₂ > 5%Ni/CeZrO₂, which is also the trend of their relative catalytic performance.

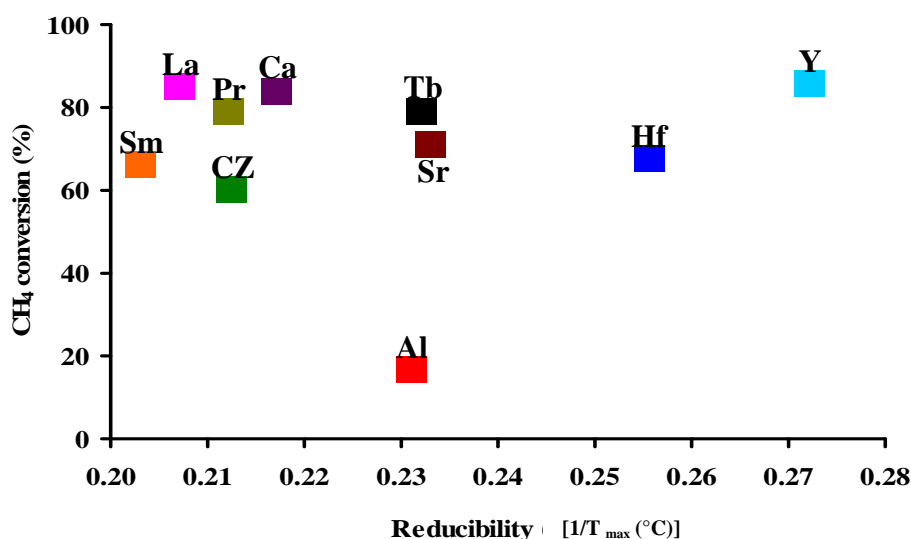


Figure 4.24 Structure/activity correlation plots of activity vs. reducibility for dry reforming of CH₄ reaction in the presence of steam.

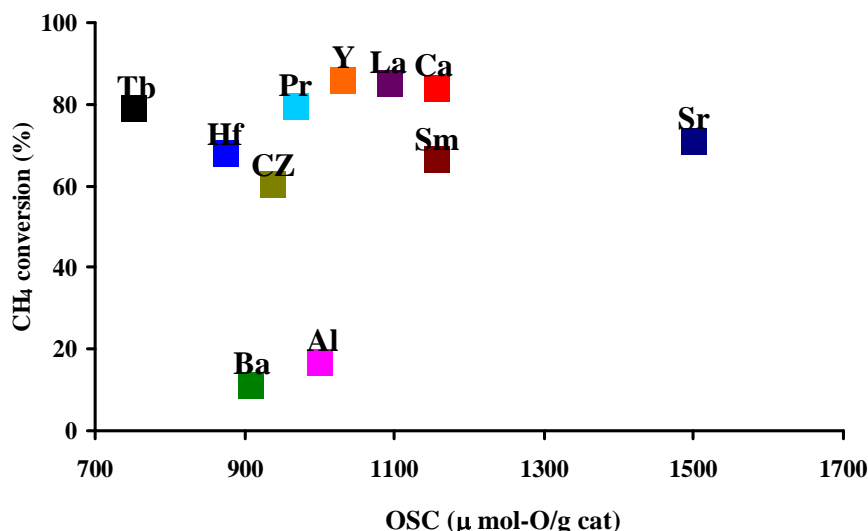


Figure 4.25 Structure/activity correlation plots of activity vs. OSC for dry reforming of CH₄ reaction in the presence of steam.

Figure 4.25 represents the correlation plot of activity vs. OSC. An increase in OSC leads to an improvement in the resultant catalytic activity; however, there is an outlier in this plot too. Among the different catalysts tested, 5%Ni/CeZrSrO₂ exhibited highest OSC; however, the performance of this catalyst is unsatisfactory. On the other hand, 5%Ni/CeZrTbO₂ showed the lowest OSC but yielded high performance. From the present investigation, it is quite apparent that reasonable OSC and high reducibility lead to excellent catalytic activity for dry reforming process. An example is 5%Ni/CeZrYO₂ which exhibits excellent performance in dry reforming reaction. The superior performance of the above catalyst can be explained in terms of high reducibility and reasonable OSC.

From this research, some 5%Ni/CeZrMO₂ ternary mixed oxide catalysts exhibited higher performance than 5%Ni/CeZrO₂ binary mixed oxide catalysts due to higher OSC and reducibility of the catalysts. In the presence of steam, the doped elements improved the hydrophilic property of the catalysts resulting in higher activity and stability. The previous literature [101] reported that the hydrophilic property of polysulfone membrane has been improved by adding sulfated Y-doped zirconia particles. The adding of Y has stabilized the metastable tetragonal phase of

ZrO₂ and more point defects and oxygen vacancies. Guan et al. [102] also reported that rare earth oxide CeO₂ and La₂O₃ doped TiO₂/SiO₂ films have better hydrophilicity than a pure TiO₂ film. The surface of the films has more oxygen vacancies and hydroxyl groups due to addition of rare earth oxide and SiO₂.

CHAPTER V

CONCLUSIONS

5.1 Binary mixed oxide catalyst

In this research, it was clearly revealed that the catalysts obtained by surfactant-assisted templating route show the higher activity than the one obtained by co-precipitation method. Also, within the limitation of the surfactant ratios used, the amount of surfactant employed during the course of support preparation seems to affect the activity of the catalyst. The catalysts prepared with the higher surfactant/metal molar ratio exhibited better activity and enhanced stability. Suitable structure/activity relationship (SAR) was formulated in order to explain the marked difference in activity and stability of the catalysts prepared with different CTAB/(Ce+Zr) molar ratios. The characteristics which are absolutely necessary for good performance in dry reforming process are high OSC, high surface area, easy reducibility, lower cerium content and higher nickel content on the surface. Accordingly, the surfactant-assisted templating route is a promising method to prepare the catalyst for dry reforming of CH₄ with high surface area, better dispersion of Ni species, and high OSC. However, this catalyst was prone to deactivation when steam was introduced along with the dry reforming feed gas. The inherent hydrophilic nature of the ceria-zirconia support is the main cause for the apparent deactivation in the presence of steam.

5.2 Ternary mixed oxide catalyst

5%Ni/CeZrMO₂ (M= Al, Ba, Ca, Hf, La, Pr, Sm, Sr, Tb, and Y) ternary mixed oxides were prepared by surfactant-assisted templating route with CTAB/(Ce+Zr) molar ratios of 0.5. The catalytic performance of Ni-based catalysts was investigated for catalytic dry reforming of methane with and without steam. Among the various formulations tested, the best three catalysts are 5%Ni/CeZrCaO₂, 5%Ni/CeZrLaO₂,

and 5%Ni/CeZrYO₂. They exhibit high activity and stability compared to other members of the ternary mixed oxide family and also to the catalysts belonging to binary oxide family due to their high OSC. The addition of steam to the dry reforming feed resulted in the increasing of methane conversion and significantly lower carbon deposition. Moreover, the catalysts show a good stability even at low temperature like 500°C.

From the study, it can be concluded that the ternary mixed oxide catalysts , 5%Ni/CeZrMO₂, prepared by surfactant-assisted templating route using the surfactant/metal molar ratio ~ 0.5 are promising catalysts for dry reforming of methane both in the absence and presence of steam and also at low temperature, thus being potential candidates for plausible membrane reactor applications.

5.3 Further Works

From this work, it can prove that 5%Ni/CeZrMO₂ (M= Ca, La, and Y) are the promising catalysts for dry reforming of methane with high activity and stability at 500 °C in the presence of steam. The productivity of the reaction could be further improved by the following studies:

1. The coupling dry reforming reaction with steam reforming and partial oxidation reaction.
2. Palladium membrane assisted dry reforming reaction in the presence of steam over ternary mixed oxide-based catalysts.

REFERENCES

- [1] Chen, L., Wu, Q., Zhang, J., and Zhang, J. Effect of preparation methods on structure and performance of Ni/Ce_{0.75}Zr_{0.25}O₂ catalysts for CH₄-CO₂ reforming. *Fuel* 87 (2008): 2901-2907.
- [2] Qin, D., and Lapszewicz, J. Study of mixed steam and CO₂ reforming of CH₄ to syngas on MgO-support metals. *Catalysis Today* 21 (1994): 551-560.
- [3] Edwards, J. H., and Maittra, A. M. The chemistry of methane reforming with carbon dioxide and its current and potential applications. *Fuel Processing Technology* 42 (1995): 269-289.
- [4] Rostrup-Nielsen, J. R., and Hansen, J. H. B. CO₂-reforming of methane over transition metals. *Journal of Catalysis* 144 (1993): 38-49.
- [5] Wang, Y. H., Liu, H. M., and Xu, B. Q. Durable Ni/MgO catalysts for CO₂ reforming of methane: Activity and metal-support interaction. *Journal of Molecular Catalysis A: Chemical* 299 (2009): 44-52.
- [6] Yokota, O., and others. Stoichiometric consideration of steam reforming of methane on Ni/Al₂O₃ catalyst at 650 °C by using a solar furnace simulation. *International Journal of Hydrogen Energy* 25 (2000): 81-86.
- [7] Luna, A. E. C., and Iriate, M. E. Carbon dioxide reforming of methane over a metal modified Ni-Al₂O₃ catalyst. *Applied Catalysis A: General*, 343 (2008): 10-15.
- [8] Takahashi, R., Sato, S., Sodesawa, T., and Tomiyama, S. CO₂-reforming of methane over Ni/SiO₂ catalyst prepared by homogeneous precipitation in sol-gel-derived silica gel. *Applied Catalysis A: General* 286 (2005): 142-147.
- [9] Pompeo, F., Nichio, N. N., González, M. G., and Montes, M. Characterization of Ni/SiO₂ and Ni/Li-SiO₂ catalysts for methane dry reforming, *Catalysis Today* 107-108 (2005): 856-862.
- [10] Courson, C., Makaga, E., Petit, C., and Kiennemann, A. Development of Ni catalysts for gas production from biomass gasification. Reactivity in steam- and dry-reforming. *Catalysis Today* 63 (2000): 427-437.

- [11] Laosiripojana, N., and Assabumrungrat, S. Catalytic dry reforming of methane over high surface area ceria. *Applied Catalysis B: Environmental* 60 (2005): 107-116.
- [12] Wei, J. M., Xu, B. Q., Li, J. L., Cheng, Z. X., and Zhu, Q. M. Highly active and stable Ni/ZrO₂ catalyst for syngas production by CO₂ reforming of methane. *Applied Catalysis A: General* 196 (2000): L167-L172.
- [13] Montoya, J. A., Pascual, E. R., Gimón, C., Del Angel, P., and Monzón, A. Methane reforming with CO₂ over Ni/ZrO₂-CeO₂ catalysts prepared by sol-gel. *Catalysis Today* 63 (2000): 71-85.
- [14] Roh, H. S., Jun, K. W., Dong, W. S., Chang, J. S., Park, S. E., and Joe, Y. I. Highly active and stable Ni/Ce-ZrO₂ catalyst for H₂ production from methane. *Journal of Molecular Catalysis A: Chemical* 181 (2002): 137-142.
- [15] Dong, W. S., Roh, H. S., Jun, K. W., Park, S. E., and Oh, Y. S., Methane reforming over Ni/Ce-ZrO₂ catalysts: effect of Ni content, *Applied Catalysis A: General*. 226 (2002): 63-72.
- [16] Roh, H. S., Jun, K.W., Dong, W. S., Park, S. E., and Baek, Y. S. Highly stable Ni catalyst supported on Ce-ZrO₂ for oxy-steam reforming of methane. *Catalysis Letters* 74 (2001): 31-36.
- [17] Roh, H. S., Jun, K.W., and Park, S.E., Methane-reforming reactions over Ni/Ce-ZrO₂/θ-Al₂O₃ catalysts. *Applied Catalysis A: General* 251 (2003): 275-283.
- [18] Srisiriwat, N., Therdthianwong, S., and Therdthianwong, A. Oxidative steam reforming of ethanol over Ni/Al₂O₃ catalysts promoted by CeO₂, ZrO₂ and CeO₂-ZrO₂. *International Journal of Hydrogen Energy* 34 (2009): 2224-2234.
- [19] Gao, J., Liang, D., Hou, Z., Fei, J., and Zheng, X. Production of syngas via autothermal reforming of methane in a fluidized-bed reactor over the combined CeO₂-ZrO₂/SiO₂ supported Ni catalysts. *International Journal of Hydrogen Energy* 33 (2008): 5493-5500.
- [20] Leitenburg, C., Trovarelli, A., Llorca, J., Cavani, F., and Bini, G. The effect of doping CeO₂ with zirconium in the oxidation of isobutane. *Applied Catalysis A: General* 139 (1996): 161-173.

- [21] Roh, H. S., Platon, A., Wang, Y., and King, D. L. Catalyst deactivation and regeneration in low temperature ethanol steam reforming with Rh/CeO₂-ZrO₂ catalysts. *Catalysis Letters* 110 (2006): 1-6.
- [22] Roh, H. S., Potdar, H. S., Jun, K. W., Kim, J. W., and Oh, Y. S. Carbon dioxide reforming of methane over Ni incorporated into Ce-ZrO₂ catalysts. *Applied Catalysis A: General* 276 (2004): 231-239.
- [23] Pengpanich, S., Meeyoo, V., Rirksomboon, T., and Bunyakiat, K. Catalytic oxidation of methane over CeO₂-ZrO₂ mixed oxide solid solution catalysts prepared via urea hydrolysis. *Applied Catalysis A: General* 234 (2002): 221-233.
- [24] Hori, C. E., and others. Thermal stability of oxygen storage properties in a mixed CeO₂-ZrO₂ system. *Applied Catalysis B: Environmental* 16 (1998): 105-117.
- [25] Zhang, D. L. Processing of advanced materials using high-energy mechanical milling. *Progress in Material Science* 49 (2004): 537-560.
- [26] Roh, H. S., Potdar, H. S., and Jun, K. W., Carbon dioxide reforming of methane over co-precipitated Ni-CeO₂, Ni-ZrO₂ and Ni-Ce-ZrO₂ catalysts, *Catalysis Today*, 93-95 (2004): 39-44.
- [27] Laosiripojana, N., and Assabumrungrat, S. Methane steam reforming over Ni/Ce-ZrO₂ catalyst: Influences of Ce-ZrO₂ support on reactivity, resistance toward carbon formation, and intrinsic reaction kinetics. *Applied Catalysis A: General* 290 (2005): 200-211.
- [28] Otsuka, K., Wang, Y., and Nakamura, M. Direct conversion of methane to synthesis gas through gas-solid reaction using CeO₂-ZrO₂ solid solution at moderate temperature. *Applied Catalysis A: General* 183 (1999): 317-324.
- [29] Terribile, D., Trovarelli, A., Llorca, J., Leitenbrug, C., and Dolcetti, G. The preparation of high surface area CeO₂-ZrO mixed oxides by surfactant-assisted approach. *Catalysis Today* 43 (1998): 79-88.
- [30] Laosiripojana, N., Chadwick D., and Assabumrungrat, S. Effect of high surface area CeO₂ and Ce-ZrO₂ supports over Ni catalyst on CH₄ reforming with H₂O in the presence of O₂, H₂, and CO₂. *Chemical Engineering Journal* 138 (2008): 264-273.

- [31] Rezaei, M., Alavi, S. M., Sahebdehfar, S., and Yan, Z. F. A highly stable catalyst in methane reforming with carbon dioxide. *Scripta Materialia* 61 (2009): 173-176.
- [32] Kumar, P., Sun, Y., and Idem, R. O. Comparative Study of Ni-based Mixed Oxide Catalyst for Carbon Dioxide Reforming of Methane. *Energy & Fuel* 22 (2008): 3575-31582.
- [33] Kumar, P., Sun, Y., and Idem, R. O. Nickel-based ceria, zirconia, and ceria-zirconia catalytic systems for low-temperature carbon dioxide reforming of methane. *Energy & Fuel* 21 (2007): 3133-3123.
- [34] Roh, H. S., Koo, K. Y., and Yoon, W. L. Combined reforming of methane over co-precipitated Ni-CeO₂, Ni-ZrO₂ and Ni-Ce_{0.8}Zr_{0.2}O₂ catalysts to produce synthesis gas for gas to liquid (GTL) process. *Catalysis Today* 146 (2009): 71-75.
- [35] Lemonidou, A. A., and Vasalos, I. A. Carbon dioxide reforming of methane over 5 wt. % Ni/CaO-Al₂O₃ catalyst. *Applied Catalysis A: General* 228 (2002): 227-235.
- [36] Laosiripojana, N., Sutthisripok, W., and Assabumrungrat, S. Reactivity of high surface area CeO₂ synthesized by surfactant-assisted method to ethanol decomposition with and without steam. *Chemical Engineering Journal* 127 (2007): 31-38.
- [37] Xu, J., and others. Methane steam reforming for hydrogen production using low water-ratios without carbon formation over ceria coated Ni catalysts. *Applied Catalysis A: General* 345 (2008): 119-127.
- [38] Roh, H. S., and others. Combined reforming of methane over supported Ni catalysts. *Catalysis Letters* 117 (2007): 85-90.
- [39] Choudhary, V. R., and Rajput, A.M. Simultaneous carbon dioxide and steam reforming of methane to syngas over NiO-CaO catalyst. *Industrial Engineering Chemical Research* 35 (1996): 3934-3939.
- [40] Qin, D., Lapszewicz, J., and Jiang, X. Comparison of partial oxidation and steam-CO₂ mixed reforming of CH₄ to syngas on MgO-supported metals. *Journal of Catalysis* 159 (1996): 140-149.

- [41] Koo, K. Y., Roh, H. S., Jung, U. H., Seo, D. J., Seo, Y. S., and Yoon, W. L. Combined H₂O and CO₂ reforming of CH₄ over nano-sized Ni/MgO-Al₂O₃ catalysts for synthesis gas production for gas to liquid (GTL): Effect of Mg/Al mixed ratio on coke formation. *Catalysis Today* 146 (2009): 166-171.
- [42] Choudhary, V. R., and Mondal, K. C. CO₂ reforming of methane combined with steam reforming or partial oxidation of methane to syngas over NdCoO₃ perovskite-type mixed metal-oxide catalyst. *Applied Energy* 83 (2006): 1024-1032.
- [43] Raju, A. S. K., Park, C. S., and Norbeck, J. M. Synthesis gas production using steam hydrogasification and steam reforming. *Fuel Processing Technology* 90 (2009): 330-336.
- [44] Roh, H. S., Koo, K. Y., and Joshi, J. U. D. Combined H₂O and CO₂ reforming of methane over Ni-Ce-ZrO₂ catalysts for gas to liquids (GTL). *Catalysis Letters* 125 (2008): 283-288.
- [45] Li, C. L., Fu, Y. L., Bian, G. Z., Xie, Y. N., Hu, T. D., and Zhang, J. Effect of steam in CO₂ reforming of CH₄ over a Ni/CeO₂-ZrO₂-Al₂O₃ catalyst. *Kinetics and Catalysis* 45 (2004): 719-723.
- [46] Cao, L., Ni, C., Yuan, Z., and Wang, S. Correlation between catalytic selectivity and oxygen storage capacity in autothermal reforming of methane over Rh/Ce_{0.45}Zr_{0.45}RE_{0.1} catalysts (RE = La, Pr, Nd, Sm, Eu, Gd, Tb). *Catalysis Communication* 10 (2009): 1192-1195.
- [47] Li, M., Liu, Z., Hu, Y., Wang, M., and Li, H. Effect of doping elements on catalytic performance of CeO₂-ZrO₂ solid solutions. *Journal of Rare Earths* 26 (2008): 357-361.
- [48] Aneggi, E., Leitenburg, C., Dolcetti, G., and Trovarelli, A., Promotional effect of rare earths and transition metals in the combustion of diesel soot over CeO₂ and CeO₂-ZrO₂, *Catalysis Today* 114 (2006): 40-47.
- [49] Mei, D., Chen, Y., Zhong, J., Wei, Z., Ma, D., and Gong, M. Catalytic partial oxidation of methane over Ni/CeO₂ - ZrO₂ -Al₂O₃. *Journal of Rare Earths* 25 (2007): 311 - 315.

- [50] Wu, X., Yang, B., and Weng, D. Effect of Ce–Zr mixed oxides on the thermal stability of transition aluminas at elevated temperature *Journal of Alloys and Compounds* 376 (2004): 241–245.
- [51] Frolova, E. V., Ivanovskaya, M., Sadykov, V., Alikina, G., Lukashevich, A., and Neophytides, S. Properties of Ce-Zr-La-O nano-system with ruthenium modified surface. *Progress in Solid State Chemistry* 33 (2005): 317-325.
- [52] Fan, G., Feng, C., and Zhang, Z. Surface and texture properties of Tb-doped ceria-zirconia solid solution prepared by sol-gel method. *Journal of Rare Earths* 25 (2007): 42-47.
- [53] Mikulova, J., Rossignol, S., Ge´rardy, F., Mesnard, D., Kappenstein, C., and Duprez, D. Properties of cerium–zirconium mixed oxides partially substituted by neodymium: Comparison with Zr–Ce–Pr–O ternary oxides. *Journal of Solid State Chemistry* 179 (2006): 2511–2520.
- [54] Strobel, R., Krumeich, F., Pratsinis, S. E., and Baiker, A. Flame-derived Pt/Ba/Ce_xZr_{1-x}O₂: Influence of support on thermal deterioration and behavior as NO_x storage-reduction catalysts. *Journal of Catalysis* 243 (2006): 229–238.
- [55] Fernandez-Garcia, M., Mart´inez-Arias, A., Guerrero-Ruiz, A., Conesa, J. C., and Soria, J. Ce–Zr–Ca ternary mixed oxides: structural characteristics and oxygen handling properties. *Journal of Catalysis* 211 (2002): 326–334.
- [56] Sherif, S. A., Barbir, F., and Veziroglu, T. N. Wind energy and the hydrogen economy-review of the technology. *Solar Energy* 78 (2005): 647–660.
- [57] Hu, Y. H., and Ruckenstein, E. Catalytic conversion of methane to synthesis gas by partial oxidation and CO₂ reforming. *Advance in Catalysis* 48 (2004): 297–345.
- [58] Ding, R., Yan, Z., Song, L., and Liu, X. A review of dry reforming of methane over various catalysts. *Journal of Natural Gas Chemistry* 10 (2001): 237-255.
- [59] Bond, G. C. Metal-Catalysed reactions of hydrocarbons. Fundamental and Applied Catalysts. *Springer* (2005): 77-78.
- [60] Pinna, F. Supported metal catalysts preparation. *Catalysis Today* 41 (1998): 129-137.

- [61] Basic operating principles of the sorption apparatus [Online]. 1990. Available from:
<http://saf.chem.ox.ac.uk/Instruments/BET/sorptprin.htm>.
- [62] Mnasiero, P., and Graziani, M. Use of CeO₂-based oxides in the three-way catalysis. *Catalysis Today* 50 (1999): 285-298.
- [63] Reiche, M.A., Maciejewski, M., and Baiker, A. Characterization by temperature programmed reduction. *Catalysis Today* 56 (2000): 347–355.
- [64] Skoog, D.A. Principle of instrument analysis, pp. 363-364. New York: Harcourt Brace Collage Publishers, 1997.
- [65] Leonid, V.A. Elements of X-ray crystallography, pp. 425. New York: Mcgraw-hill, 1997.
- [66] Raman spectroscopy, [Online] Available from:
<http://www.physics.iisc.ernet.in/~asood/res.htm>.
- [67] Flewitt, P. E. J., and Wild, R. K.. Physical methods for materials characterization, ISBN: 0750302038. Great Britain : Bookcraft, 1994.
- [68] Strobel, R., Krumeich, F., Pratsinis, and S. E.; Baiker, A. Flame-derived Pt/Ba/Ce_xZr_{1-x}O₂: Influence of support on thermal deterioration and behavior as NO_x storage-reduction catalysts. *Journal of Catalysis* 243 (2006): 229–238.
- [69] An, Y., Shen, M., and Wang, J. Comparison of the microstructure and oxygen storage capacity modification of Ce_{0.67}Zr_{0.33}O₂ from CaO and MgO doping. *Journal of Alloys and Compounds* 441 (2007): 305–310.
- [70] Wang, H., Chen, Y., Zhang, Q., Zhu, Q., Gong, M., and Zhao, M. Catalytic methanol decomposition to carbon monoxide and hydrogen over Pd/CeO₂-ZrO₂-La₂O₃ with different Ce/Zr molar ratios. *Journal of Natural Gas Chemistry* 18 (2009): 211–216.
- [71] Rossignol, S., Descorme, C., Kappenstein, C., and Duprez, D. Synthesis structure and catalytic properties of Zr–Ce–Pr–O mixed oxides. *Journal of Material Chemistry* 11 (2001): 2587–2592.
- [72] Wang, J., Shen, M., An, Y., and Wang, J. Ce–Zr–Sr mixed oxide prepared by the reversed microemulsion method for improved Pd-only three-way catalysts. *Catalysis Communications* 10 (2008): 103–107.

- [73] Hu, Y., Yin, P., Liang, T., Jiang, W., and Liu, B. Rare Earth Doping Effects on Properties of Ceria-Zirconia Solid Solution. *Journal of Rare Earths* 24 (2006): 86-89.
- [74] López-Luke, T., and others. Effect of the CTAB concentration on the upconversion emission of $\text{ZrO}_2:\text{Er}^{3+}$ nanocrystals. *Optical Materials* 29 (2006): 31-37.
- [75] BaO, H., Li, L., and Zhang, H. Influence of cetyltrimethylammonium bromide on physicochemical properties and microstructures of chitosan-IPP nanoparticles in aqueous solution. *Journal of Colloid and Interface Science* 328 (2008): 270-277.
- [76] Fally, F., and others. Modification of the oxygen storage capacity of $\text{CeO}_2\text{-ZrO}_2$ mixed oxides after redox cycling aging. *Catalysis Today* 59 (2000): 373-386.
- [77] Potdar, H. S., and others. Preparation of ceria-zirconia ($\text{Ce}_{0.75}\text{Zr}_{0.25}\text{O}_2$) powders by microwave-hydrothermal (MH) route. *Materials Chemistry and Physics* 74 (2002): 306-312.
- [78] Dharmaraj, N., Prabu, P., Nagarajan, S., Kim, C. H., Park, J. H., and Kim, H. Y. Synthesis of nickel oxide nanoparticles using nickel acetate and poly(vinyl acetate) precursor. *Materials Science and Engineering: B* 128 (2006): 111-114.
- [79] Li, X. K., Liu, L., Li, Z. H., Wu, D., and Shen, S. D. The characterization of ultrafine carbon powders by SAXS and Raman spectra. *Letters to the editor / Carbon* 38 (2000): 623-641.
- [80] Atribak, I., Bueno-López, A., and García, A. Role of yttrium loading in the physico-chemical properties and soot combustion activity of ceria and ceria-zirconia catalysts. *Journal of Molecular Catalysis A: Chemical* 300 (2009): 103-110.
- [81] Kang, Z., and Kang, Z. Quaternary oxide of cerium, terbium, praseodymium and zirconium for three-way catalysts. *Journal of Rare Earths* 24 (2006): 314-319.

- [82]. Wu, Q., Chen, J., and Zhan, J. Effect of yttrium and praseodymium on properties of $\text{Ce}_{0.75}\text{Zr}_{0.25}\text{O}_2$ solid solution for $\text{CH}_4\text{-CO}_2$ reforming. *Fuel Processing Technology*, 89 (2008): 993-999.
- [83] Markaryan, G. L., and others. Red-ox properties and phase composition of $\text{CeO}_2\text{-ZrO}_2$ and $\text{Y}_2\text{O}_3\text{-CeO}_2\text{-ZrO}_2$ solid solutions. *Colloids and Surfaces A: Physicochemical and Engineering Aspects* 151 (1999): 435-447.
- [84] Ghita, R.V., Negriila, C., Manea, A. S., Logofatu, C., Cernea, M., and Lazarescu, M. F. X-ray Photoelectron spectroscopy study on n-type GaAs. *Journal of optoelectronics and Advanced Materials* 5 (2003): 859-863.
- [85] Grosvenor, A. P., Cavell, R. G., Mar, A., and Blyth, R. I. R. Analysis of the electronic structure of Hf ($\text{Si}_{0.5}\text{As}_{0.5}$)As by X-ray photoelectron and photoemission spectroscopy. *Journal of Solid State Chemistry* 180 (2007): 2670-2681.
- [86] Perkins, C. L., Trenary, M., Tanaka, T., and Otani, S., X-ray photoelectron spectroscopy investigation of the initial oxygen adsorption sites on the LaB_6 (100) surface. *Surface Science* 1(1999): L222-L228.
- [87] He, H., Dai, H. X., and Au, C. T. Defective structure, oxygen mobility, oxygen storage capacity, and redox properties of RE-based (RE = Ce, Pr). *Catalysis Today* 1 (2004): 245-254.
- [88] Rao, G. R., Kadowaki, Y., Kondoh, H., and Nozoye, H. Surface alloy formation at the Sm/Ru(001) interface: evidence from Ru3d core-level emission. *Surface Science* 327 (1995): 293-300.
- [89] Jia, T., Wang, W., Long, F., Fu, Z., Wang, H., and Zhang, Q. Synthesis, characterization and luminescence properties of Y-doped and Tb-doped ZnO nanocrystals. *Materials Science and Engineering: B* 162 (2009): 179-184.
- [90]. Ohno, S., Hatabayashi, K., Chikamutsu, A., Hirose, Y., Shimada, T., and Hasegawa, T. XPS study of Sm_2TiO_7 thin films of layered perovskite structure. *Photon Factory Activity Report* 26 (2008): 87.
- [91] Pompeo, F., Gazzoli, D., and Nichio, N. N. Stability improvements of Ni/ $\alpha\text{-Al}_2\text{O}_3$ catalysts to obtain hydrogen from methane reforming. *International Journal of Hydrogen Energy* 34 (2009): 2260-2268.

- [92] Yue, B., Zhou, R., Zheng, X., and Lu, W. Promotional effect of Ca on the Pd/Ce-Zr/Al₂O₃ catalyst for low temperature catalytic combustion of methane. *Fuel Processing Technology* 89 (2008): 728-735.
- [93] Benkacem, T., and Agoudjil, N. Synthesis of Mesoporous Titania with Surfactant and its Characterization. *American Journal of Applied Sciences* 5 (2008): 1437-1441.
- [94] Rezai, M., and others. Synthesis of pure tetragonal zirconium oxide with high surface area. *Journal of Membrane Science* 42 (2007): 1228-1237.
- [95] Reddy, B. M., Khan, A., Yamada, A., Kobayashi, Y., T., Loridant, S., and Volta, J. C. Raman and X-ray photoelectron spectroscopy study of CeO₂-ZrO₂ and V₂O₅/CeO₂-ZrO₂ catalysts. *Langmuir* 19 (2003): 3025-3030.
- [96] Reddy, B. M., and Khan, A. Nanosized CeO₂SiO₂, CeO₂TiO₂, and CeO₂ZrO₂ mixed oxides: influence of supporting oxide on thermal stability and oxygen storage properties of ceria. *Catalysis Surveys from Asia*, 9 (2005): 155-171.
- [97] Khan A., and Smirniotis, P. G. Relationship between temperature-programmed reduction profile and activity of modified ferrite-based catalysts for WGS reaction. *Journal of Molecular Catalysis A: Chemical* 280 (2008): 43-51.
- [98] Pfau, A., and Schierbaum, K. D. The electronic structure of stoichiometric and reduced CeO₂ surfaces: an XPS, UPS and HREELS study. *Surface Science* 321 (1994): 71-78.
- [99] Reddy, B. M., Khan, A., Yamada, Y., Kobayashi, T., Loridant, S., and Volta, J. C. Structural characterization of CeO₂-MO₂ (M = Si⁴⁺, Ti⁴⁺, and Zr⁴⁺) mixed oxides by Raman spectroscopy, x-ray photoelectron spectroscopy, and other techniques. *Journal of Physical Chemistry B*, 107 (2003): 11475-11484.
- [100] Wagner, C.D., Moulder, J.F., Davis, L.E., and Riggs, W.M. Handbook of x-ray photoelectron spectroscopy. G.E. Muilenberg, Perkin-Elmer Corporation, Minnesota, 1978.
- [101] Zhang, Y., Cui, P., Dua, T., Shan, L., and Wang, Y. Development of a sulfated Y-doped nonstoichiometric zirconia/polysulfone composite membrane for treatment of wastewater containing oil. *Separation and Purification Technology* 70 (2009): 153-159.

- [102] Guan, K. S., and Yin, Y. S. Effect of rare earth addition on super- hydrophilic property of $\text{TiO}_2/\text{SiO}_2$ composite film. *Materials Chemistry and Physics* 92 (2005): 10–15.

APPENDICES

Appendix A

The TPR spectra of CeZrMO_2 , 5%Ni/ CeZrO_2 , and pure metal oxides are shown as following:

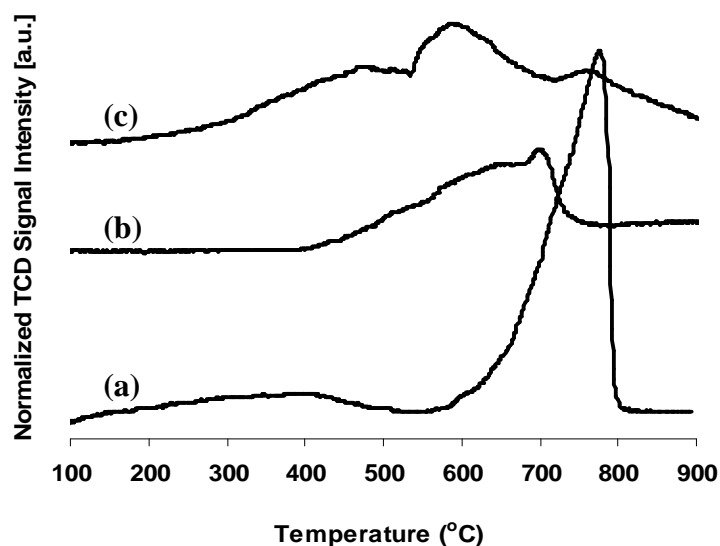


Figure A1 TPR profiles of the ternary mixed oxide support and catalyst calcinated at 650 °C (a) CaO (b) CeZrCa (c) 5%Ni/CeZrCa

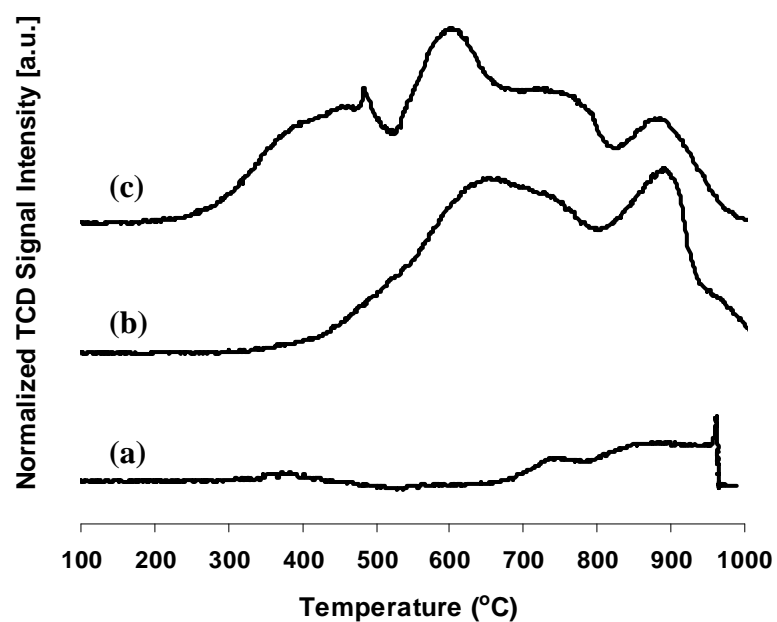


Figure A2 TPR profiles of the ternary mixed oxide support and catalyst calcinated at 650 °C (a) Sm_2O_3 (b) CeZrSm (c) 5%Ni/CeZrSm

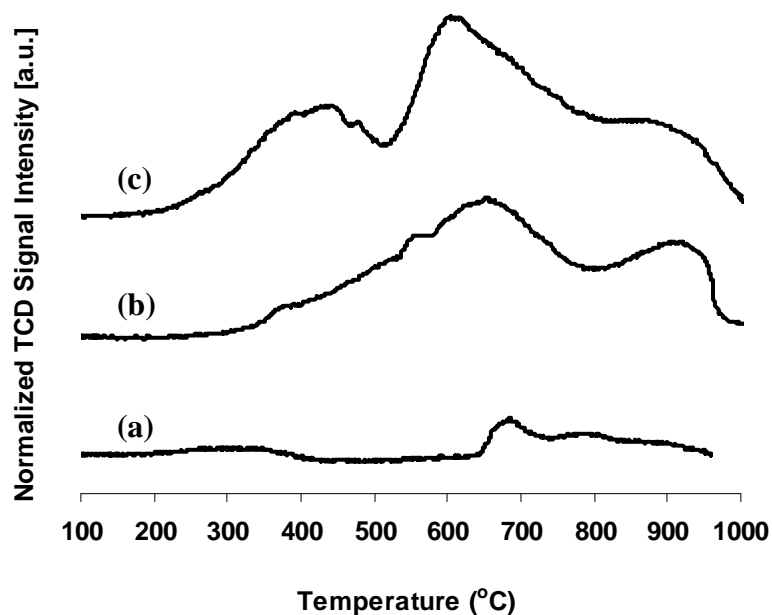


Figure A3 TPR profiles of the ternary mixed oxide support and catalyst calcinated at 650 °C (a) Tb_2O_3 (b) CeZrTb (c) 5%Ni/CeZrTb

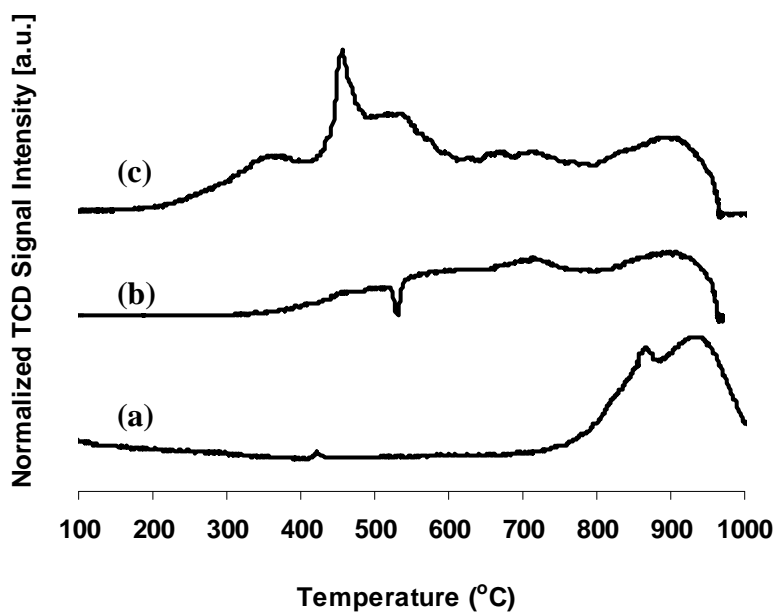


Figure A4 TPR profiles of the ternary mixed oxide support and catalyst calcinated at 650 °C (a) Y_2O_3 (b) CeZrY (c) 5%Ni/CeZrY

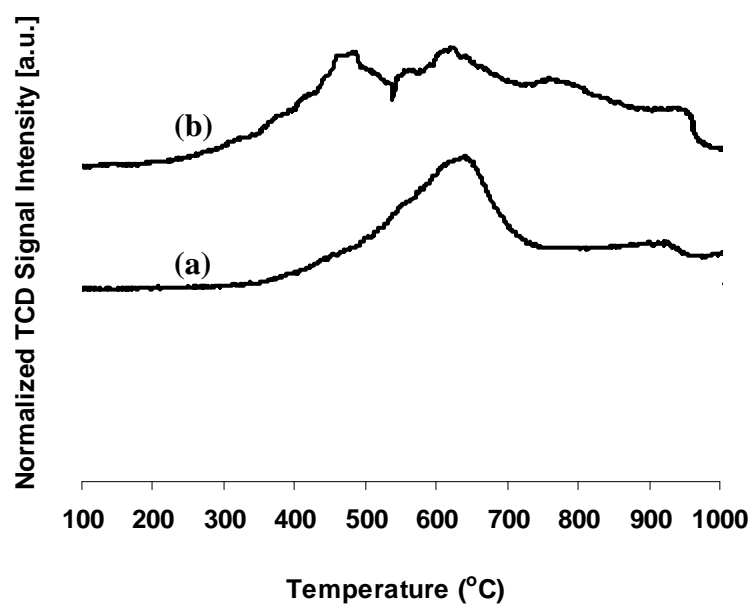


Figure A5 TPR profiles of the ternary mixed oxide support and catalyst calcinated at 650 °C (a) La_2O_3 (b) CeZrLa (c) 5%Ni/CeZrLa

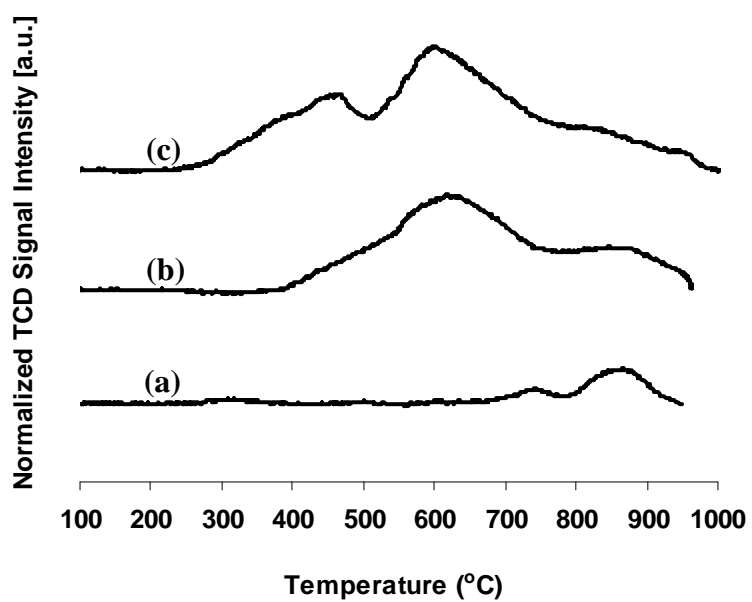


Figure A6 TPR profiles of the ternary mixed oxide support and catalyst calcinated at 650 °C (a) Pr_2O_3 (b) CeZrPr (c) 5%Ni/CeZrPr

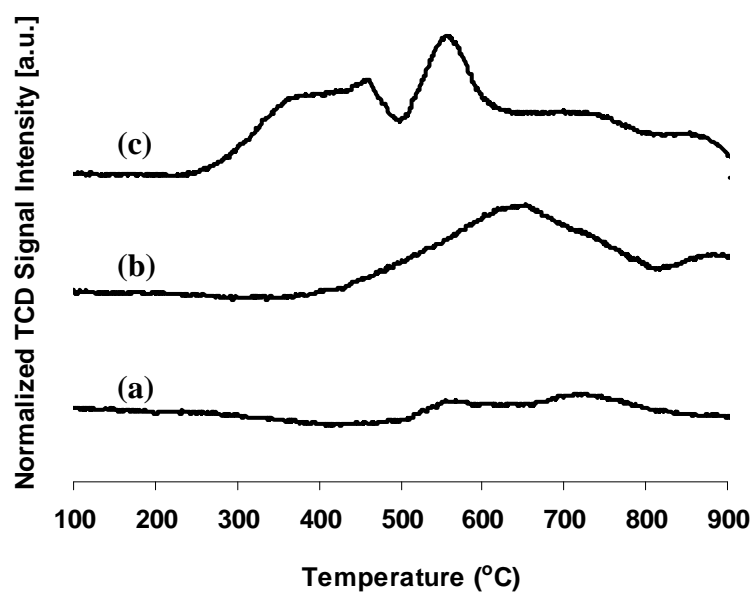


Figure A7 TPR profiles of the ternary mixed oxide support and catalyst calcinated at 650 °C (a) HfO_2 (b) CeZrHf (c) 5%Ni/ CeZrHf

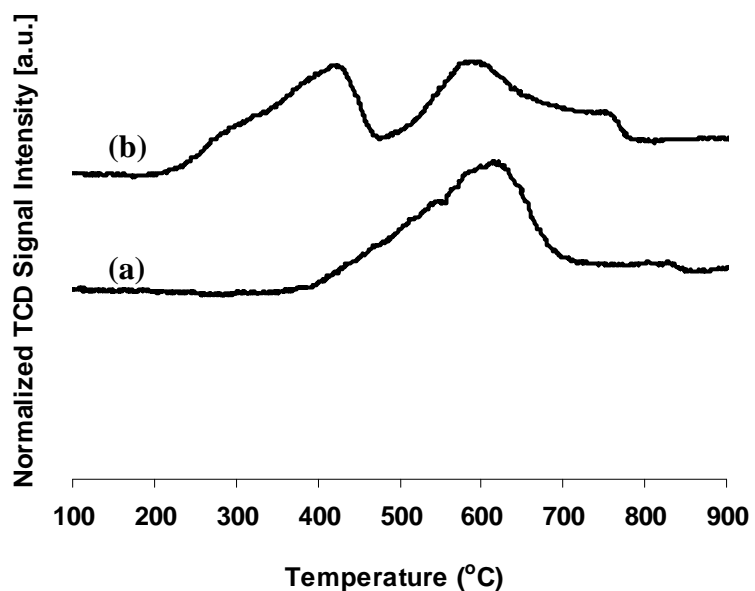


Figure A8 TPR profiles of the ternary mixed oxide support and catalyst calcinated at 650 °C (a) Al_2O_3 (b) CeZrAl (c) 5%Ni/ CeZrAl

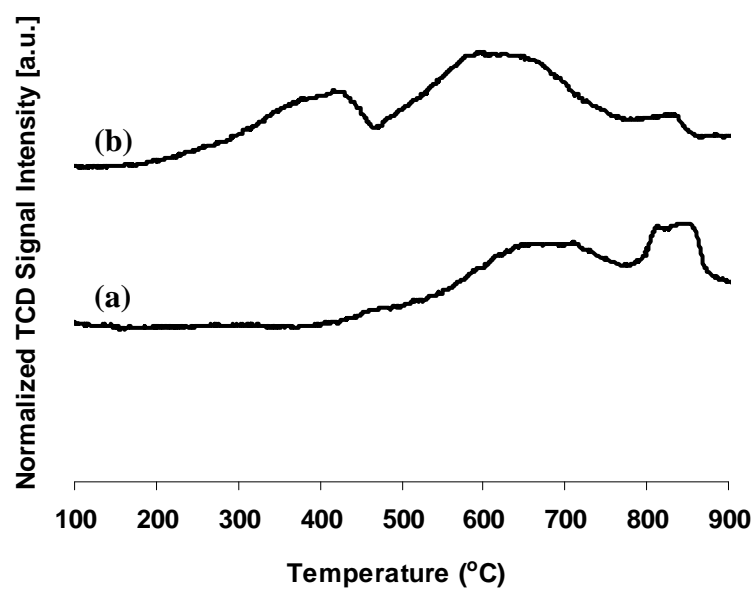


Figure A9 TPR profiles of the ternary mixed oxide support and catalyst calcinated at 650 °C (a) Sr_2O_3 (b) CeZrSr (c) 5%Ni/CeZrSr

The Raman spectra of CeZrMO_2 are shown as following:

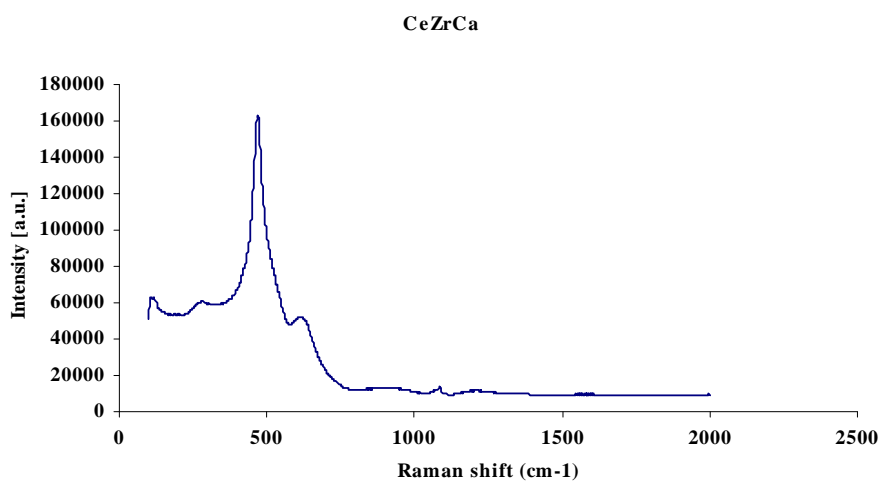


Figure A10 RS spectrum of CeZrCaO_2

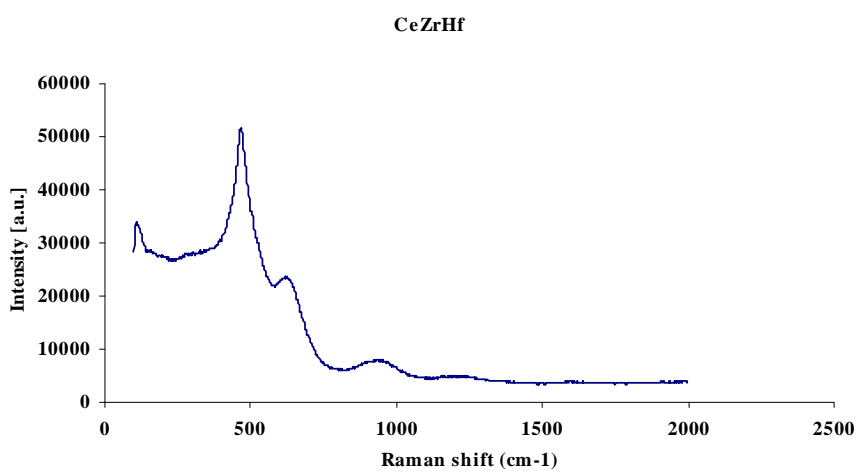


Figure A11 RS spectrum of CeZrHfO_2

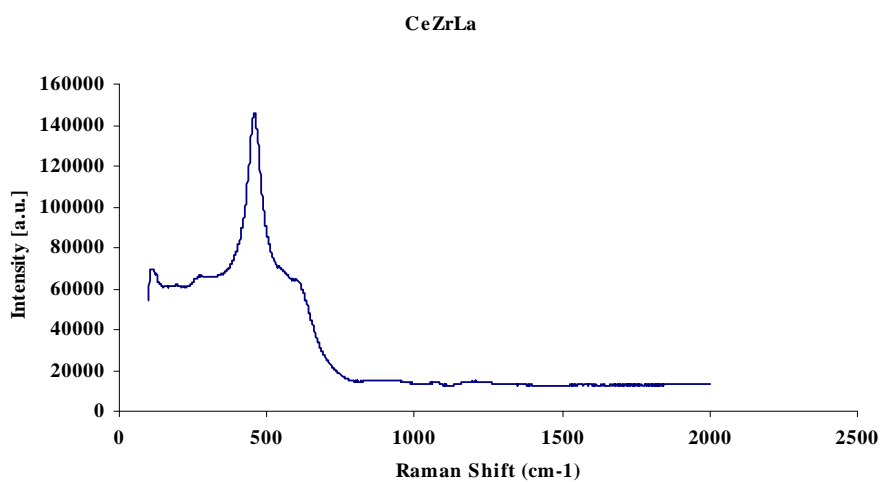


Figure A12 RS spectrum of CeZrLaO₂

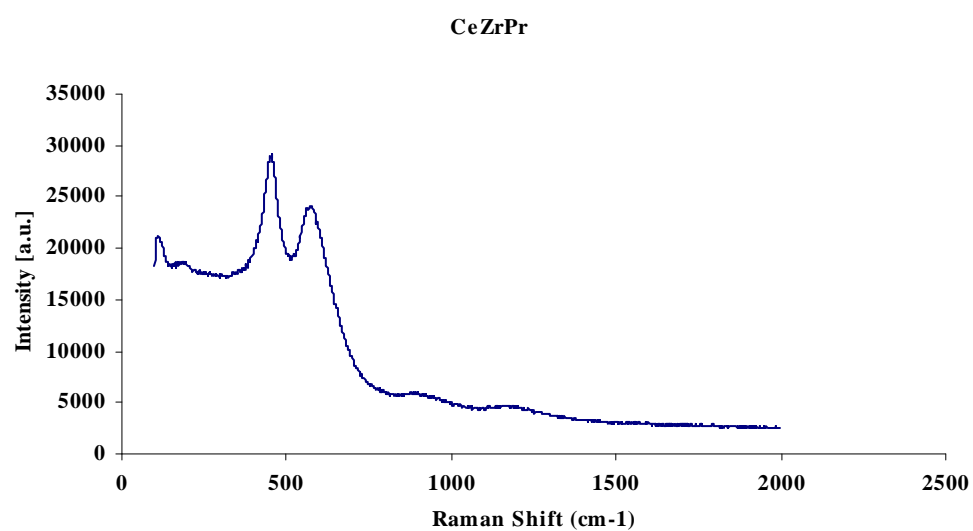


Figure A13 RS spectrum of CeZrPrO₂

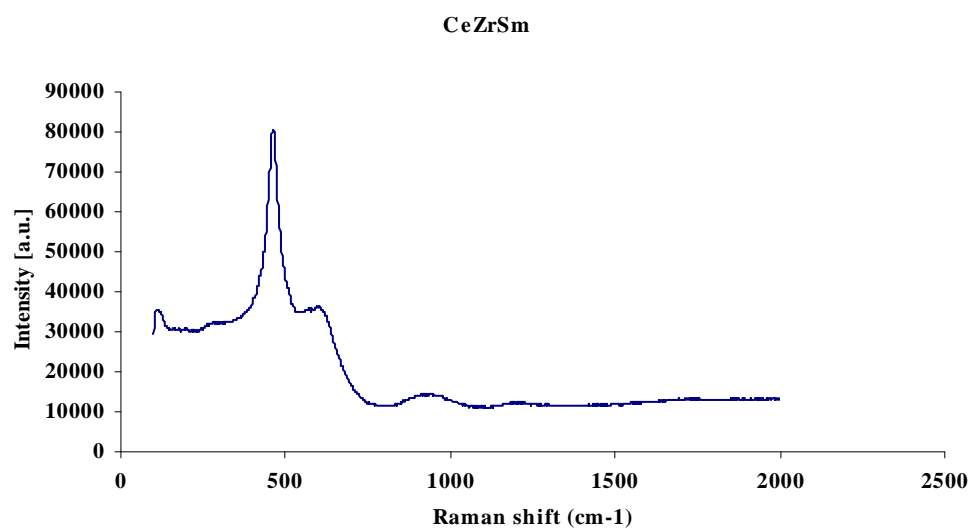


Figure A14 RS spectrum of CeZrSmO₂

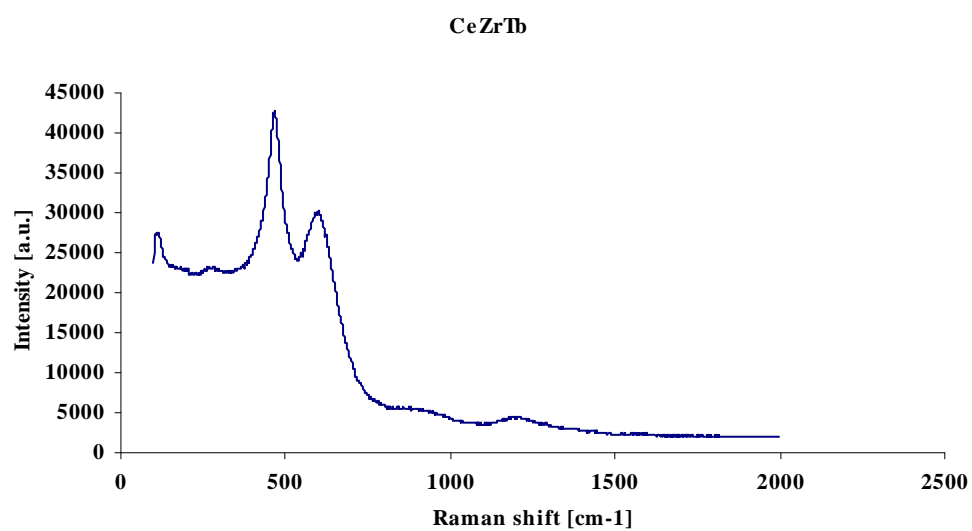


Figure A15 RS spectrum of CeZrTbO₂

The XRD patterns of CeZrMO_2 are shown as following:

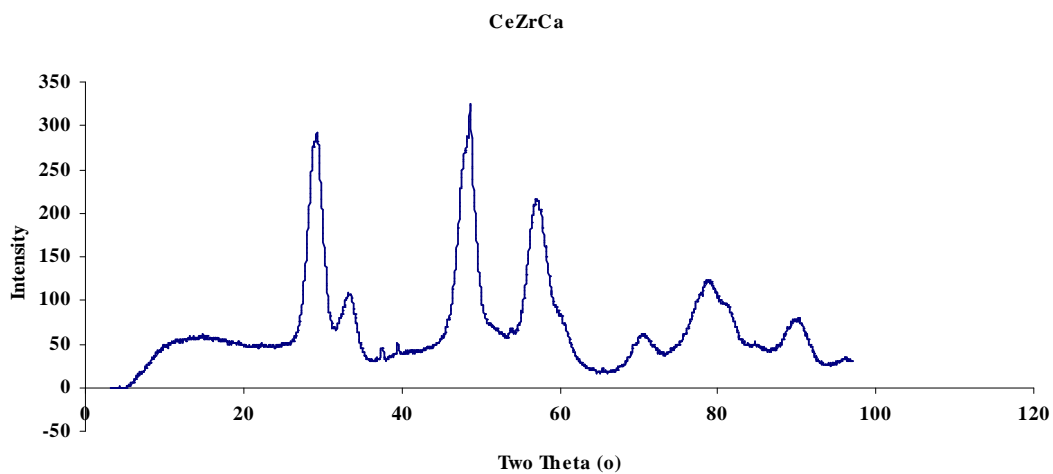


Figure A16 XRD pattern of CeZrCaO_2

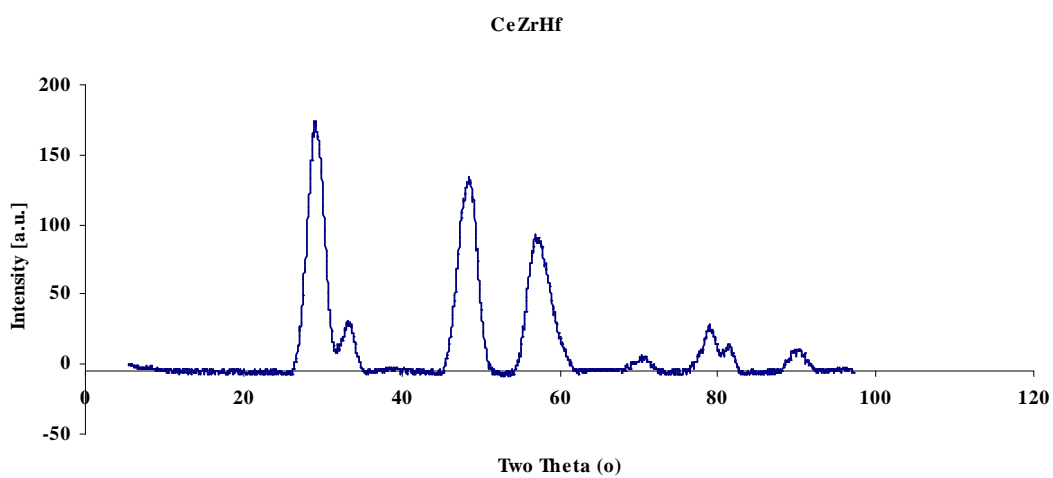


Figure A17 XRD pattern of CeZrHfO_2

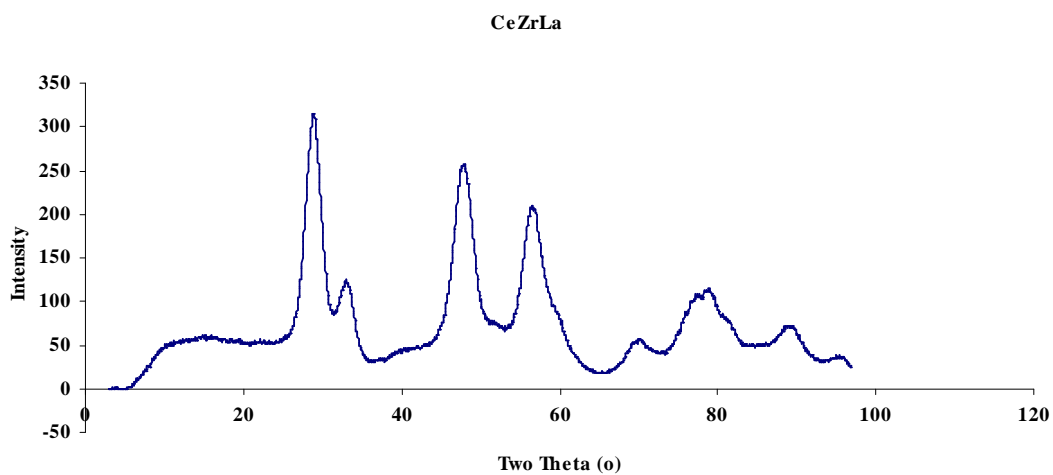


Figure A178 XRD pattern of CeZrLaO₂

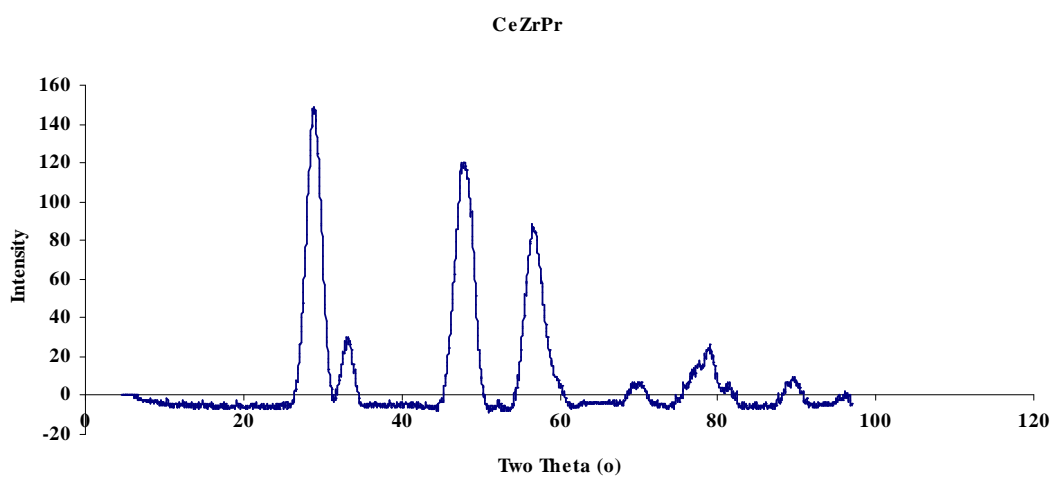


Figure A19 XRD pattern of CeZrPrO₂

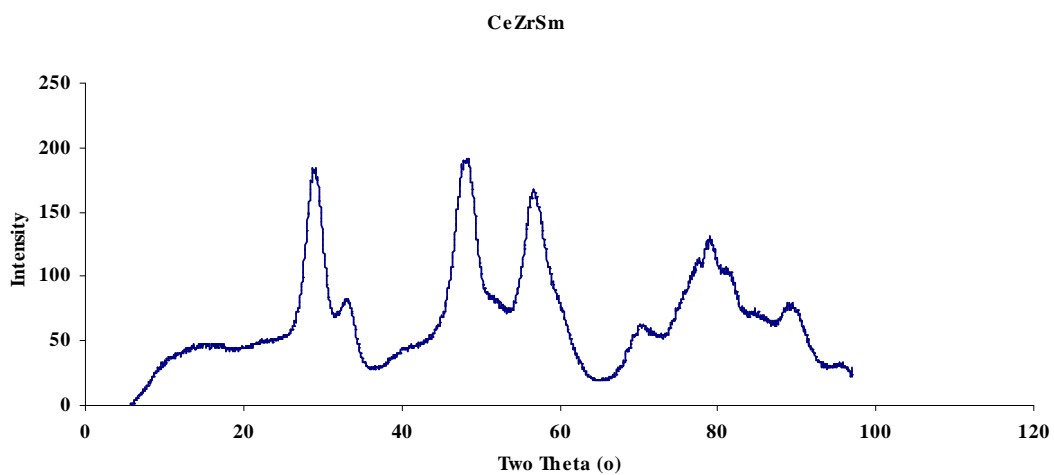


Figure A20 XRD pattern of CeZrSmO₂

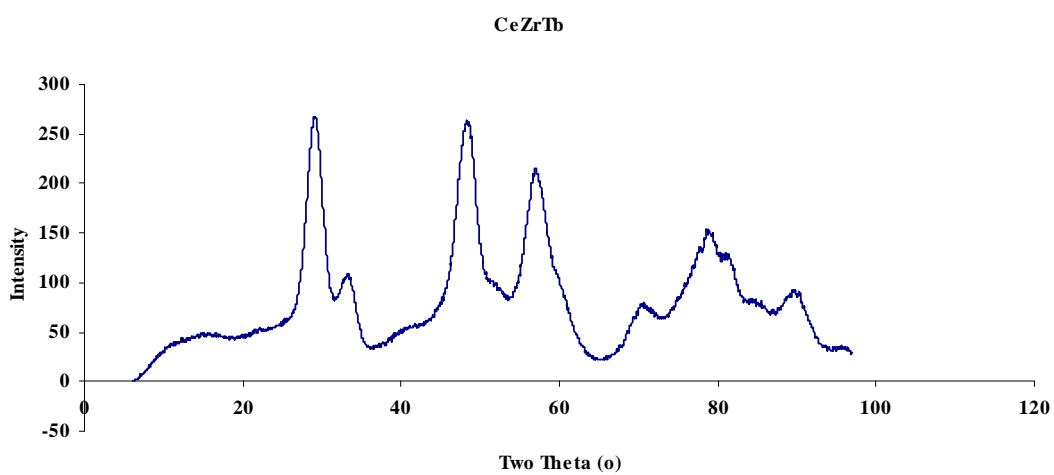


Figure A21 XRD pattern of CeZrTbO₂

Appendix B

Table B1 The productivity calculation of 5%NiCe_{0.6}Zr_{0.4}, CTAB 1.25, without steam, 800 °C

File name	temp C	Time (min)	Read	Time (h)	Calculation	H2 %	CO2 %	N2%	CH4 %	CO %
			Fin (mL/m)		Fout (mL/m)					
5%NiCe _{0.6} Zr _{0.4} , 1.25, W/O	800	60	100	1	150.73	41.903616	6.988079	13.177624	4.289997	33.636548
5%NiCe _{0.6} Zr _{0.4} , 1.25, W/O	800	120	100	2	152.66	41.668225	6.532884	13.010354	4.246194	34.537271
5%NiCe _{0.6} Zr _{0.4} , 1.25, W/O	800	180	100	3	154.96	41.418351	5.931089	12.817268	4.137078	35.691255
5%NiCe _{0.6} Zr _{0.4} , 1.25, W/O	800	240	100	4	157.91	41.282601	5.260262	12.577842	3.975251	36.899133
5%NiCe _{0.6} Zr _{0.4} , 1.25, W/O	800	300	100	5	161.04	41.069704	4.559083	12.333266	3.816749	38.216526
5%NiCe _{0.6} Zr _{0.4} , 1.25, W/O	800	360	100	6	163.60	40.898669	3.968920	12.140416	3.680859	39.306499
5%NiCe _{0.6} Zr _{0.4} , 1.25, W/O	801	420	101	7	165.66	40.862294	3.578048	11.989712	3.537175	40.028839
5%NiCe _{0.6} Zr _{0.4} , 1.25, W/O	802	480	102	8	167.06	40.867637	3.323168	11.889082	3.454839	40.461592

CO/H2	CO/CO2	H2/CO	CO2/CH4	C- CH4(%)	C-CO2(%)	Y-H2 (%)	S-H2(%)
0.80	4.81	1.25	1.63	84.15	73.19	77.41	91.99
0.83	5.29	1.21	1.54	84.11	74.62	77.96	92.69
0.86	6.02	1.16	1.43	84.29	76.61	78.66	93.33
0.89	7.01	1.12	1.32	84.61	78.86	79.90	94.43
0.93	8.38	1.07	1.19	84.93	81.31	81.06	95.44
0.96	9.90	1.04	1.08	85.24	83.47	82.01	96.21
0.98	11.19	1.02	1.01	85.78	85.06	82.14	95.76
0.99	12.18	1.01	0.96	86.13	86.15	82.03	95.24

Table B2 The productivity calculation of 5%NiCe_{0.6}Zr_{0.4}, CTAB 1.25, with steam 0.03 cc/min, 800 °C

File name	temp C	Time (min)	Read	Time (h)	Calculation	H ₂ %	CO ₂ %	N ₂ %	CH ₄ %	CO %	CO/H ₂	CO/CO ₂
			Fin (mL/m)		Fout (mL/m)							
5%NiCe _{0.6} Zr _{0.4} , 1.25 WS	800	60	100	1	159.87	38.902813	4.797156	12.424136	4.581593	39.290567	1.01	8.19
5%NiCe _{0.6} Zr _{0.4} , 1.25 WS	800	120	100	2	161.06	37.443381	4.748748	12.332218	5.644292	39.839162	1.06	8.39
5%NiCe _{0.6} Zr _{0.4} , 1.25 WS	800	180	100	3	157.47	36.050653	5.851732	12.613563	6.981899	38.499913	1.07	6.58
5%NiCe _{0.6} Zr _{0.4} , 1.25 WS	800	240	100	4	153.42	34.787253	7.210359	12.946541	8.287784	36.765744	1.06	5.10
5%NiCe _{0.6} Zr _{0.4} , 1.25 WS	800	300	100	5	149.97	33.875619	8.489995	13.243844	9.336506	35.051416	1.03	4.13
5%NiCe _{0.6} Zr _{0.4} , 1.25 WS	800	360	100	6	146.97	32.744537	9.606386	13.514702	10.496661	33.635097	1.03	3.50
5%NiCe _{0.6} Zr _{0.4} , 1.25 WS	800	420	100	7	145.28	31.922438	10.433490	13.671390	11.333453	32.636519	1.02	3.13
5%NiCe _{0.6} Zr _{0.4} , 1.25 WS	801	480	101	8	143.56	30.937419	11.040270	13.835097	12.232247	31.952453	1.03	2.89
		CH ₄ in	CO ₂ in	N ₂ in	H ₂ O in	total mole	H ₂ O out	H ₂ out	CO ₂ out	N ₂ out	CH ₄ out	CO out
		(mol/min)	(mol/min)	(mol/min)	(mol/min)		(mol/min)	(mol/min)	(mol/min)	(mol/min)	(mol/min)	(mol/min)
		0.006211	0.005982	0.003024	0.001666667	0.024340	0.000000	0.009469	0.001168	0.003024	0.001115	0.009563
						0.024521	0.000000	0.009182	0.001164	0.003024	0.001384	0.009769
						0.023974	0.000000	0.008643	0.001403	0.003024	0.001674	0.009230
						0.023358	0.000000	0.008125	0.001684	0.003024	0.001936	0.008588
						0.022833	0.000000	0.007735	0.001939	0.003024	0.002132	0.008003
						0.022376	0.000000	0.007327	0.002149	0.003024	0.002349	0.007526
						0.022119	0.000000	0.007061	0.002308	0.003024	0.002507	0.007219
						0.021857	0.000000	0.006762	0.002413	0.003024	0.002674	0.006984
	nCH ₄ A	nCH ₄ B	X _{CH₄ A}	X _{CH₄ B}	Total X _{CH₄}	X _{CO₂ A}	H ₂ from A	H ₂ from B	S-H ₂ (%)	Y-H ₂ (%)	H ₂ /CO	CO ₂ /CH ₄
	(mol/min)	(mol/min)	%	%	%	%	mol/min	mol/min				
	0.004782	0.000314	76.99	5.06	82.05	79.93	0.009563	0.001257	87.51	76.23	0.99	1.05
	0.004885	-0.000058	78.64	0.00	78.64	81.65	0.009769	0.000000	93.99	73.91	0.94	0.84
	0.004615	-0.000078	74.30	0.00	74.30	77.15	0.009230	0.000000	93.64	69.58	0.94	0.84
	0.004294	-0.000019	69.13	0.00	69.13	71.78	0.008588	0.000000	94.62	65.41	0.95	0.87
	0.004002	0.000077	64.43	1.25	65.68	66.90	0.008003	0.000310	93.04	62.27	0.97	0.91
	0.003763	0.000099	60.59	1.60	62.18	62.91	0.007526	0.000397	92.47	58.98	0.97	0.92
	0.003609	0.000095	58.11	0.00	58.11	60.34	0.007219	0.000000	97.81	56.84	0.98	0.92
	0.003492	0.000045	56.22	1.00	57.22	58.38	0.006984	0.000248	93.50	54.44	0.97	0.90

VITAE

Name: Mrs. Thitinat Sukonket

Date of Birth: September 19, 1975

Residence: 154/52 Banggrui-Sainoi Road Tambon Banggrui, A.Banggrui
Nonthaburi 11130

Education:

- 1997** B.Sc. Industrial Chemistry, King Monkut's Institute Technology North Bangkok, Thailand
- 2000** M.Sc. Petrochemistry and Polymer Science, Chulalongkorn University, Thailand.

Presentation at the national and international conference

- 2006** Cr-Based Intermetallic Diffusion Barriers for Stainless Steel Supported Palladium Membrane, MPSGC, December 11-15, 2006, National University of Singapore, Singapore
- 2008** Development of Intermetallic Diffusion Barrier for Palladium Membrane Supported on Porous Stainless Steel, KZA Workshop 2008, July 19-20, 2008, Sogang University, Seoul, Korea
- 2009** Design and Development of High Performance Catalysts for Multi-Feedstock Hydrogen Production, 8th World Congress of Chemical Engineering, August 23-27, 2009, Montreal, Quebec, Canada
- 2010** CO₂ reforming of methane over Ni/Ce_{0.5}-Zr_{0.33}-M_{0.16}O₂ in the presence of steam, Pure and Applied Chemistry International Conference (PACCON2010), January 20-23, 2010, Ubonratchathani University, Ubonratchathani, Thailand